Alma Mater Studiorum – Università di Bologna

DOTTORATO DI RICERCA IN

Scienze Chimiche

ciclo XXIV

Settore concorsuale di afferenza: 03/A1

Settore scientifico disciplinare: CHIM/01

ELECTROSYNTHESIS AND CHARACTERIZATION OF STRUCTURED CATALYSTS

Presentata da: Marco Monti

Coordinatore del dottorato:

Prof. Adriana Bigi

Relatore:

Prof. Domenica Tonelli

Esame finale anno 2012

INDICE

1. PREFACE

Hydrogen is considered one of the most important energy carrier in the development of new system for energy production because it is very effective, not pollutant and could be obtained from several sources, such as fossil fuels (methane, carbon), water or biomasses [1].

It has a high energy content [2] and thus it could be considered a valid green alternative to fossil fuels [1]. However the produced H_2 could be clean and sustainable only if it is derived from renewable sources [3].

Nowadays about 48% of the world's hydrogen gas is generated from natural gas, 30% from oil, about 18% from coal and only about 4% from electrolysis system, due to high costs of this process [4]. It is mainly used in refinery processes such as hydrotreating and in the chemical industry for the production of NH_3 and methanol, which is one of the main building-blocks of the modern chemistry.

In the future H_2 could be also employed in the automotive industry as fuel-cells, gas turbines and engines technologies. Its employment as a fuel could lead to an increase in the efficiency and in the performances of engines with a really important decrease in the emissions of pollutants, although these aims need a major effort in the research in order to obtain cheaper and more efficient H_2 production processes. Moreover two other relevant issues regarding the hydrogen technology that have to be optimized are the problems connected to its distribution and storage [5].

Recently there has been an international attention on the development of new hydrogen technologies as a potential solution to the current fears about energy shortage. For example, since 2006 the U.S. Department of Energy has developed a multi-year plan with aggressive milestones and targets for the development of hydrogen infrastructure, fuel cells and storage technologies [6,7].

The delocalization of H_2 production would be the best choice to be developed in order to avoid the setting up of expensive structures for its distribution and for the advantages with respect to the market. On the other hand the overall effect of the establishment of a delocalized production system would lead to an increase of costs and a lower efficiency of production [5].

1.1 HYDROGEN PRODUCTION

Hydrogen can be produced from a variety of feedstock including fossil as well as renewable resources. Various chemical, biological, electrolytic, thermolytic, photolytic and thermochemical processes exist for this purpose and they are in different stages of development [5].

A brief summary of hydrogen production systems is outlined afterward. They can be mainly divided in systems employing renewable sources or hydrocarbon fuels processing.

1.1.1 HYDROGEN FROM HYDROCARBON FUELS PROCESSING

Hydrocarbon reforming is the main method employed in H_2 production and there are four main used techniques: steam reforming (SR), partial oxidation (POX), autothermal reforming (ATR) and dry reforming (DR). All of them produce a gas stream composed primarily of H_2 and CO (syngas), with also CO_2. Steam reforming and catalytic partial oxidation (CPO) are two different processes will be later described briefly. In the first one methane reacts with water while in the second one the hydrocarbon is oxidized by oxygen; the routes are endothermic and exothermic respectively. The autothermal reforming is a combination of two processes, the POX which provides the heat and the SR which increases the amount of hydrogen produced [7]. In DR CH_4 reacts with CO_2 by an endothermic reaction [8]. Fuel processing reactors are designed to maximize hydrogen production and minimize carbon production using appropriate operating conditions such as temperature, pressure, residence time, etc. [7].

Pyrolysis is another technique that employs hydrocarbon decomposition to produce hydrogen. It can be applied to any organic substrate and can be also used for the production of hydrocarbons, carbon spheres and nanotubes production. It does not need the presence of water or air and so it can be considered a low emission process if the substrate does not contain humidity or oxygen. On the contrary CO and CO_2 emissions would be very relevant. Among the advantages of the process are fuel flexibility, relative simplicity, clean carbon by-products and reduction in emissions.

Another example of H_2 production from hydrocarbons is plasma reforming. The overall reaction is the same involved in the conventional reforming but the energy and the free radicals used are provided by plasma that is typically generated with electricity or heat. When water or steam are injected with the fuel, H·, OH· and O· are formed together with electrons creating the conditions for both reductive and oxidative reaction. It should overcome many limitations of other methods such as costs and deterioration of catalysts, limitation of hydrogen production from heavy hydrocarbons, size and weight requirements, and it is more sulfur tolerant. On the other hand, the electrical requirements and the high electrode erosion at high pressure are reported to be the main disadvantages [7].

1.1.2 HYDROGEN FROM RENEWABLE SOURCES

These methods employ mainly biomasses or water as feedstock for hydrogen production. Biomasses are the most likely renewable organic substitute to petroleum and they are available from a wide range of different sources such as animal and agricultural wastes, municipal solid wastes, crop residues, sawdust, aquatic plants and many others [2,7].

Gasification technology is a variation of pyrolisis. It is commonly used with biomasses and coal, and it is based upon partial oxidation of the materials into a mixture of H_2, CH_4, N_2, CO,

CO_2 and tar. A reformer may be placed downstream the gassifier to increase the H_2 content. However, this system requires a massive amount of biomass to be fed continuously in the reactor and large plants. It can achieve efficiencies between 35-50% but the high logistics costs limit the number of gasification plants. Development of smaller and efficiently distributed gasification plants may be required to this technology for cost effective hydrogen production [7].

Bio-hydrogen production includes different technologies based on the employment of different microorganisms. This technology that has substantially increased over the last several years. However nowadays only a small fraction of naturally occurring microorganisms has been discovered and characterized, but they have been also modified to improve their characteristics. This kind of technology is at the beginning of its development and many steps should be make for its optimization [7].

In addition to the previous described approaches, water can be used as feed for many hydrogen production techniques. Electrolysis consists in the conversion of electrical energy to chemical energy by passing an electrical current through two electrodes to break water to produce hydrogen, with oxygen as useful by-product. It is more expensive than large scale fuel processing techniques and it results in higher emissions respect to other technologies, such as gas reforming, if non-renewable power generation is used to produce electricity.

In thermochemical water splitting (thermolysis), the heat alone is used to decompose water to hydrogen and oxygen. There are many projects investigating several processes focused on improving materials, lowering costs and increasing efficiency of this technology that mainly suffers from the high decomposition temperature of water.

Finally, another example of a technique employed in hydrogen production from renewable sources is photoelectrolysis, that uses sunlight to directly decompose water into hydrogen and oxygen. It employs semiconductor materials similar to those used in photovoltaic technology. The hydrogen production efficiency is generally limited by the imperfections in the crystalline structure of the photoelectrodes, bulk and surface properties, and the resistance of materials to the corrosion from the electrolyte [7].

2. AIM

This work has been focused on the electrochemical synthesis of catalytic precursors for the steam reforming and the catalytic partial oxidation reactions and their characterization.

The catalytic precursors have been prepared through the synthesis of layered double hydroxide (LDH) compounds that contain Rh, Mg and Al by a method known as electrobase generation method. FeCrAlY alloy foams have been used as supports to exploit several advantages of supported catalysis respect to pellets catalysts.

To achieve a better performance of the electrochemical method, all the parameters that affect the electrosynthesis such as the applied potential, the time of synthesis and the pH have been investigated. As far as LDHs precipitation is very sensible to pH, a particular attention has been given to the correlation between the evolution of pH at the working electrode surface and the applied potential in order to identify the best working conditions for the synthesis. Pt gauzes and plates have been used as supports in order to avoid problems caused by the complex geometry of the foams, and NiAl and MgAl LDHs have also been investigated in order to avoid the high costs due to the Rh consumption.

The characterization of each sample has been a key point of the study in order to understand the modification in morphology and reactivity as result of the change of synthesis conditions.

The work has been carried out in collaboration with the Department of Industrial and Materials Chemistry where the catalytic tests have been performed in order to check the activity of the prepared catalysts in the CPO and SR of methane reactions.

3. INTRODUCTION

A brief overview of catalytic reactions, catalysts and of the synthesis methods is reported below for a better comprehension of the subsequently described work.

3.1 STEAM REFORMING OF METHANE

The steam reforming of methane is the main commercial route for hydrogen and syngas production [9] and about 50% of hydrogen demand is satisfied by means of methane SR [10]. It consists of an endothermic reaction between the hydrocarbon and vaporized water that can be written as:

$$CH_4 + H_2O \rightarrow CO + 3H_2 \qquad \Delta H°=206 \text{ KJ/mol [11]} \qquad (3.1.1)$$

$$CO + H_2O \rightarrow CO_2 + H_2 \qquad \Delta H°=-41 \text{ KJ/mol [11]} \qquad (3.1.2)$$

The second reaction is referred as the water gas shift reaction (WGS), that is slightly exothermic and takes place spontaneously as far as the syngas produced by SR reacts with the remaining water present in the reactor [5, 7, 11].

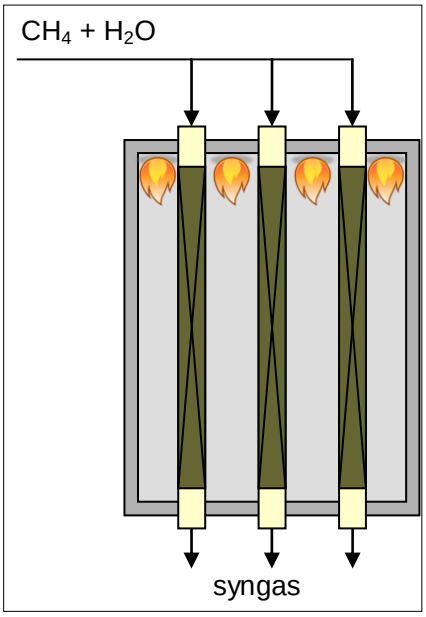

Figure 1: Schematic representation of typical SR reactor

Due to the endothermicity of the reaction, the thermodynamic equilibrium is favored at high temperature [10]. The steam reforming takes place over catalysts in vertical tubes, which are supported in parallel rows in a radiant furnace. Reformers are usually operated at

high temperatures and pressure. The thermal efficiency of the process is around 95%, but only 50% is absorbed by SR. The heat is often supplied from the combustion of some of the methane feed-gas. Usually, it occurs at a temperature of 700-1100 °C [12, 13, 14, 15].

The methane SR offers the best H_2/CO molar ratio among hydrocarbon reforming reactions (3:1), furthermore the carbon monoxide present in the products gas stream can be further converted to CO_2 and H_2 through the WGS reaction (3.1.2).

Carbon dioxide produced in the reformer and WGS reactors is typically removed from the process gas by chemical solvent absorption or by pressure swing absorption processes. The level of carbon oxides that remains in the H_2 stream after the CO_2 removal absorber is reduced to a minimum by methanation, that is essentially the reverse reaction of the steam reforming. This traditional process produces H_2 at a purity from 95 to 98%, with the impurity being predominantly methane [11].

In steam reforming plant the reactors suffer from non-uniform distribution of heat fluxes and from profound effect on high temperature catalyst and tubes lifetime [13].

Generally, the catalysts employed in this reaction can be divided in non-precious metals based catalysts (tipically Ni), and precious metals (Group VIII) based catalysts (tipically Pt or Rh) [7]. As far as Ni-like catalysts are concerned, the methane adsorbs dissociatively on Ni surface with no molecular species as precursor. This requires that the CH_4 molecule has enough energy to overcome a barrier of about 50 kJ/mol and that it strikes two adjacent free Ni sites. The adsorbed methyl group undergoes further step-wise dehydrogenation, yielding carbon [11]:

$$CH_4 \leftrightharpoons CH_3^* \rightarrow CH_2^* \rightarrow CH^* \leftrightharpoons C^* \qquad (3.1.3)$$

Group VIII based catalysts seem to have the same catalytic path as Ni based catalysts, but they exhibit a much higher specific activity, particulary Rh seems to be the most active metal. However, the high cost of Rh is driving the researchers to develop alternative catalysts such as Co based catalysts [7].

One of the main reasons that lead to the deactivation of catalysts is the formation of carbon over the catalytic surface, particularly at intermediate and high temperatures [7, 11]. Carbon deposition takes place by the Boudouard reaction and by the direct decomposition of methane:

$$2CO \rightarrow C + CO_2 \qquad \Delta H°=-172 \text{ kJ/mol [11]} \qquad (3.1.4)$$

$$CH_4 \rightarrow C + 2H_2 \qquad \Delta H°=75 \text{ kJ/mol [11]} \qquad (3.1.5)$$

Moreover, carbon formation is catalyzed by Ni surface and usually takes place in the form of whiskers with a Ni particle at the top of a fibre. The rate of carbon formation is much more lower on noble metals than on Ni, which is ascribed to a smaller dissolution of carbon into

those metals. By the way, rhodium and ruthenium display the highest selectivity for the carbon-free operation, and this can be due to the high reforming activity combined with the low carbon growth rates [11].

Nickel and noble metal-based catalysts have been reported to be active also for CO_2 reforming, without coke formation in the case of precious metal based catalysts [7, 11].

To limit the carbon deposition that poisons the active phase an excess of steam is usually employed in the feed stream and alkali (K) or alkali earths (Mg, Ca, metals) are introduced in catalyst formulations to accelerate carbon removal from the catalyst surface [7, 11].

Zeolites and ceramic monoliths have been employed to support catalysts in SR process [16, 17]. Moreover layered double hydroxides with different composition have been used as catalyst precursors. After calcination they have been used as bulk catalysts in powder [18, 19, 20] and supported catalysts on FeCrAlY foams [21] for this reaction.

3.2 PARTIAL OXIDATION OF METHANE

As the steam reforming is a very intensive energy process, extensive work has been done over the years in order to develop other more attractive options [11]. The catalytic partial oxidation of methane offers a promising alternative to the steam reforming for hydrogen and CO (syngas) production [22] since a process based on this reaction would be much more energy efficient than the energy intensive SR process [11].

As outlined before, the partial oxidation of methane is a slight exothermic reaction where a hydrocarbon reacts with oxygen to produce carbon monoxide and hydrogen. During this process several reactions take place [8], but the general reaction can be written in the case of methane as:

$$CH_4 + 0.5O_2 \rightarrow CO + 2H_2 \qquad \Delta H°=-36 \text{ KJ/mol [11,22]} \qquad (3.2.1)$$

Typically the non-catalytic partial oxidation occurs with flame temperatures of 1300-1500 °C while the operating temperature can be lowered if a catalyst is added. However the control temperature has been proved hard because of coke and hot spots formation due to the exothermic nature of the reaction [7**].**

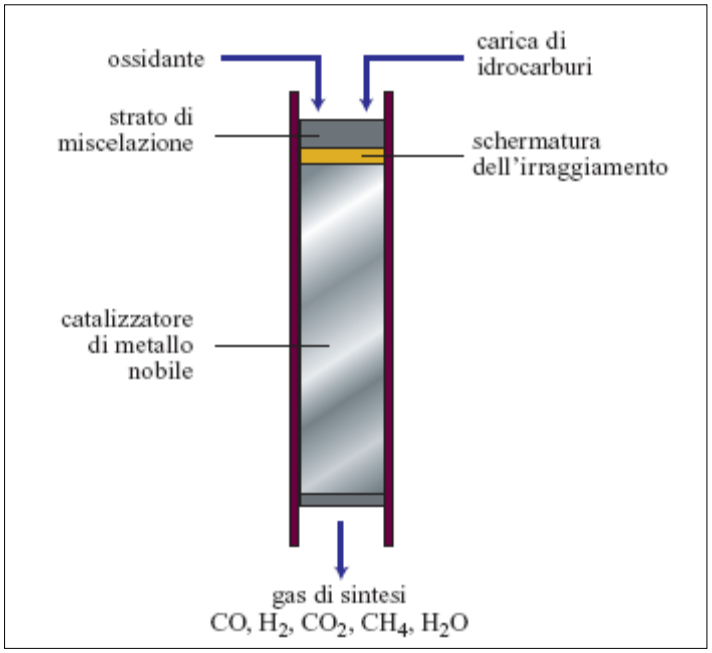

Figure 2: Schematic representation of typical CPO reactor

The gas stream obtained from this reaction presents a H_2/CO molar ratio 2:1, so it can be further used in the methanol production, in a Fischer-Tropsch reactor for the production of hydrocarbons or in a water gas shift plant to increase the hydrogen production. The composition of the product gas depends on temperature, pressure, input gas composition, and also on kinetic factors too.

The high conversion of CH_4 and the high syngas selectivity for short contact times make it possible to use this reaction also in small reactors with excellent results [20]. However CPO has not been able to replace steam reforming in the syngas and hydrogen production. This is due to its severe reaction conditions such as the high operating temperature and the high gas flux that may cause the runaway of the reactor and that are a heavy source of mechanical and thermal stress for the catalysts. In fact since exothermic combustion reactions generate heat in the catalyst bed, the temperature can substantially increase when high space velocities are used [8]. Moreover the heat production is really important in the scale-up of the process because its removal could be a very complex parameter to improve. However, it can be seen that as the temperature increases the selectivity to CO and H_2 increses as well. Therefore, very high methane conversion (> 90%) and selectivity (> 90%) to synthesis gas can be obtained above 1200-1300 °C. Moreover, methane, carbon dioxide and water concentrations increase at high pressures but the increasing of the reaction temperature can compensate for the effect of pressure [8].

A debate is still ongoing on the exact mechanism of methane activation and the sequence of syngas and hydrogen production and two distinct mechanisms are proposed for explaining this reaction.

The indirect pathway postulates that CH_4 is first totally oxidized to CO_2 and H_2O (a strongly exothermic reaction) and then reformed to produce syngas (with endothermic steam

and dry reforming reactions). One major proof of the existence of such an exothermic–endothermic sequence has been the observation of an axial temperature profile with sharp hot-spot temperatures at the entrance of the reactor [23].

The direct pathway postulates the formation of H_2 and CO as primary products. The main evidence in favor of a direct path is the observation of syngas at extremely short contact times, in the presence of unreacted O_2. H_2O and CO_2 are in this case interpreted as non-selective oxidation products. The mechanism was proposed to consist of the dissociative adsorption of CH_4 with formation of carbon species and H adsorbed atoms, followed by the associative desorption of two H atoms to H_2 formation and the oxidation of C to CO.

Depending on the sampling technique, on the type of reactor and on the operating conditions, different product distributions were obtained and different mechanisms were thus inferred, either direct, indirect, or mixed [23].

However in recent works the collected data seems to indicate that a "mixed" pathway, as the one occurring on Rh-based catalysts, takes place. The division of the reactor in an oxidation and a reforming zone has been observed, and the length of the oxidation zone depends on the total flow rate and the stoichiometry of the reactants [23, 24]. The oxidation zone is located in the first part of the reactor, where H_2 and CO are produced by direct oxidation in the presence of gas phase O_2 together with CO_2 and H_2O (produced by total oxidation). In the reforming zone, only steam reforming is active [23, 24], no dry reforming was observed. If a CO molecule stays long enough at the surface of the catalyst then CO_2 is formed by reaction with a O adsorbed atom [24] and the contribution of WGS varies with the C to O feed ratio [23].

As for the SR process, carbon formation occurs on the metal catalysts. This behavior cannot be avoided by increasing the O_2/CH_4 ratio or by increasing the operating temperature without increasing also the potential explosion hazards, separation problems, gas phase reactions and decreased the synthesis gas selectivities. Carbon deposition evolves as for the SR process by the Boudouard reaction (3.1.4) or by catalytic methane decomposition (3.1.5) [8].

In catalytic partial oxidation, catalysts are based on transition metals such as Ni or Co and on noble metals (Rh, Ru, Pt, …) similarly to those employed in SR.

High yields and selectivities to synthesis gas (> 85%) can be obtained over nickel and cobalt supported on various oxides, under conditions of apparently low temperature and very short residence times. However, some noble metals could, on a laboratory scale, catalyze methane partial oxidation to the thermodynamic equilibrium composition of product gases with little or no carbon deposition. It was found that the relative rate of carbon deposition follows the order Ni > Pd > Rh, Ru, Pt, Ir.

In CPO reaction bulk catalysts, where the active phase is supported on alumina powder, could be employed [23]. However, several supported catalysts have been developed on different structures, such as Al_2O_3 [24, 25,26] and zirconia [25] foams, pellets [25, 26], cordierite monoliths [25, 26], due to the problems related to heat diffusion and optimization of the catalyst employment. Mixed oxides obtained from LHD precursors of various

compositions has also been employed for CPO reaction as bulk catalysts [27, 28, 20, 29]. Moreover, the same compounds have been used to develop structured catalysts on FeCrAlY foams [20, 21].

3.3 LAYERED DOUBLE HYDROXIDES (LDH) COMPOUNDS

LDHs have been used as catalyst precursors for the SR [18, 19, 30] and CPO [23,24, 27, 28, 29] of natural gas.

In this work layered double hydroxides have been studied and employed as catalytic precursors, after deposition on FeCrAlY foams. They belong to a family of compounds called clays that could be mainly divided in two large groups: anionic and cationic clays. Both types are made up of several hydroxide layers. In cationic clays these layers present a negative charge and they are mostly composed by Si and Al hydroxides. The negative charge is balanced by cations situated in the interlayer region. On the contrary, anionic clays are characterized by positive charge layers and interlayer anions to obtain the electroneutrality.

LDHs or hydrotalcite-like (HT-like) compounds are anionic clays materials. A few kinds of anionic clays have been found in nature but most of them could be artificially synthesized in the laboratory [31]. These layered materials have rich intercalation properties. The structure of most of them corresponds to that of the mineral hydrotalcite which is a natural magnesium-aluminum hydroxycarbonate ($Mg_6Al_2(OH)_{16}CO_3 \cdot 4H_2O$). These compounds consist of positively charged brucite-type octahedral sheets alternating with interlayers containing carbonate anions, in the natural mineral, or other exchangeable anions in the synthetic HT-like compounds, together with water molecules [32]. Brucite is the common magnesium hydroxide $Mg(OH)_2$.

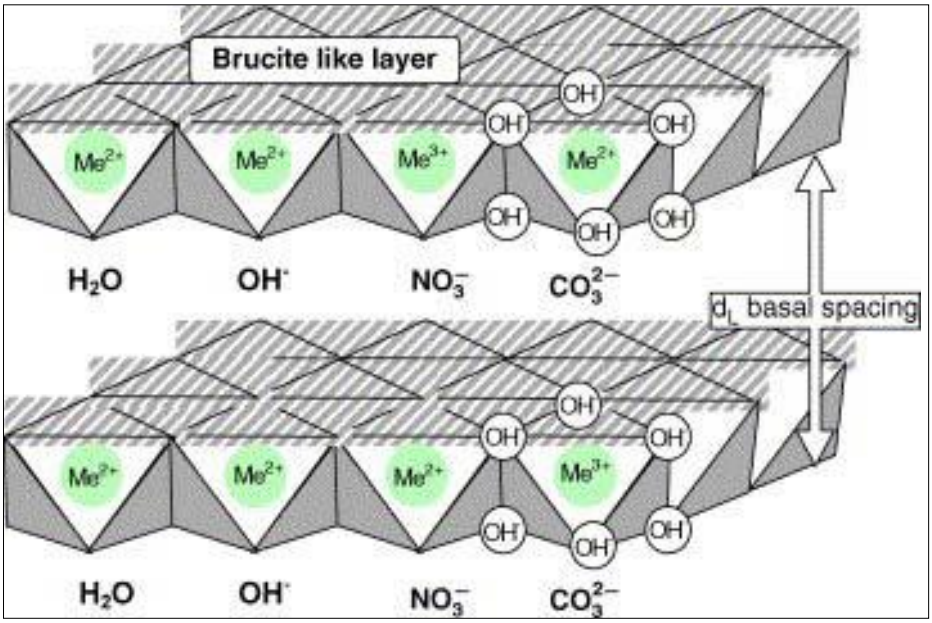

Figure 3: Schematic representation of LDH compounds structures

LDHs can be represented by the general formula $[M_{1-x}^{2+}M_x^{3+}(OH)_2]^{x+}(A^{n-})_{x/n}\cdot mH_2O$, where M^{2+} and M^{3+} are divalent and trivalent cations, respectively. The value of x is equal to the molar ratio of $M^{3+}/(M^{2+}+M^{3+})$, whereas A is the interlayer anion of valence n. The identity of M^{2+}, M^{3+}, x and A^{n-}, and the x value may vary over a wide range, thus giving rise to a large class of isostructural materials with different physicochemical properties [33].

The divalent and trivalent metal listed in Table 1 are all found to form LDHs through replacing, fully or partially, Mg^{2+} or Al^{3+}, in the brucite-like layer [31]. In general ions that have ionic radius similar to that of Mg^{2+} can be accommodated in the holes of the close-packed OH groups in the brucite-like sheets to form LDHs [31,33].

M^{2+}	Radius (nm)	M^{3+}	Radius (nm)
Fe	0.061	Al	0.054
Co	0.065	Co	0.055
Ni	0.069	Fe	0.055
Mg	0.072	Mn	0.058
Cu	0.073	Ga	0.062
Zn	0.074	Rh	0.067
Mn	0.083	Ru	0.068
Pd	0.086	Cr	0.069
Ti	0.086	V	0.074
Cd	0.095	In	0.080
Ca	0.100	Y	0.090
		La	0.103
V^{4+}	0.058		
Ti^{4+}	0.061	Li^{+}	0.076
Sn^{4+}	0.069	Na^{+}	0.102
Zr^{4+}	0.072		

Table 1: Divalent and trivalent metals found in LDH compounds

Some tetravalent cations such as V^{4+}, Ti^{4+}, Zr^{4+} or Sn^{4+} may also be incorporated in to the HT-like layers [31, 34]. However, some evidences reveal that M^{4+} cations form amorphous oxide particles instead of incorporating into the layers [31]. In a very similar way, monovalent cations, Li^+ or $Li_{1-x}Na_x$, together with Al^{3+}, can form a similar series of LDH compounds, with atomic ratio Al/Li or Al/(Li + Na) fixed at 2 and various counteranions intercalated among the sheets [34]. A more outstanding feature is that multi-metal cations can be incorporated simultaneously into the LDH structure if an x value in the general formula is chosen in a valid range [31]. The value of x is reported to be between 0.2 and 0.33 [34] or 0.4 [31] to obtain a pure LDH phase. If x values are outside this range, hydroxides or other impurities may be formed [31].

The anion located in the interlayer gallery can be anyone as far as it has a sufficient charge density. Up to now, many kinds of anions have been intercalated into the LDH interlayer, including common inorganic anions (Cl^-, F^-, CO_3^{2-}, NO_3^-, etc.), organic anions (carboxylates, dicarboxylates, alkylsulfates, alkanesulfonates, etc.), complex anions ($Fe(CN)_6^{4-}$/$Fe(CN)_6^{3-}$, metal-porphyrin and phthalocyanine complexes), iso- and hetero-polyoxometalates (POMs) ($Mo_7O_{24}^{6-}$, $W_7O_{24}^{6-}$, $V_{10}O_{28}^{6-}$, OsO_4^{2-}, $PMo_{12}O_{40}^{3-}$, $PW_{12}O_{40}^{3-}$, $PW_6Mo_6O_{40}^{3-}$, etc.) [31, 34], polymeric anions (polyvinylsulfonate, polystyrenesulfonate, polyacrylate, polyaniline, ionized polyvinyl alcohol, polyethylene glycol, etc.) and biochemical anions (amino acids, DNA with 500‑1000 base pairs, CMP, AMP, GMP, ATP, ADP, etc.) [34].

LDH materials can be directly synthesized using precipitation at a varying or constant pH. The pH is one of the most important parameters in the precipitation of this kind of materials and a defined interval of pH corresponds to the precipitation of a hydroxide or a LDH.

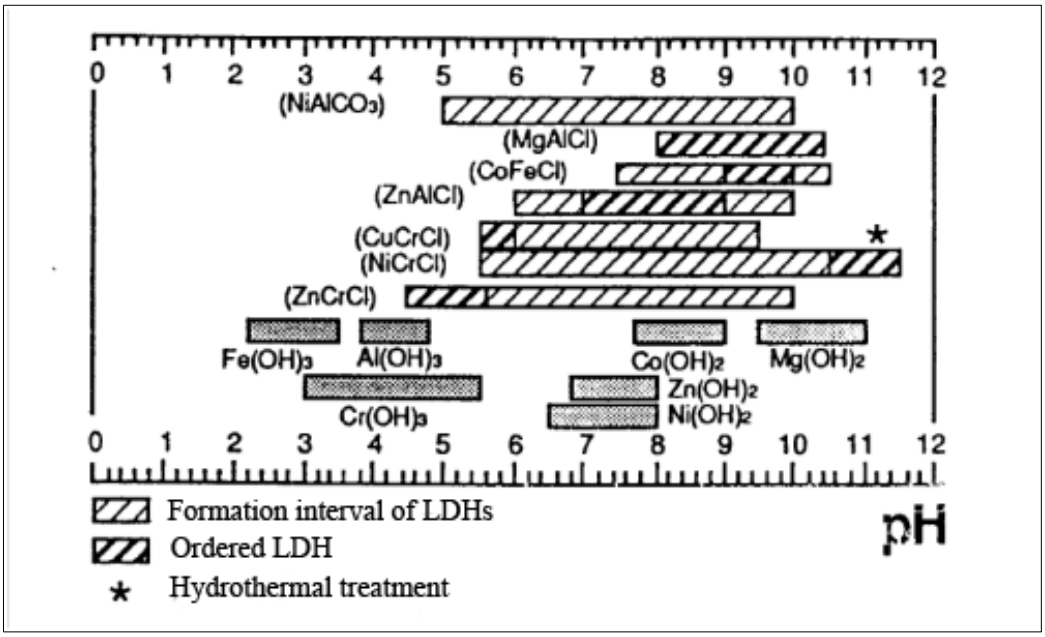

Figure 4: Precipitation intervals of LDH compounds

Layered double hydroxides are highly insoluble materials, at least at the relatively high pH used in their preparation. Thus, in principle, all that appears necessary is to mix together soluble precursor salts, and, if convenient, to replace the initially incorporated anion with the one desired. The reality is much more complicated, as it is so often with seemingly simple inorganic materials. Nonetheless, nearly all the used preparative methods are variants of these reactions of precipitation by base and selective displacement of anions from precursors. For reasons explained later, the exact form of the product, including such important features as particle size and crystallinity and the base strength of the material, is expected to be extremely sensitive to the precise preparative details. Several LDH materials have been prepared while allowing the pH to vary in order to study their formation.

If a titration is carried out from a solution containing divalent and trivalent metals, that has usually an acid pH, some interesting behaviors could be noticed. LDH forms at a pH well below that necessary to form the most soluble hydroxide (as far as the pH of the solution is concerned), a fact that leads to the initial recognition of LDH as a distinct phase. The common pH curve exhibits, in fact, two plateau. The first plateau is associated with the formation of the least soluble metal hydroxide, with the second plateau occurring during LDH formation. This type of titration curve has been observed for almost all materials containing Al as the trivalent metal. $Al(OH)_3$ is formed first at a pH of about 4, with LDH resulting from conversion of this initial precipitate to the final product. The materials formed in this way are initially in the form of aggregates of poor crystallinity, and presumably they arise from the adherence of divalent metal and additional hydroxide ions to the $Al(OH)_3$ precipitate, followed by rearrangement, heteronucleation of the LDH, and dissolution of the initial $Al(OH)_3$ precipitate.

One common refinement of this technique is precipitation at a nominally constant pH [34]. It is the simplest and most commonly used method and it is called co-precipitation method. Aqueous solutions of M^{2+} and M^{3+} cations and of the anion that is to be incorporated into the LDHs are used as precursors. In order to ensure simultaneous precipitation of two or more cations, it is necessary to carry out the synthesis under conditions of supersaturation. There are generally two types of co-precipitation conditions, namely co-precipitation at low supersaturation and co-precipitation at high supersaturation. Co-precipitation at low supersaturation is performed by slow addition of mixed solutions of divalent and trivalent metal salts, at the selected ratio, into a reactor containing an aqueous solution of the desired interlayer anion. A second solution of a base is then added into the reactor, simultaneously, at such a rate as to maintain the desired pH for co-precipitation of the two metal salts. In slight contrast to the former method, co-precipitation at high supersaturation requires the addition of a mixed salt solution to an alkaline solution containing the desired interlayer anion. Co-precipitation at high supersaturation generally gives rise to less crystalline materials compared to those obtained at low supersaturation, due to the formation of a large number of crystallization nuclei. After precipitation at low and high supersaturation, an aging process is

conducted for a period, ranging from a few hours to several days, to increase the yields and crystallinity of the materials [33].

A number of studies have reported the synthesis of LDHs using the urea hydrolysis method. Urea has a few unique properties, such as its weak Bronsted base characteristic and high solubility in water. Furthermore its hydrolysis rate that can be easily controlled, making it an attractive agent to precipitate several metal ions as hydroxides or as insoluble salts a suitable anion is present in the solution. The optimum conditions to prepare LDHs with good crystal quality, in a relatively short time, have been suggested to involve dissolving solid urea in a 0.5M solution of the chosen metal chlorides to give a urea/metal ion molar ratio of 3.3. The compounds prepared using this method display homogeneous sizes and platelet-like primary particles with well-defined hexagonal shapes, which may be very interesting from the viewpoint of nanotechnology since LDHs offer nano-size two-dimensional spaces for the creation of functional materials.

LDHs can be also prepared by the ion exchange method. This method is useful when the co-precipitation method is not applicable, e.g. when the involved divalent or trivalent metal cations or the anions are unstable in the alkaline solution, or when the direct reaction between the metal ions and the guest anions is more favorable. In this method, the guests are exchanged with the anions present in the interlayer regions of the LDHs to produce specific anion-pillared LDHs [33].

Another common method to produce LDHs is rehydration/reconstruction using the structural ‘‘memory effect’’. This method involves calcination of LDHs to remove the interlayer water, interlayer anions, and the hydroxyl groups, resulting in mixed metal oxides. It is interesting to note that the calcined LDHs are able to regenerate the layered structure when they are exposed to water and anions. In addition, the intercalated anions do not need to be the same species originally present in the interlayer of the uncalcined LDHs. Therefore this is an important method to synthesize LDHs with desired inorganic or organic anions to fulfill specific application requirements [33].

Besides the aforementioned methods, other reported synthesis methods of LDHs include the secondary intercalation method (involving dissolution of LDH and the re-co-precipitation method), salt-oxide method, surface synthesis, template synthesis, and so on [33].

Moreover, electrochemical methods have also been developed in the last years for the synthesis of LDH compounds [35]. The electrobase generation is one of them, and it consists in the production of an alkaline pH next to the surface of an electrode immersed in a metal solution, allowing the precipitation of mixed hydroxides on the electrode surface. It is however deeply described afterward.

A LDH can be transformed to the corresponding mixed oxide by a high temperature treatment, which typically involves reaction such as dehydration, dehydroxylation, decomposition of anions and oxide segregation. This process is of great importance in deriving oxide and oxide-supported catalysts [31]. In fact, hydrotalcites allow the formation of highly-dispersed and stable metal particles on the surface after calcination and reduction. It

is known that metal species highly dispersed over supports, are less involved in sintering, so that the rate of carbon deposition is reduced, since large metal particles stimulate carbon formation [29].

3.4 STRUCTURED CATALYSTS

In recent years structured catalysts have been developed for several reactions in order to obtain more efficient processes exploiting some peculiarities of the employed materials such as mechanical resistance or thermal conductivity.

They are essentially defined solid structures such as monoliths, foams or fibers on which the active catalytic phase is deposited. In this way it is possible to avoid some disadvantages of the classic packed-bed catalyst as below outlined. The substrates are usually composed of ceramic or metallic materials. Factors such as cost, weight, thermal resistance, heat management, and so on dictate which material is used in a specific application [36]. Through the application of these new structures, traditional unit operations and reactors can be replaced by new, highly productive and energy-efficient reactors [37].

In this work only gas-phase processes have been considered, so some advantages of structured catalysts employment for these systems will be discussed. The geometry and the physicochemical properties of the supporting material are very important features in the choice of the support. The most important physical characteristics of material, when used as a catalyst support, is the size of the channels or pores through which the gaseous reactants and products traverse. The catalyst coating the structured support is usually composed of a high surface area inorganic oxide carrier, for example Al_2O_3, upon which catalytic centers of metals or metal oxides are dispersed [38].

The structured catalytic system most widely used is the monolithic reactor. Monoliths are also called honeycombs because the first monoliths had a cross-section like a honeycomb structure [38, 39]. Monolith structures are essentially a single structure with many thin, vertical, parallel channels, separated from each other by walls. The channels are usually rectangular, but triangles, hexagons, or more complex geometries also exist. To increase the surface area, internal fins can also be provided. To enhance turbulence inside monolith channels, patented monolith structures have also been developed in which either corrugation has been provided or channels have been interconnected for radial transport [37]. They offer great advantages over pellet catalysts but the most important one being the low-pressure drop associated with the high flow rates [38, 39].

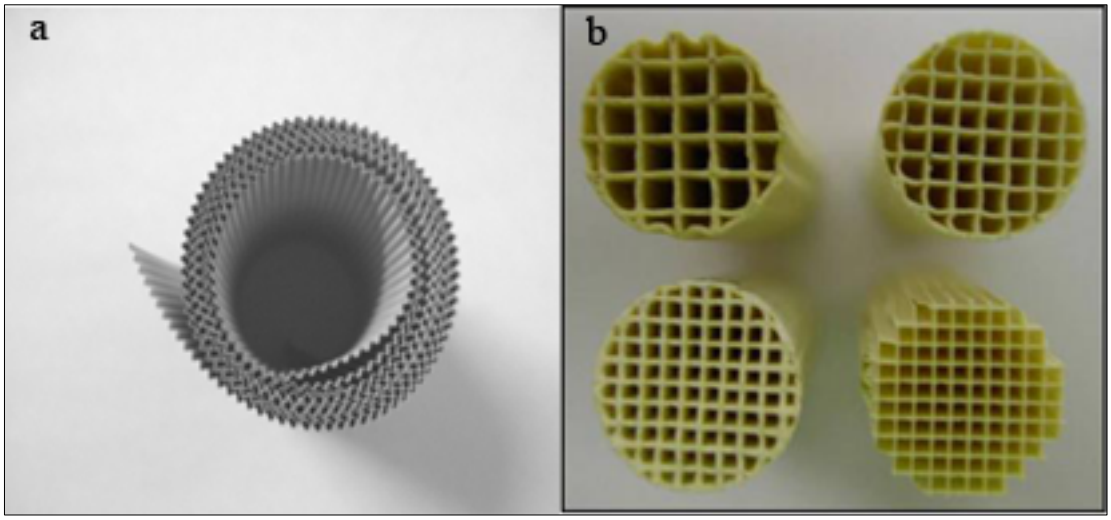

Figure 5: Metallic (a) and ceramic (b) monoliths

Foams are characterized by irregular, open pore structure (~75-85% porosity), which allows improved radial mixing, attrition/crushing resistance, as well as low pressure drop [40]. It is thus possible to produce foams with a very low volume density that enables their material requirements and, consequently, the production costs are greatly reduced [41].

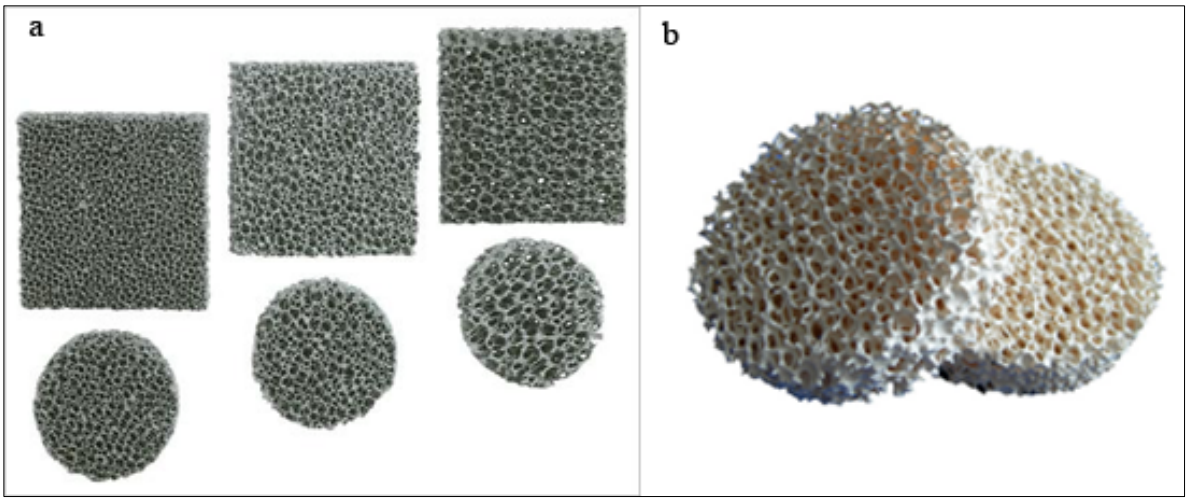

Figure 6: Metallic (a) and ceramic (b) foams

Felts and fibres are not deeply studied yet; the very open nature of these materials result in low pressure drop, while the fibrous structure offers a high surface area for coating active catalyst material. Additionally, the malleable nature of the felt offers a benefit in terms of flexible catalyst design [40].

Extrusion method is actually the main procedure to manufacture ceramic monoliths at an industrial scale. The progressive perfection of this technique has permitted the preparation of monoliths with high cell densities, the optimization of the fluid dynamic properties and the

design with different shapes that lead to an improved behavior of the catalysts with respect to phenomena such as the mass or heat transfer [39]. Amongst the various processing methods for fabricating ceramics foams, the most common one consists of the incorporation of organic phases, that are then eliminated during firing, and of the partial sintering of ceramics. Another approach is the replication of polymer foams by impregnation or CVD coating [42].

Structured ceramic catalysts have been classified as coated and incorporated [39]. "Coated-type" catalysts are based on an inert ceramic substrate of low-surface area, which is coated with a thin film of porous material allowing the dispersion of the corresponding active phases. The "incorporated" catalysts are instead characterized by having their active phases distributed, not only on the exterior walls of the monolith but also within them [39].

An important difference between ceramic and metallic structures is the thermal conductance of metallic support which is much larger [43]. Thus is a very important feature as heat diffusion plays a key role in the development of the process of interests. An additional advantage of the metal substrates is the easy way to produce different and complicated forms adapted to a wide variety of problems and uses.

Metallic monoliths are conventionally made from rolled layers of corrugated (usually sinusoidal or triangular) and flat sheets [44]. The metallic foams have been mainly produced by the nucleation and subsequent growth of gas bubbles in a liquid or semi-liquid metal, which leads to a non-uniform pore structure in size and orientation. Moreover, some imperfections such as corrugated or broken walls may occur during the cooling process. Another method is based on the employment of templates that could be removed after the casting or the deposition of the metal. With this method the porous structure could be adjusted according to the template and no pore obstruction occurs [45].

The metallic foam combines a high heat conductivity, porosity and geometric surface area that make the overall heat transfer coefficients of foam-based catalysts be up to two orders of magnitude greater than conventional catalysts. With respect to more-common ceramic reticulated materials, the use of metal foams is expected to minimize the occurrence of hot spots in the catalyst when highly exotermic reactions are performed, while avoiding mechanical strength and thermal shock limitations due to their physicochemical characteristics [46, 47]. The high thermal conductivity makes them interesting candidates also for endothermic and exothermic reactions because they allow a better heat diffusion [47].

The choice of a metal alloy to be used as metallic catalytic substrate depends on the properties related to the use of the catalyst (mechanical, thermal and chemical resistance under operation conditions) and on the properties related to the catalytic coating adhesion, and to the fabrication process. High temperature oxidation resistant alloys were developed in the 1960s, based on Fe, Cr, Al and Y. The formation of a self-healing protective "skin" of alumina allows the ultra-thin steel to withstand the high temperatures and corrosive conditions in auto exhaust and other environmental uses. These materials have also a particularly high thermal shock resistance and high melting and softening points respect to others, and facilitate the development of high cell densities with very low-pressure losses. In addition to the main

components of these ferritic steels, chromium (17–22%) and aluminum (5–8%), other reactive elements (Y or others) are present in small quantities because they are fundamental to improve the oxidation resistance of the alloy and to aid oxide adhesion.

3.5 COATING METHODS

Several methods for the coating of the previously described structured supports have been developed, and some of them are outlined below.

As far as metallic structures are concerned, in some cases a pretreatment of the metallic surface could allow a better adhesion of the catalytic layer. One of these is the anodic oxidation method that is generally applied to structures containing aluminum with the aim to obtain a porous alumina layer on the surface. It consists in the application of a direct current (or a direct voltage) to an electrolyte in contact with an aluminum surface. There is a competitive formation of an oxide layer and dissolution of the substrate, generating a porous layer. The method is either used as a pretreatment before another coating method or as a way to obtain a thin porous layer than can be directly impregnated with the active phase [48]. Like anodic oxidation, thermal oxidation is another method for a surface modification. It can be used either as a pretreatment step to increase the catalyst adhesion or as a catalyst support preparation. It is often applied to FeCrAl substrates where during segregation at high temperature, aluminum oxides are preferably formed on the upper part of the substrate in the range of 1 µm thickness. Finally, a chemical oxidation of the substrate is sometimes carried out. The substrate is immersed in HCl solution to increase the surface roughness and then in HNO_3 to favor the formation of an Al_2O_3 layer [48]. However, the exact procedures vary with the type of structure and the specific application [38, 39].

With respect to the coating techniques, wash-coating is probably the most widely used for coating catalyst supporting structures. In these procedures, the involved structures are dipped into suitable slurries, kept in the particle dispersion for a certain period of time and finally withdrawn. Once the metallic monolith is withdrawn, the excess slurry must be drained. To form a thin oxide layer on the metal surface the metallic structure has to be dried and calcined to suitable temperatures [49].

Pulsed laser deposition is another technique employed for the film growth. A short ultraviolet laser pulse of high light intensity is used to vaporize material from a target and to deposit thin layers in a vacuum chamber. Depending on the broad spectrum of wavelengths as well as on the pulse energy, this process can be used to deposit a large variety of different compounds [48].

In chemical vapor deposition one or more molecular precursors of the desired species are vaporized by heating the solid and then they react or decompose on the surface of the substrate to produce the desired film.

High-surface area ceramic coatings can be prepared via sol-gel methods from liquid organic or inorganic precursor materials. Impregnation of the structure can be done directly with a sol and upon drying and calcination, a well-adhered coating layer can be formed in situ upon the support walls [48, 51].

As far as conductive supports such as metallic structures are concerned several electrochemical methods could be employed to cover the structure surface with metal, hydroxides or oxides in addition to the previously described methods.

Electrophoretic deposition is a colloidal process wherein a direct current electric field is applied across a stable suspension of charged particles attracting them to an oppositely charged electrode. The cathode consists of the substrate to coat. The thickness of the coating depends on the working conditions [48].

Among these methods, electrochemical syntheses are achieved when a reaction occurs passing an electric current between two electrodes in an electrolyte solution and the synthesis reaction takes place at the electrode-electrolyte interface [35].

Electrochemical deposition uses ionic solutions and produces a coating, usually metallic, on a surface by the action of electric current. The deposition of a metallic coating onto a conductive support may be\ achieved by the reduction, on the negative charged support, of the positively charged metallic ions to their metallic form [48].

In anodic oxidation a metal ion, in a lower oxidation state, is oxidized to a higher oxidation state at the anode while hydrogen is produced at the cathode. The pH of the electrolyte is chosen in such a way that the lower oxidation state is stable while the higher oxidation state readily undergoes hydrolysis to yield the metal oxide or hydroxide. The anodic oxidation technique is especially suited for the synthesis of compounds with metal ions in unusual high oxidation states. An example is the stabilization of Fe(IV), Co(IV), Ni(IV), or Cu(III) which can be achieved only partially in complex ternary oxide systems by conventional ceramic techniques [35].

On the contrary, electrobase generation method exploits several reduction reactions to increase the pH next to the working electrode surface, allowing the precipitation of single and multiple hydroxides. It has been employed in this work for the covering of FeCrAlY foams with a LDH layer that constitute the catalytic precursor. For this reason, a deeper explanation of the method and its advantages is given.

3.5.1 ELECTROBASE GENERATION METHOD

There are several techniques for the electrochemical synthesis of hydroxides or LDHs and some of them have been listed previously. As outlined before, LDHs can be prepared by the electrobase generation method. In this process when a current or a potential is applied to the electrochemical cell several reactions, that involve the electrolyte ions and water, occurs and

lead to a raise of pH occurs. They obviously change in respect with the choice of the electrolyte. In the case of nitrates the main reactions should be:

$H^+ + e^- \rightarrow H_{ads}$ or H_{abs} (3.5.1)

$2H^+ + 2e^- \rightarrow H_2$ E°= 0.000 V (3.5.2)

$NO_3^- + 2H^+ + 2e^- \rightarrow NO_2^- + H_2O$ E°= 0.934 V (3.5.3)

$NO_3^- + 10H^+ + 8e^- \rightarrow NH_4^+ + 3H_2O$ E°= 0.360 V (3.5.4)

$2H_2O + 2e^- \rightarrow H_2 + 2OH^-$ E°= -0.828 V (3.5.5)

$NO_3^- + H_2O + 2e^- \rightarrow NO_2^- + 2OH^-$ E°= 0.010 V (3.5.6)

$NO_3^- + 7H_2O + 8e^- \rightarrow NH_4^+ + 10OH^-$ E°= -0.120 V (3.5.7)

These reactions are effectively competitive in respect to the metal ion reduction reaction:

$M^{n+} + ne^- \rightarrow M^0$

From a thermodynamic point of view, the reactions with a more positive E° would be preferred if a negative current or potential is applied to the electrochemical system. In the case of nitrates, usually metal deposition does not take place. On the contrary, metal ions precipitate in the form of hydroxide or LDH if a multi-metal system is involved [35].

The reactions involved in this process could be divided into three classes: reactions that consume H^+ (3.5.1, 3.5.2, 3.5.3, 3.5.4), water electrolysis (3.5.5), and anion reduction reactions (3.5.6, 3.5.7). The relative importance of the three classes in the base electrogeneration is not known.

Most of the investigations on the mechanism assume the overwhelming role of nitrate [35]. However, a study [52] on the electrosynthesis of $Mg(OH)_2$ as a model reaction have shown that the yield of magnesium hydroxide is much higher from a Mg-chloride than from a Mg-nitrate bath, under all deposition conditions. Since the chloride ion does not participate in any anion reduction reactions, reactions 3.5.1, 3.5.2 and 3.5.5 are the only ones responsible for electrogeneration of base in a chloride bath. It appears that these reactions are important as nitrate reduction in the electrosynthesis of hydroxides. Extending this technique, nickel hydroxide has been electrosynthesized from chloride and sulfate baths [53] with comparable yields as from a nitrate bath. Other experiments where Cu^{2+}, Tl^+, Bi^{3+}, and Pb^{2+} hydroxides where synthesized in a perchlorate bath showed that *E*° value is not the only crucial parameter

for the success of this class of electrosynthetic reactions, but other unknown kinetic factors also play a crucial role [54].

For easily reducible metals, such as Rh^{3+}, the reduction to metal may become competitive In acid solution, the formal potential of Rh reduction is 0.76 V, but it decreases when increasing pH, according to the relative Pourbaix's diagram. A control and, if necessary, an adjustment of the initial pH of the solution is therefore needed in order to avoid the metal precipitation [20].

In an actual synthesis, one or more of these synthetic parameters have to be empirically selected by performing a large number of trials, keeping in view the product quality [35].

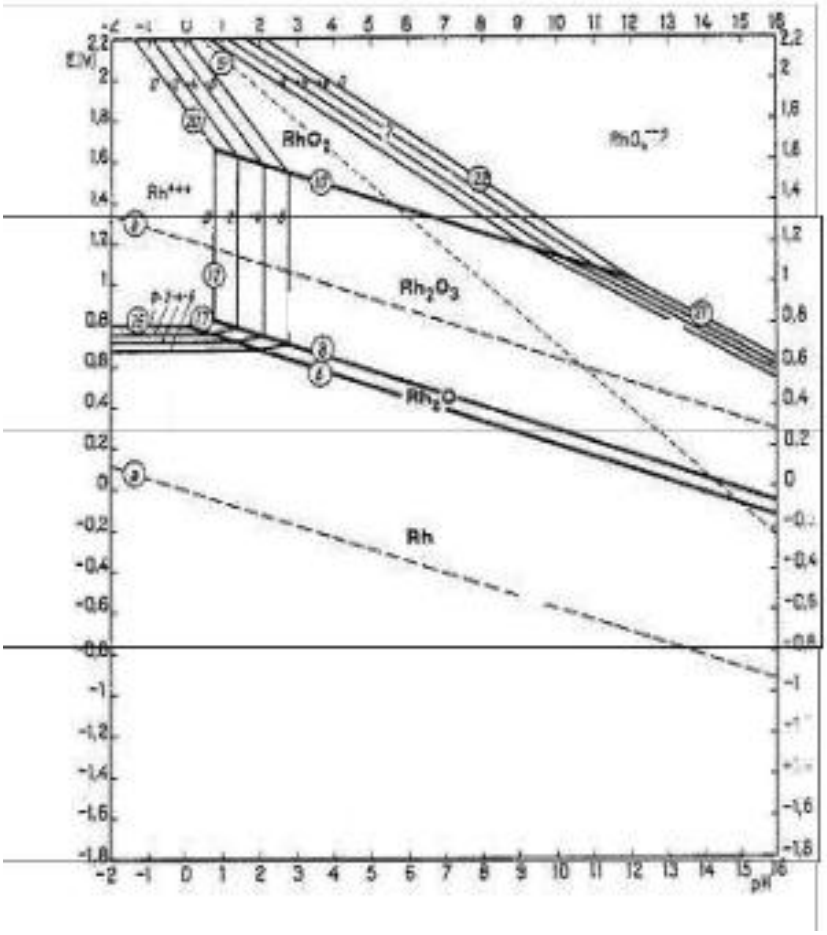

Figure 7: Pourbaix's diagram for rhodium

The electrochemical synthesis can be divided in galvanostatic and potentiostatic synthesis. In a galvanostatic experiment a delicate control can be performed over the rate of the reaction leading to deposits with good adhesion and a controlled morphology. However, the cell potential drifts as the reactant activity decreases and this may lead to a multiplicity of products. On the other hand, a potentiostatic synthesis is carried out with a three-electrode cell by polarizing the electrode to a desired potential with respect to a reference electrode. In this case the cell current usually decays rapidly as the reaction proceeds, both due to low rates of diffusion of the reactant molecules from the bulk to the electrode surface as well as due to

decrease in activity of the reactant. However, the reaction is likely to yield a pure single-phase product depending on the applied potential [35]. In this work the potentiostatic route has been applied in order to achieve electrobase generation at the surface of the working electrode.

. There are several features that make this technique interesting in respect to others. It takes place really close to the electrode and the product deposited is in the form of a thin film or a coating [35]. The thickness of the film can be modified from about 100 nm to a few microns, just changing the deposition time [55]. Further, a solid-liquid interface facilitates the growth of homogeneous coatings on substrates of any shape, especially if a suitably shaped counter electrode is employed to provide uniform polarization. It is a low-temperature technique, the kinetic control can be exercised by controlling the current passed through the cell, while thermodynamic control can be exercised by choosing the applied potential. In an electrochemical synthesis the main reaction must be an oxidation or a reduction reaction. By fine-tuning the applied cell potential, the oxidizing or reducing power can be continuously varied and suitably selected, that is not a so simple feature to obtain in a chemical synthesis. The film composition can be controlled by varying the bath composition, the experiments are simple to perform, and the instruments are inexpensive and readily available [35]. Moreover, it does not need expensive equipment and it is cost-effective.

There are, however, some disadvantages. Being an ambient temperature technique, electrosynthesis often leads to poorly ordered products, making unequivocal structural characterization difficult. Often, the product comes with X-ray amorphous impurities. Further electrodeposition can only be carried out on conducting substrates [35].

Therefore, the success of an electrosynthetic reaction depends on several parameters such as the choice of electrodes and electrolytes, the type of cell to be employed, the temperature, the pH, the concentration, and the composition of the working solution and the electrochemical technique employed [35].

In the last years, this method has been already applied to electrodes modification in order to increase the electrocatalytic activity for methanol oxidation [56] and to develop amperometric enzymatic [57, 58] sensors.

4. EXPERIMENTAL

All the solutions have been prepared with distilled water, and the pH adjustment is achieved (when requested) by adding a few HNO_3 1 M drops to the stirred solution. The pH is monitored with a 338 pH-meter (Amel).

The electrochemical measurements have been performed using an AUTOLAB PGSTAT128N (Metrohm) and different electrochemical cells as will be outlined later. The explanation of the set ups is described in chapter 5. A Pt gauze (Sigma Aldrich) and a saturated calomel electrode (Amel) have been used as counter electrode (CE) reference electrode (RE), respectively.

All the metallic foams have been cut from sheet (thickness = 1.2 cm) with a brass cylinder of the desired diameter. The pores per inch (ppi) and the diameter of the foams have been varied for reasons later discussed in chapter 5. The contact with the potentiostat is always achieved by sticking a Pt wire (Sigma Aldrich) in the center of the foam cylinder.

4.1 pH MEASUREMENTS

The measurement of the overpotential in a nitrate solution between the metallic foam (diameter 0.8 or 1.0 cm, 80 ppi or 60 ppi) and the Pt plate has been carried out in a classical three electrode electrochemical cell. A 0.3 M KNO_3 (Sigma Aldrich) solution has been employed as both supporting electrolyte and nitrates source. The two working electrodes (WE) have been cleaned before the measurement. The Pt plate (Sigma Aldrich) is sonicated for 10 min in a HNO_3 (Carlo Erba) 0.1 M solution, while the FeCrAlY foam is immersed for 10 min in acetone (Aldrich). The cyclic voltammetry has been performed from 0 to -1.3 V at a 0.05 V/s scan rate.

A rough estimation of the evolution of the pH near to the electrode surface when a cathodic potential was applied (from -0.9 V to -1.3 V) in a nitrates solution was obtained by adding a few drops of acid-base indicators to a KNO_3 0.3 M solution. The employed indicators and the relative toning intervals are shown in Table 2.

Indicator	Toning interval
Cresol Red	6.8/7.9
Fenolftalein	8.2
Timolftalein	9.8
Alizarin	11

Table 2: Acid-base indicators and toning pH

A foam with a diameter of 0.8 cm and a 80 ppi has been employed as WE after a 10 min immersion in acetone. The chronoamperometry is not carried out for 2000 s, but it has been stopped if the color change of the indicator is detected before.

The measure of the pH with the glass electrode (Metrohm) has been achieved using a pX1000 module (Metrohm) of the Autolab. In order to register the value nearby the surface of the WE, a Pt gauze (Sigma Aldrich) has been rolled around the membrane of a glass electrode connected to the pX1000 module. In this way the pH of the small amount of liquid in close contact with the electrode is measured. The pX1000 module with the relative glass electrode has been calibrated before every measurement with a pH 2.00 and a pH 9.21 buffer solutions (Hamilton). The pH generated in the closeness of the working electrode immersed in pure water, 0.3 M KNO_3, 0.3 M NH_4NO_3 and in the solutions containing the nitrates of the metals (0.03 M) used for the synthesis have been measured. A screening of potentials ranging from -0.5 V to -1.3 V has been made. For comparison purposes, titrations with NaOH 0.1 M (Aldrich) have been carried out for each working solution.

The electrosynthesis of single hydroxides and LDH compounds have been carried out on Pt plates. All the syntheses have been carried out using an aqueous solution containing the salts of the metals to be deposited (0.03 M) and KNO_3 (0.3 M) as supporting electrolyte. The electrosynthesis of the Ni^{2+}, Mg^{2+} and Al^{3+} single hydroxides, and NiAl and MgAl LDHs in 2:1 and 3:1 molar ratios have been performed. The initial pH of the plating solution was adjusted to 3.8, when necessary, to optimize the efficiency of the base generation. The electrochemical syntheses have been performed by chronoamperometry applying a cathodic potential in the -0.5 V and -1.3 V range for 1000 s.

4.2 CATALYSTS PREPARATION

The catalysts preparation consists in different phases and could be outlined as indicated in the following scheme:

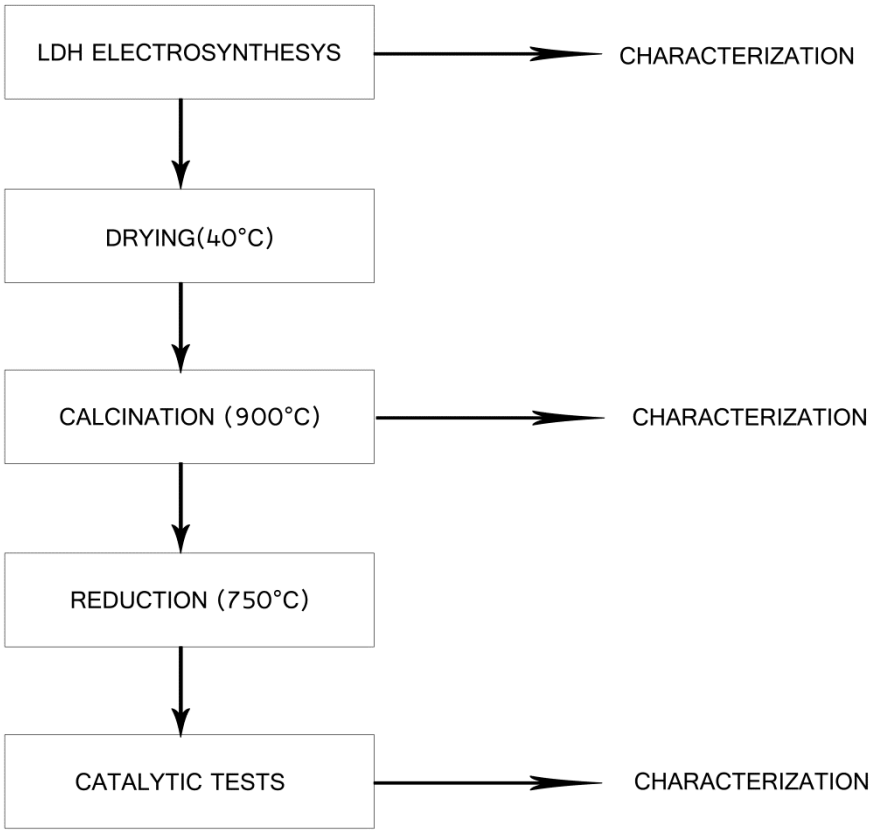

Figure 8: Schematic representation of the synthesis of the catalyst

As said before in this work the main interest is given to the first step, but also some useful informations from subsequent characterization are discussed.

In the first step the synthesis is conducted by electrogeneration of base method, and the drying process in a oven at 40°C is needed to eliminate the water and to slightly enhance the adhesion of the LDH to the support. A first characterization is performed in order to check the quality of the HT-like phase deposited. Then during the calcination process at high temperature the mixed hydroxides have been turned into mixed oxide. Another characterization step is performed to check the transformation process and to study the differences in the surface coatings caused by the chemical transformation and the thermal stress. The reduction step is needed in order to reduce the Rh^{3+} present in the mixed oxides structure into well dispersed metallic Rh that constitutes the real catalytic active phase. Another characterization session has been performed in order to check the presence of Rh^{0}. Finally catalytic tests have been performed in order to check the activity of catalysts in CPO and SR reactions. The last characterization session is performed to control possible

modifications on the catalyst structure due to the operative conditions and the formation of carbon on the catalyst surface.

Catalysts has been synthesized by cronoamperometry technique at room temperature and this mean that a constant potential (in the -0.9/-1.3 V range) has been applied to the foam for a defined time (in the 1000-3000 s range). The electrochemical cell geometry has been varied during the work, and further informations and explanations are given in chapter 5.

The working solution contains nitrates of the desired metals, with a variable atomic ratio and a total concentration of 0.03 M. The composition of the different solution ands the relative molar ratios have been reported in Table 3.

Elements	Molar ratio
Mg:Al	3:1
Rh:Mg:Al	11:70:19
Rh:Mg:Al	5:70:25
Rh:Mg:Al	2:70:28
Rh:Ni:Mg:Al	5:15:55:25

Table 3: Electrolytic solution composition and molar ratios

When the supporting electrolyte was 0.3 M KNO_3, only a few measurements have been carried out without the adjustment of the pH of the initial solution. Normally the pH has been adjusted to 3.8 with concentrated KOH (Sigma Aldrich). All the potentials have been measured with respect to a SCE. The working electrode is the FeCrAlY foam (80 or 60 ppi) with a diameter of 0.8 cm or 1 cm. The contact with the potentiostat has been obtained by sticking one or three Pt wires, dependly on the experiment, into the foam.

After electrodeposition, the foams have been gently rinsed with distilled water and then dried at 40°C in oven. The catalysts were obtained by calcination at 900 °C for 12 h of coated foam pellets in a muffle.

Catalytic partial oxidation of methane tests have been carried out in a quartz reactor (inner diameter 8mm or 10 mm) operating at atmospheric pressure. Two cylinders of the foams (8mm×10mm or 10mm×10mm) have been loaded in the isothermal zone of the reactor. The foams fit well with the diameter of the reactor to minimize any by-pass. Catalysts have been reduced in situ before the tests in an equimolar H_2/N_2 mixture (7.0 L/h) for 2 h at 750 °C. Catalytic tests were performed keeping the temperature of the oven constant at 750 °C and allowing the temperature of the catalyst to vary depending on the endothermicity/exothermicity of the process. The effect of the concentration of the gas mixture was studied, $CH_4/O_2/He$ = 2/1/20 and 2/1/4 (v/v), while keeping constant the gas-hourly-space-velocity (GHSV) values, 28,000 h^{-1} for the 8mm×10mm foams and 17500 h^{-1} for the 10mm×10mm foams. No large pressure drop was observed during the tests. The gas phase temperature at the inlet of the catalytic bed was measured by a moveable chromel–

alumel thermocouple sliding in a quartz wire inside the catalytic bed. The reaction products were analysed online after water condensation by a PerkinElmer Autosystem XL gas chromatograph, equipped with two thermal conductivity detectors (TCD) and two Carbosphere columns using He as the carrier gas for the analysis of CH_4, O_2, CO and CO_2 and N_2 for the H_2 analysis.

Steam reforming tests were performed in an Incolloy 800 HT reactor (inner diameter 10 mm), placed inside an electric oven. 6 foam cylinders (10mm×10mm) were loaded in the isothermal zone of the reactor whilst the bottom and top section of the tube were filled with beads of corundum. A thermocouple wire was inserted along the axial direction of the reactor, into which a chromel-aluminum thermocouple could be slid to measure the temperature at the inlet of the reactor. Catalytic tests were performed at T_{oven} = 920 ºC, P = 10 bar, steam-to-carbon ratio S/C = 2.5 and τ = 3 s The feed was provided by a cylinder for the gas and a HPLC pump for water. Water was vaporized using a heater at 280°C and then mixed with the gas before entering the reactor. Catalysts were activated by in situ reduction at 750°C for 2 h with a H_2/N_2 equimolar flow. Wet syngas passed through a water condenser to separate the major amount of non-reacted water. Dry syngas was then analyzed on line by using two gas-chromatographs equipped with TCD: a Thermo Focus GC and a Perkin Elmer CLARUS 500, equipped with Carbosieve S-II 100-120 mesh-packed columns. The Focus GC analyzed the H_2 and used N_2 as carrier gas. The CLARUS was used to measure the other products (CO, CO2, and CH4) and the carrier gas was He.

4.3 SAMPLES CHARACTERIZATION

Most of the samples synthesized on Pt plates and on FeCrAlY foams have been morphologically analyzed by scanning electron microscope (SEM) and an indication of composition has been obtained by EDS analysis. This technique can give in fact just an indication and not a precise quantification of the elements present in the sample, particularly as far as foams are concerned mainly because of their complex and not planar structure. SEM and EDS characterization has been performed by using an EVO 50 Series Instrument (LEO ZEISS) equipped with both an INCAEnergy 350 EDS micro-analysis system and an INCASmartMap for imaging the spatial variation of elements (Oxford Instruments Analytical). The accelerating voltage was 25 kV, the beam current 1.5 nA, and the spectra collection time 100 s.

X-ray diffraction patterns have been collected mainly for the sample synthesized on Pt plates in order to check the real presence of a hydrotalcite phase. Not always was possible to collect a good XRD pattern because of the small amount of sample deposited on the plate. As far as metallic foam samples are concerned the diffraction patterns were not collected because this kind of measurement requires a planar surface to be analyzed. X-ray diffraction (XRD) patterns were collected with Cu K_radiation (λ = 1.5418 Å) by means of a X'PertPro

PANalytical diffractometer diffractometer equipped with a fast X'Celerator detector. The 3–80° 2θ range was measured performing steps of 0.07° (2θ) and counting 120 s/step. The analyses were performed on a powder that was gently removed from a FeCrAlloy plate. A "zero background" sample holder (The Gem Dugout, State College, PA, USA) was used.

To understand the best reducing conditions Temperature Programmed Reduction (TPR) measurements have been carried out on calcind foams. TPR analyses were carried out with a H_2/Ar (5/95 v/v) gas mixture (total flow rate 1.2 L/h) in the 100–950 °C temperature range by using ThermoQuest CE Instruments TPDRO 1100.

For a few sample also μ-XRF/XRD tomographic measurements have been performed with synchrotron radiation thanks to the collaboration with dr. Wout de Nolf and dr. Gert Nuyts of the University of Antwerp at ANKA (Karlsruhe, Germany), SLS (Villigen, Switzerland) and ESRF (Grenoble, France) synchrotrons.

The experiments at ANKA synchrotron were conducted using a μ-XRF/μ-XRPD tomography setup at the FLUO beamline. A W/B4C double multilayer monochromator produces at "pink" beam of 25keV. A polymer CRL focuses the beam down to a $8\times5\mu m^2$ spot size. Diffraction patterns are collected with a 2k×2k CCD camera (Quad-RO 4320, Princeton Instruments). Fluorescence spectra were recorded with a Si(Li) detector.

The experiments at SLS synchrotron were performed at the micro-XAS beamline. A 18 KeV beam was foused on the sample by means of a Kirkpatrick–Baez mirror system, achieving a spot size of 1.5 × 3 μ m (h × v). A Pilatus 100K camera was used to record the diffraction pattern. Two KETEK SDD's (Silicon Drift Detectors) with Helium flux collected the fluorescence data.

In both beamtimes a strut from the foam was translated (Y) and rotated (ω) in the microfocussed X-ray beam. The energy dispersive detector collects fluorescence spectra for each translation and rotation step, while the area detector registers diffraction patterns. Diffraction data were processed using XRDUA software [59]. Fluorescence spectra were processed by means of PyMCA software. From the XRF spectra it is possible to extract a signal proportional to the amount of each chemical element present in the material, as a function of Y and ω. The result is called a sinogram and can be transformed into an element distribution map (XY). This map visualizes the elements in a virtual cross-section of the foam strut. From the diffraction patterns, an analog result can be obtained for crystalline phases.

5. RESULTS AND DISCUSSION

5.1 MEASUREMENT COMPARISON AND OVERPOTENTIALS

Different working electrodes (Pt plates and gauzes, FeCrAlY foams) have been used in the measurements later discussed. Therefore, a direct comparison among these measurements is not possible because of the different reactivity and conductivity of the two electrode materials. In particular, both the different nature and shape of the working electrode modifies the synthesis conditions required to precipitate the LDH phase.

At first the right overpotential for the two supports has been evaluated by cyclic voltammetry in a KNO_3 0.3 M solution. The current vs potential recorded on both supports is shown in Figure 9. The main increase of the cathodic current is related to the nitrates reduction discharge. A small peak is also observed in the curve referred to the foam and it is ascribable to the reduction of Cr^{3+} (-0.74 V) contained in the alloy. If feet of the cathodic waves are considered, the difference between the two values (about -0.9 V for the metallic foam and -0.7 V for the Pt plate) is about 0.2 V. Therefore the foam should have behavior a quite similar to that obtained with Pt by applying a more cathodic potential. This was confirmed by comparing the pH measured near the foam surface with that at Pt electrode, after applying a negative potential in a KNO_3 solution and adjusting the initial pH to 3.8. However those results will be discussed in the following.

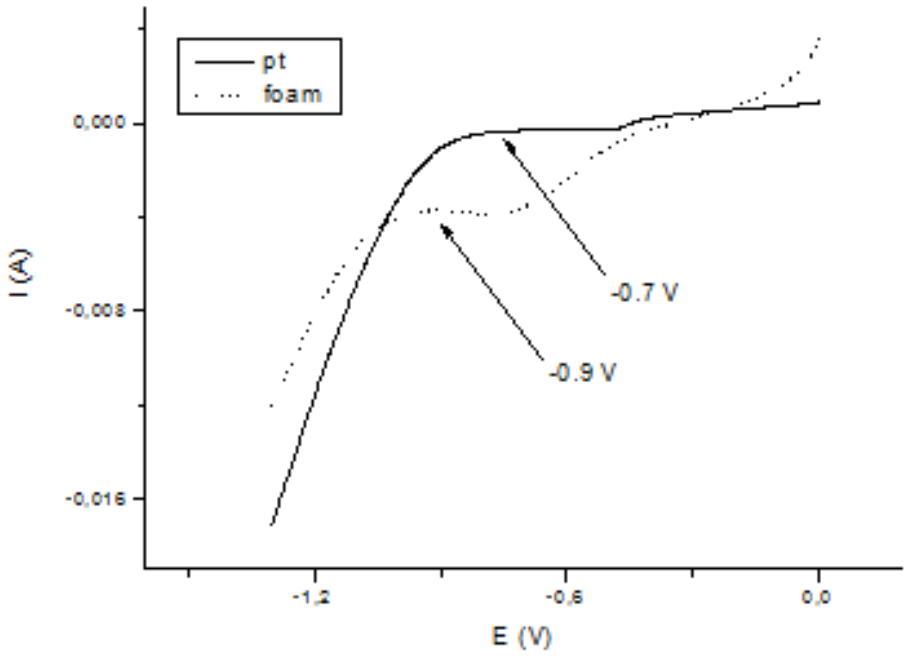

Figure 9: Nitrates reduction potential on a Pt plate (solid line) or on a FeCrAlY foam (dotted line)

5.2 CELL DESIGN, PREFERENTIAL DEPOSITION AND DIFFUSION

As previously said different electrochemical cells have been used in this work.

At first a classical electrochemical cell was used. It consists of a Pt plate or a FeCrAlY foam as working electrode, a Pt gauze as counter and a SCE as reference electrodes geometrically disposed as outlined in Figure 10.

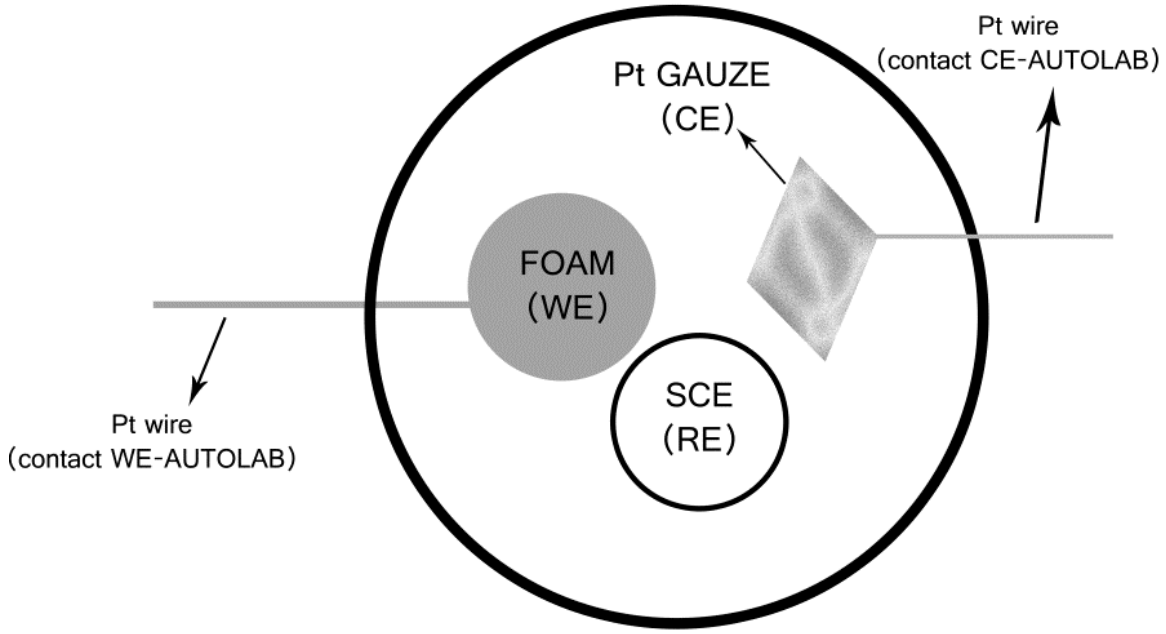

Figure 10: Schematic representation of a classical three-electrode cell

As far as the CE is in front of a side of the metallic foam a preferential deposition occurs: an important difference in the amount of the material between the 'front' side and the 'back' side of the foam has been noticed. In particular the covering on the 'back' part is very poor with a difference that could be noticed without a microanalysis system. This is obviously a really undesired side-problem since the uniformity of the covering is one of the aims that has to be achieved. This problem is linked to the different distance of the two sides of the WE from the RE and the CE which causes a different ohmic drop. In particular, the back side of the WE suffers from and enhanced ohmic drop and, therefore, the charge exchange is more hindered than at the 'front' side.

In order to obtain a better performance with the whole foam surface, allowing a more uniform deposition, a modification on the CE was done. A larger Pt gauze was fixed to the whole internal wall of the cell, creating a sort of cylindrical counter electrode with the reference and the working electrodes more or less at the centre of the Pt gauze, as shown in Figure 11.

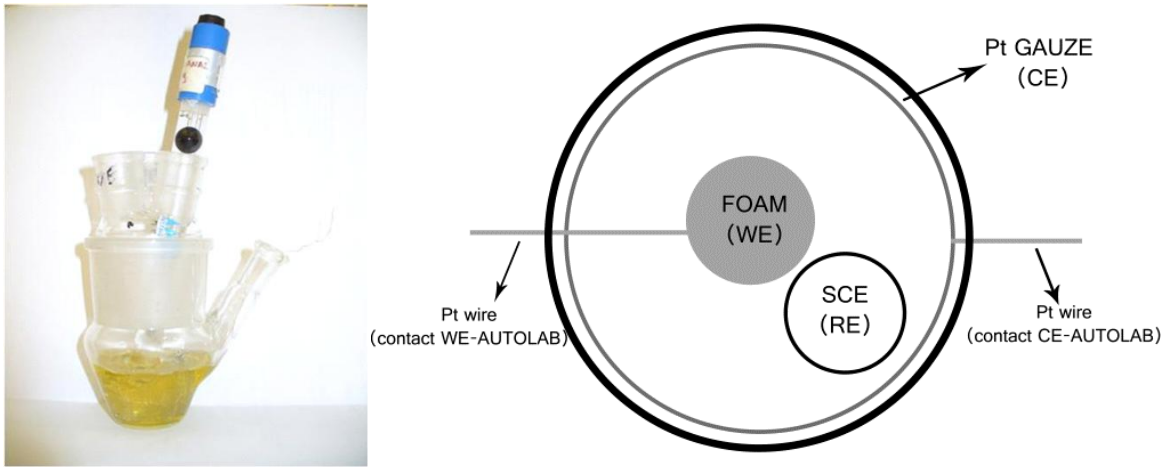

Figure 11: Round-CE electrochemical cell

With this modified three electrode electrochemical cell the preferential deposition of the solid on one side of the foam was avoided and a more uniform covering of the outer surface was obtained. Almost all the tests discussed below have been performed with this kind of electrochemical cell.

5.3 THE pH MEASUREMENTS

5.3.1 EVALUATION OF pH BY ACID-BASE INDICATORS

At first, a rough estimation of the evolution of the pH near to the electrode surface when a cathodic potential was applied in a nitrates solution was obtained by adding a few drops of acid-base indicators to the (acidified) KNO_3 0.3 M solution. The characteristic of indicators to change color in a defined pH interval was exploited to detect OH^- production.

As an example, figure 12 shows the measurement carried out using fenolftalein and timolftalein.

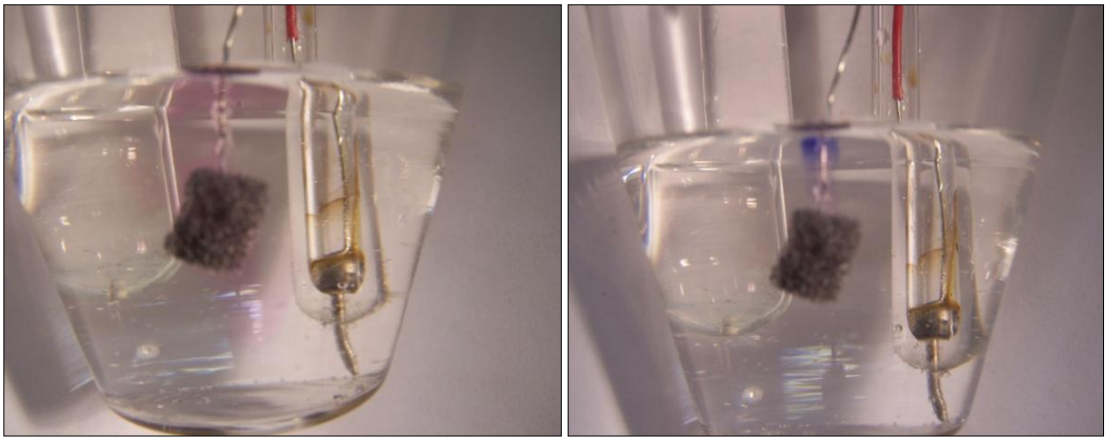

Figure 12: Monitoring of the evolution pH at the foam surface with fenolftalein (right) and timolftalein (left)

However, this estimation is not really accurate and it allows to determine a quite large pH interval. Moreover, the change of color was detected visually; therefore OH^- diffusion layer had to become enough large to be observed. For these reasons a strong influence of the acidic bulk solution was expected with the consequent underestimation of the pH generated at the electrode surface. The used indicators and they toning interval have been reported in Table 2 in the 'Experimental' section. In Table 4 the pH interval observed during the application of different potentials have been reported.

E (V)	Pt WIRE	FOAM
-0.9	8.2 < pH < 9.8	6.5 < pH < 7.5
-1.0	8.2 < pH < 9.8	7.5 < pH < 8.2
-1.2	9.8 < pH < 11	8.2 < pH < 9.8
-1.3	9.8 < pH < 11	9.8 < pH < 11

Table 4: Difference of pH reached at Pt and foam surface after the application of different potentials

As already said this kind of measurement is not really accurate; anyway it confirms some previously described results. In fact, it is possible to notice that to reach the same interval of pH a -0.2 V overpotential has to be applied to the foam with respect to the Pt wire, as expected from the discussion in Paragraph 5.1. An interval 8.2 < pH < 9.8 is in fact obtained with an applied potential of -1.0 V if a Pt wire is employed as WE, while it is necessary an applied potential of -1.2 V if the WE is a FeCrAlY foam.

5.3.2 MONITORING OF pH EVOLUTION WITH A GLASS ELECTRODE

5.3.2.1 CHOICE OF THE SUPPORTING ELECTROLYTE

The electrochemical route for the synthesis of hydroxides by base electrogeneration mainly proceeds by the nitrate reduction; KNO_3 is usually used both as supporting electrolyte and nitrate source; however, the deposition of K^+ cations together with the expected hydroxides may take place simultaneously [55]. Other species may be used as supporting electrolyte, such as NH_4NO_3; however some modifications may occur in the electrochemical reactions, so altering the pH values and, consequently, the precipitation process. Therefore, the effect of the replacement of KNO_3 by NH_4NO_3 on the pH generation in the electrode-electrolyte interface was firstly studied. To this aim different cathodic potentials were applied (from -0.7 V to -1.1 V) to a Pt wire immersed in a KNO_3 or NH_4NO_3 0.3 M solution. The evolution of the pH and the current during the application of constant potential values is reported in Figure 13.

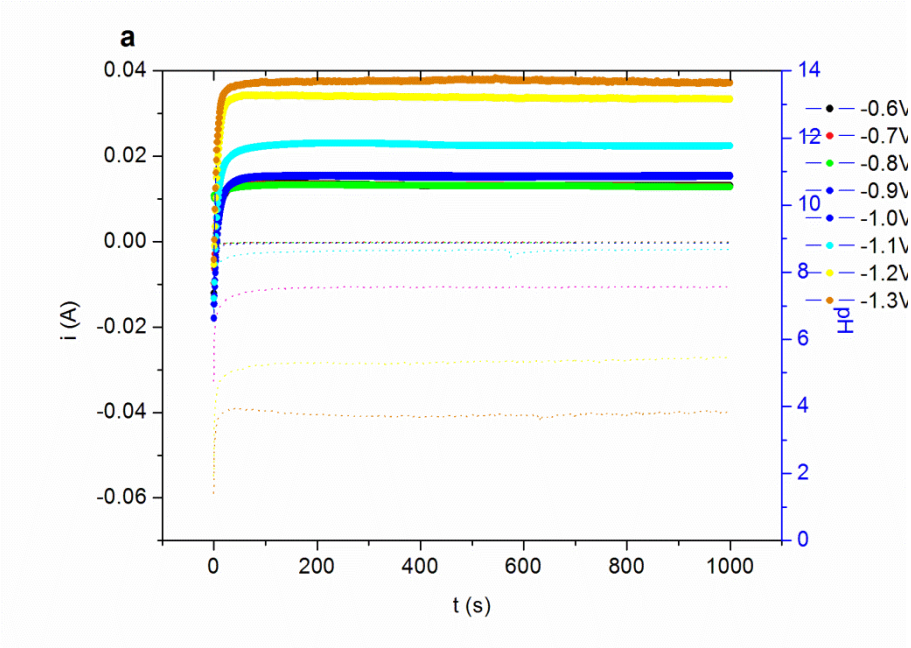

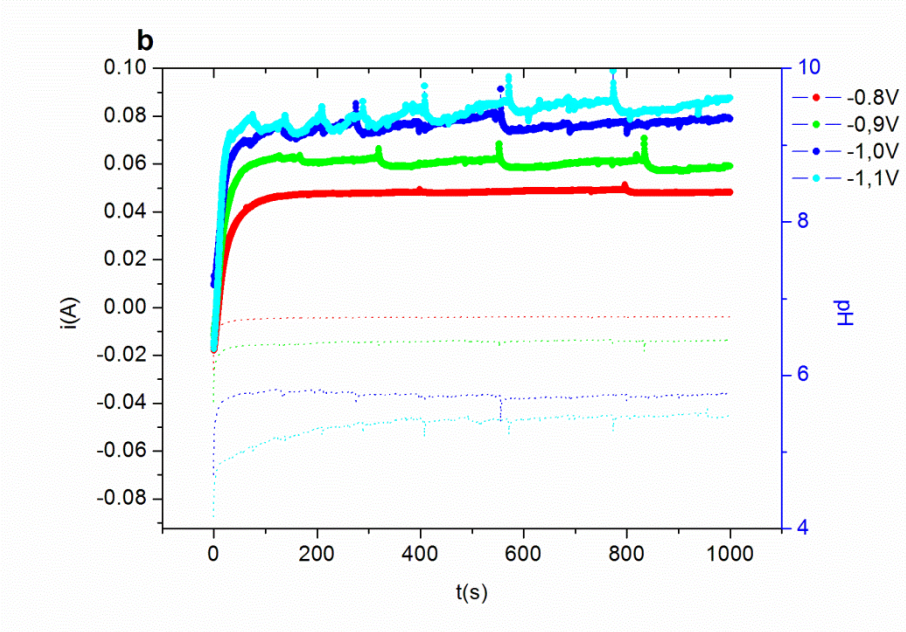

Figure 13: Evolution of pH vs time for KNO_3 (a) and NH_4NO_3 (b) at different applied potentials

The curves are characterized by a fast increase of the pH at the beginning of the measurements (ca. 30-60 s) after which a plateau is reached. Regardless of the supporting electrolyte, the more cathodic is the applied potential the steeper is the pH increase and the higher the pH plateau reached. This is due to the highest speed the nitrate reduction as confirmed by the current increase with the applied potential. However, it is worth noting that at a selected potential value some differences are observed depending on the electrolyte both in the time required to reach the plateau and in the pH value. For instance, at low potentials (E $\leq$ -1.0 V) about 60 s are required to reach the steady-state for KNO_3 while about 90 s for NH_4NO_3. Moreover, at the same applied potential, higher pHs are obtained if KNO_3 is the supporting electrolyte. Finally, it should be remarked that the use of NH_4NO_3 leads to a destabilization of the signal, which increases as the applied potential becomes more cathodic. This behavior is due to a massive H_2 bubble evolution at the WE surface caused by the reduction of hydrogen and water. Both reactions lead to an increase of the pH in the closeness of the WE [60, 61].

The lower pH increase obtained with NH_4NO_3 is likely caused by to the neutralization of part of the OH^- generated at the WE surface, because of the weak acidity of NH_4^+. Moreover, NH_4^+ is also a product of the nitrate reduction and thus its presence may shift the equilibrium of the reaction. For all these reasons KNO_3 was chosen as the supporting electrolyte for the subsequent electrodeposition tests.

The measurements above described were carried out at the pH of the bulk solution (5.5-6) containing KNO_3. Since the addition of metals leads to an increase of the acidity, to better simulate the actual synthesis conditions, the initial pH of the bulk solution was corrected to 3.8 in the following measurements. This value have been previously chosen to perform the electrosynthesis of Rh/Mg/Al compounds [20]; it was considered as the highest value suitable

for the electrosynthesis that did not allow the precipitation of any considered element and avoided the rhodium reduction. The adjustment of the initial pH with HNO_3 (Figure 14) results in a lower slope in the first part of the curves pH vs time, especially at less cathodic potential values, whereas in only slight differences of the steady state pH reached after the application of every potential are observed.

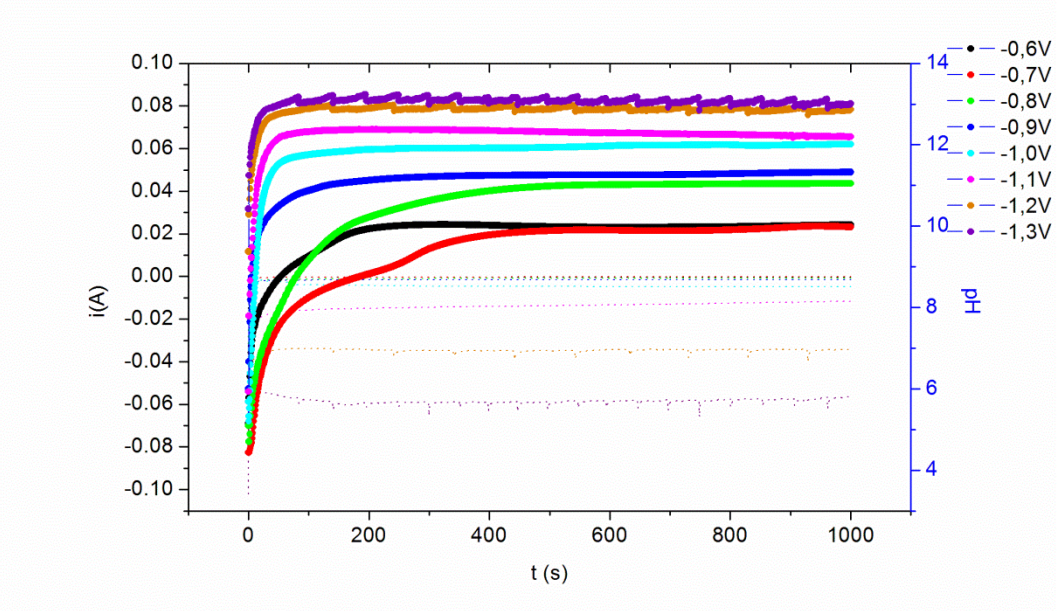

Figure 14: Evolution of pH vs time for KNO_3 after pH adjustment at different applied potentials

The currents measured become a little more cathodic than the ones in the previous tests carried out at higher initial pH; however it is worth noting that the trend followed by the current is exactly the same. More accurate comparisons among recorded current values are not possible in this work because some differences could be due to a not costant surface area of the Pt gauze employed as WE. This fact is acribable to the mounting procedure repeated for every measurement the loss of some wires from the gauze sometimes occurred. However a strict correlation between the evolution of current and pH is always observed.

In this case the oscillations ascribed to the hydrogen bubble can be also observed in the current signal. These results may be related to the more acidic starting conditions that slow down the increase of pH. Moreover, the higher H^+ concentration in the bulk solution may also explain the large bubbles production and signal oscillations at the most cathodic potentials such as -1.2 V and -1.3 V.

The monitoring of pH evolution in a solution of KNO_3 0.3 M, after the adjustment of pH to 3.8 at the surface of a metallic foam, was also carried out. This measurement has been achieved by digging a hole in the center of the foam itself in order to insert the sensible bulb of the glass electrode inside the foam. The connection between the potentiostat and the foam was obtained in the same way as in the experiments carried out with the Pt wire. Also in this case the pH increases when a higher potential is applied to the working electrode. From the

comparison with the data obtained in the same conditions when a Pt gauze is employed as WE, it was possible to observe that similar pH values was reached when a 0.2 V overpotential is applied to the metallic foam (Figure 15), in agreement with results previously discussed. In fact, when a potential of -1.3 V or -1.0 V was applied to the foam the pH values were very similar to those obtained with a Pt gauze at -1,1 V and -0,8 V, respectively. The small deviation of this trend obtained when a potential of -1.2 V was applied to the metallic foam, could be explained by the slightly different closeness of the glass electrode to the foam during the measurement.

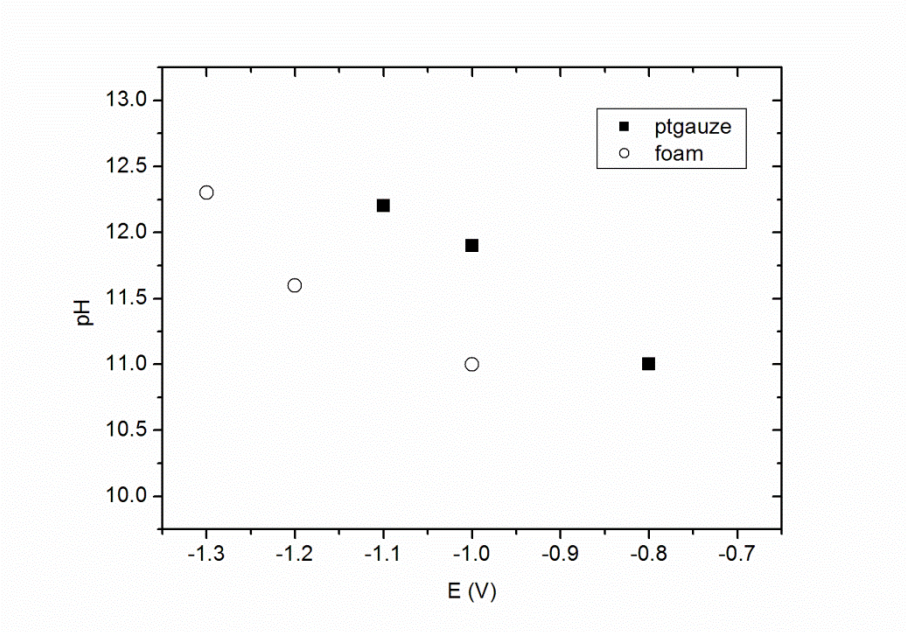

Figure 15: Comparison between pH plateau value for Pt and foam at different applied potentials

5.3.2.2 HYDROXIDES

It should be remembered that one of the main goals of the present research work is to define the optimal working potential for the electrosynthesis of a selected compound and to verify how the pH established at the electrode surface affects the properties of the deposited solids. However, in the measurements first described the pH increases due to the nitrate, H^+ or H_2O reduction and the pH value in the vicinity of the electrode depends only on the potential applied since no OH^- consumption occurs. On the contrary, during the electrosynthesis the precipitation of the cations as hydroxides makes the OH^- concentration decrease. The ratio between the rates OH^- formation and consumption determines the pH within the electrode/electrolyte interface; the former is related to the accessibility of the electrode to the nitrates as the electrosynthesis proceeds, whereas the latter depends on the cation concentration in the vicinity of the electrode, which is due to the bulk concentration and diffusion of cations towards the electrode. Therefore, to optimize the applied potential,

measurements of the interfacial pH in the presence of the precipitating cations were carried out. To this aim the electrosynthesis of three single hydroxides ($Al(OH)_3$, $Ni(OH)_2$, and $Mg(OH)_2$) were studied, first of all.

For every test a 0.03 M solution of the metal has been prepared in 0.3 M KNO_3 and its pH has been adjusted to 3.8. To determine the pH interval where the considered compounds precipitate, a titration with 0.1 M NaOH has been carried out for each nitrate solution.

5.3.2.2.1 Al(OH)3

From the titration curve it is possible to notice a single plateau as expected during the deposition of a single hydroxide. In agreement with the data reported in the literature [62] it takes place at a pH about 4 (Figure 16a).

In Figure 16a the symbols added to the titration curve correspond to the pH values near to the precipitation interval reached at the surface of the WE after the application of the corresponding potential to give an immediate correlation between the two experiments. The global evolution of pH vs time during the electrosynthesis of $Al(OH)_3$ at different cathodic potentials is displayed in Figure 16b.

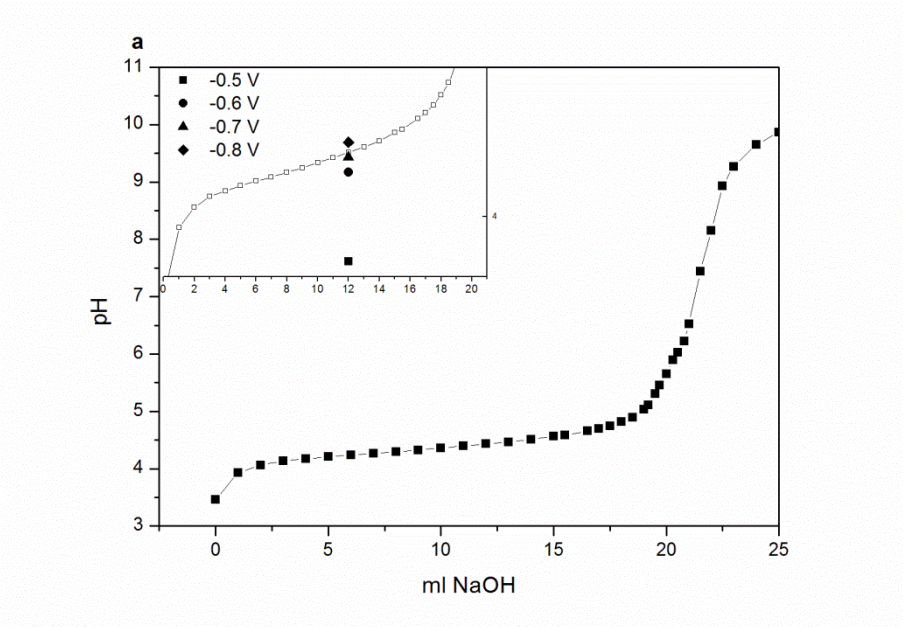

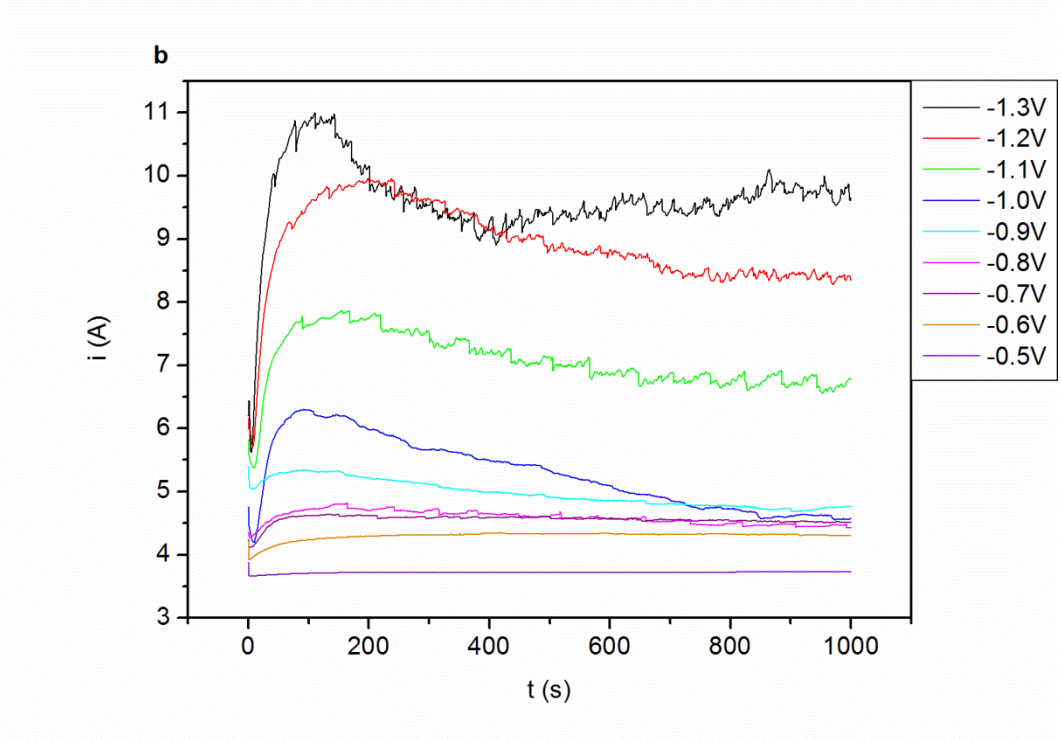

Figure 16: Titration (a) and pH evolution vs time at different applied potentials (b) for $Al(OH)_3$

As shown in Figure 16, by applying a potential in the range between -0.6 and -0.8 V the shape of the curves is similar to those previously reported during the monitoring of the pH when only the supporting electrolyte is present in solution. They present an increase of pH at the beginning of the measurement due to the OH^- production at the electrode surface until the plateau is reached. Comparing between the data obtained by titration (Figure 16a) and those related to the screening of applied potentials it is possible to observe that if a -0.5 V potential is applied to the WE almost no variation of the pH occurs. Therefore, pH (about 3.9) does not reach the value necessary for the precipitation of aluminum as hydroxide. The interval between -0.6 and -0.8 V instead corresponds to pH values in the proper range for the precipitation of $Al(OH)_3$; it would appear that the rate of OH^- production equals the rate of OH^- consumption. At a potential value of -0.9 V instead a remarkable increase of pH is observed during the first 100-200 s of the synthesis and a subsequent decrease is noticed during the remaining time of the measurement. This trend is amplified with the increase of the applied potential and it could be explainable as follows. The nitrate reductions takes place in a larger extent as the applied overpotential is higher that leads to the alkalinization of the solution near the electrode. In the meantime $Al(OH)_3$ start precipitating and, therefore, ions are promptly consumed. At higher cathodic potentials a slight decrease is observed. The plateau is not really reached probably because the OH^- production becomes less efficient. This is due to the poor conductivity of the $Al(OH)_3$ layer deposited on the electrode surface which also hinders the accessibility of NO_3^- ions. Moreover the recorded signal is more disturbed, probably due to the larger H_2 production at the WE, influencing the performance of the glass electrode. The current observed in every measurement has the typical evolution expected in

cronoaperometry with plateau values becoming more negative when the applied potential is more cathodic (Figure 17). The current signal is a bit disturbed for a potential of -1.3 V analogously to what observed during pH monitoring.

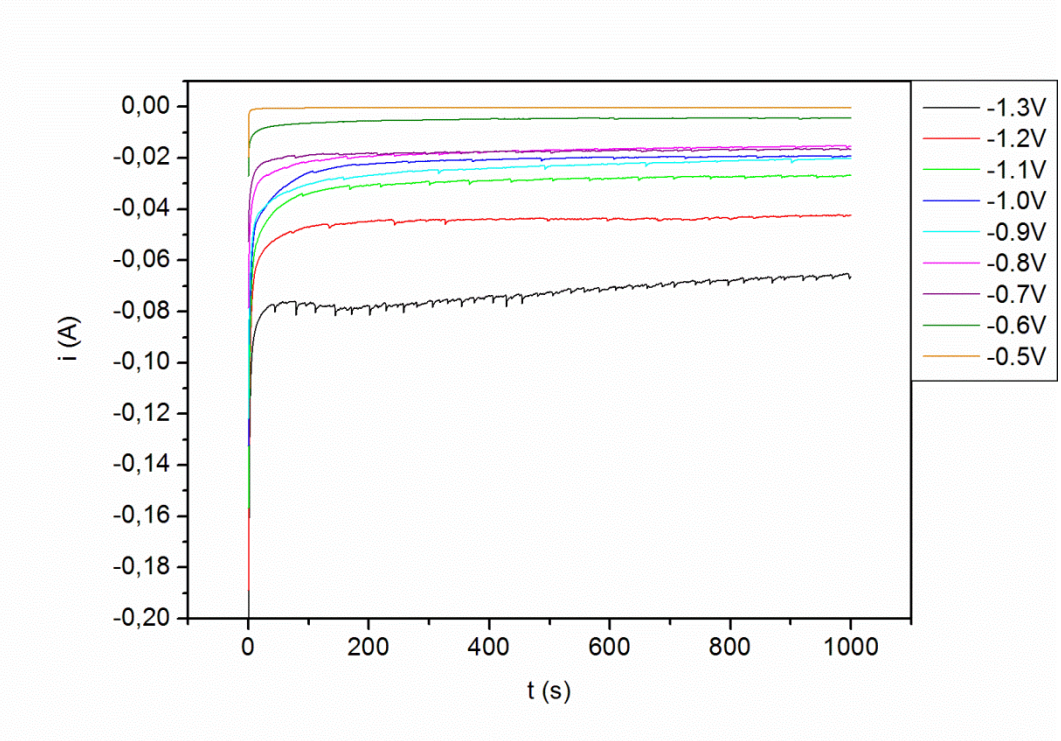

Figure 17: Current observed at different applied potentials during the synthesis of $Al(OH)_3$

5.3.2.2.2 $Ni(OH)_2$

From the titration with NaOH the precipitation interval for nickel hydroxide was observed to be comprised in the interval 7.5-8.5, as shown in Figure 18.

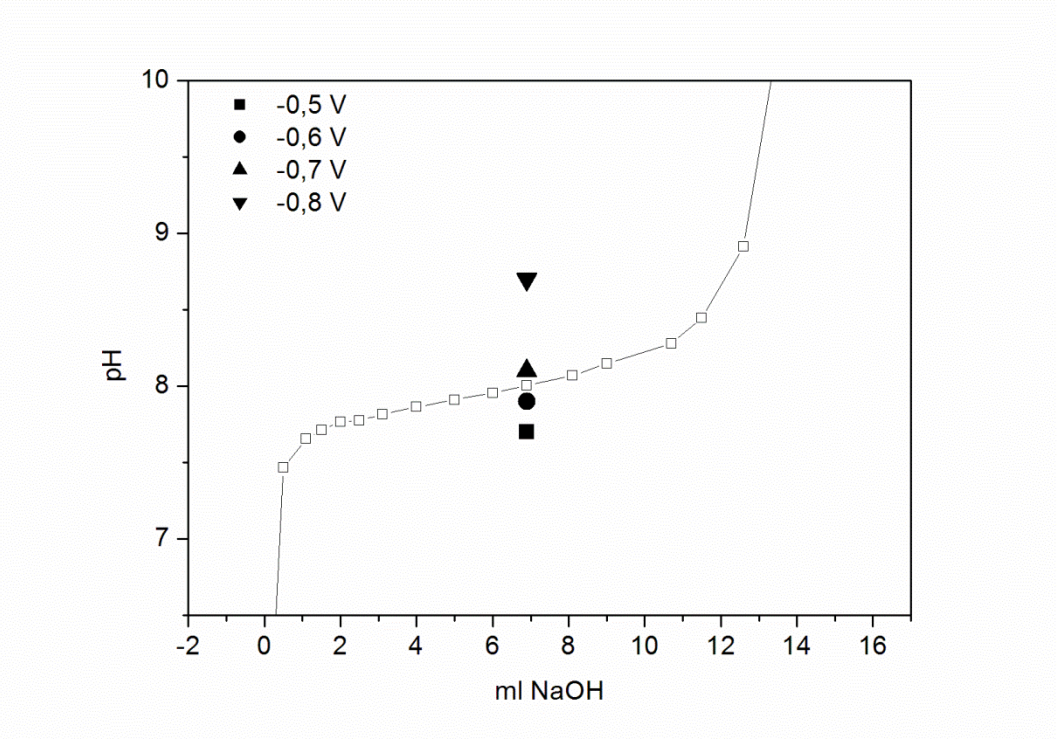

Figure 18: Titration of $Ni(OH)_2$ and pH plateau values obtained at different applied potentials

A different trend is observed in the screening of the applied potentials during the precipitation of $Ni(OH)_2$ in respect to that observed for $Al(OH)_3$, and the curves relative to evolution of pH vs time are reported in Figure 18. It could be noticed that the shape of all the curves is the same for every applied potential: an increase in the pH takes place at the beginning of the measurement and then the plateau is reached. The pH in the electrode/electrolyte layer steadily increases with the application of a more cathodic potential range (-0.5/-0.8 V). For example a -0.7 V cathodic pulse is required to reach a pH value of 8, which is included in the precipitation interval indentified by the titration, and at -0.8 V a slightly larger value (8.7) is achieved. However, the best working potentials seem to be -0.6 V and -0.7 V because they lead to a pH value that fits perfectly the interval determined by titration (Figure 18).

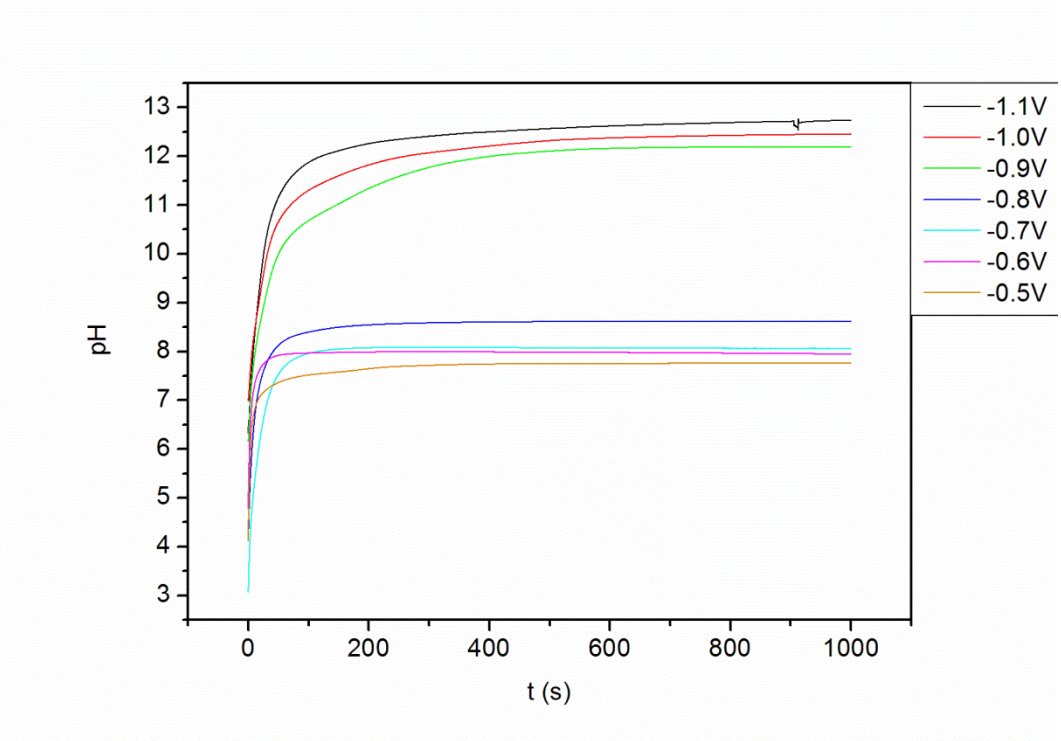

Figure 19: pH evolution vs time at different applied potentials during the synthesis of $Ni(OH)_2$

For E ≥ -0.9 V there is a very strong increase of the pH, after stabilization. Probably in this case the rate of OH^- formation exceeds its consumption and a strong increase in the interfacial pH occurs. pH stabilizes at around 12 with a slight increment during the increasing of E applied. The difference between the two kinetics of OH^- formation could be observed also comparing the time employed to reach the pH plateau. It is about 400 s at -0.9 V, 350 s at -1.0 V and 320 s at -1.1 V; that indicates that the 'steady state' could be reached more easily and the precipitation of the hydroxide has a lower influence.

Registered currents become more cathodic when the applied potential is increased, as expected, but there is not a significant difference between those recoded for E ≥ -0.9 V and those observed when -0.5 ≤ E ≤ -0.8 V as noticed instead for the evolution curves of the pH. However a lower decrease is observed when the applied potential lies in the interval -0.9 < V < -1.1 V.

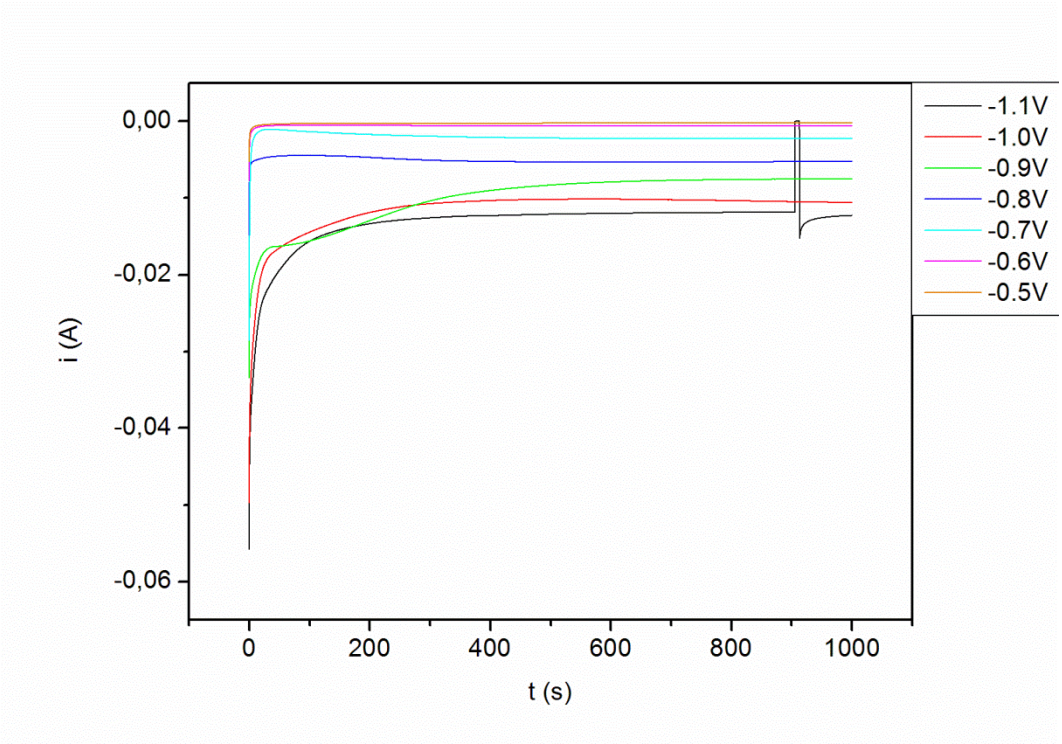

Figure 20: Current observed at different applied potentials during the synthesis of $Ni(OH)_2$

5.3.2.2.3 $Mg(OH)_2$

Also in the case $Mg(OH)_2$ the interval of precipitation was determined by titration, and it resulted to be comprised in the range 10.3-11 (Figure 21).

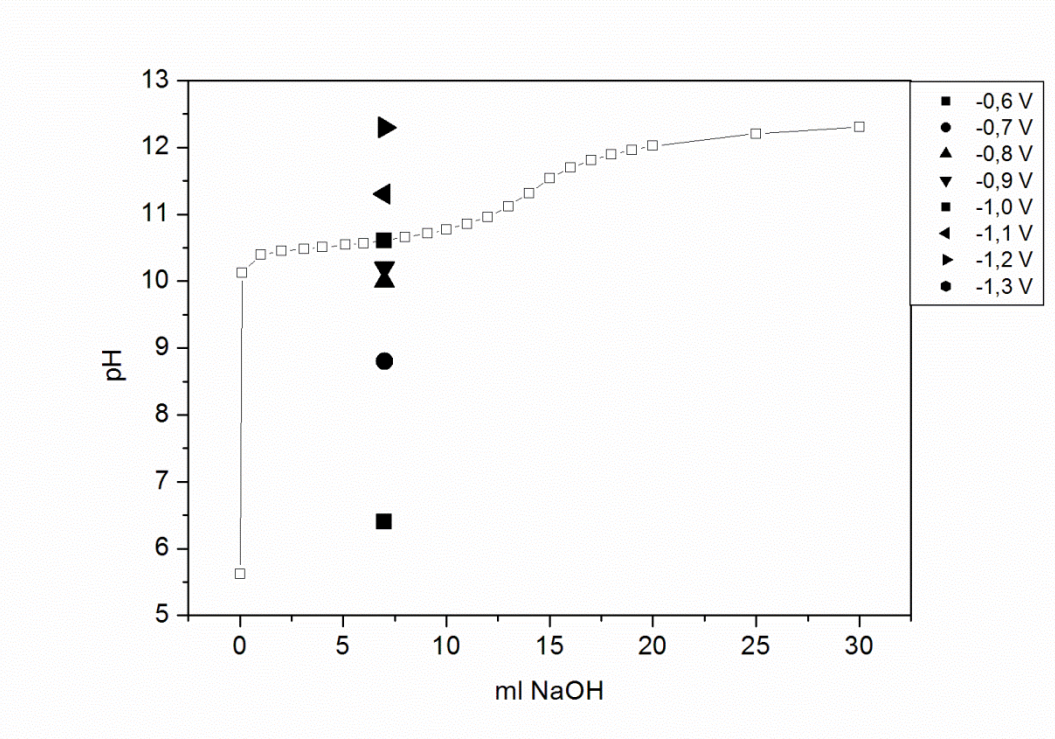

Figure 21: Titration of $Mg(OH)_2$ and pH plateau values obtained at different applied potentials

It can be noticed from the pH evolution curves reported in Figure 22, $Mg(OH)_2$ shows a trend similar to the one outlined for $Ni(OH)_2$. When a potential lower than -0.7 V is applied to the working electrode, the pH increases with the potential but it does not reach a value high enough to allow the precipitation of $Mg(OH)_2$. If the cathodic potential is higher and inside the range -0.8/-1.1 V, the pH values in the plateau lie in the interval of magnesium hydroxide precipitation as determined by titration. Moreover, a perfect overlapping with the titration curve is obtained with an applied potential of -1.0 V for which a pH=10.6is reached. Therefore, the potential can be considered the best for magnesium hydroxide synthesis reaching a pH of 10.6 (Figure 21). For potentials of -1.2 V and -1.3 V the pH stabilizes around 12.5, i.e. out of the precipitation range of the hydroxide. The H_2 evolution is observed mainly at potentials above -1.1 V and the curves become more dirty as in the previous described experiments.

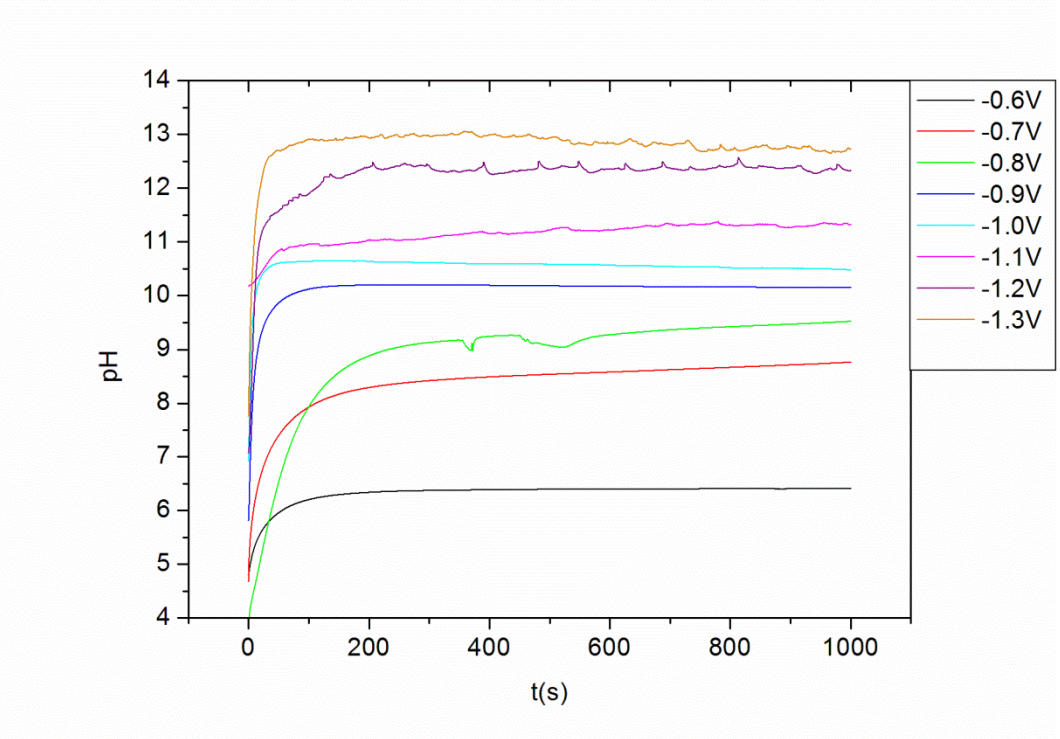

Figure 22: pH evolution vs time at different applied potentials during the synthesis of $Mg(OH)_2$

As far as the recorded currents (Figure 23) are concerned, a good correlation between the increase of potential and then increasing intensity was observed, confirming high OH^- production or H^+ consumption from the reduction reactions listed in chapter 3.5.1.. Also in this case the signal starts to oscillate at high applied pontentials due to bubbles evolution in a way similar to the pH evolution curves.

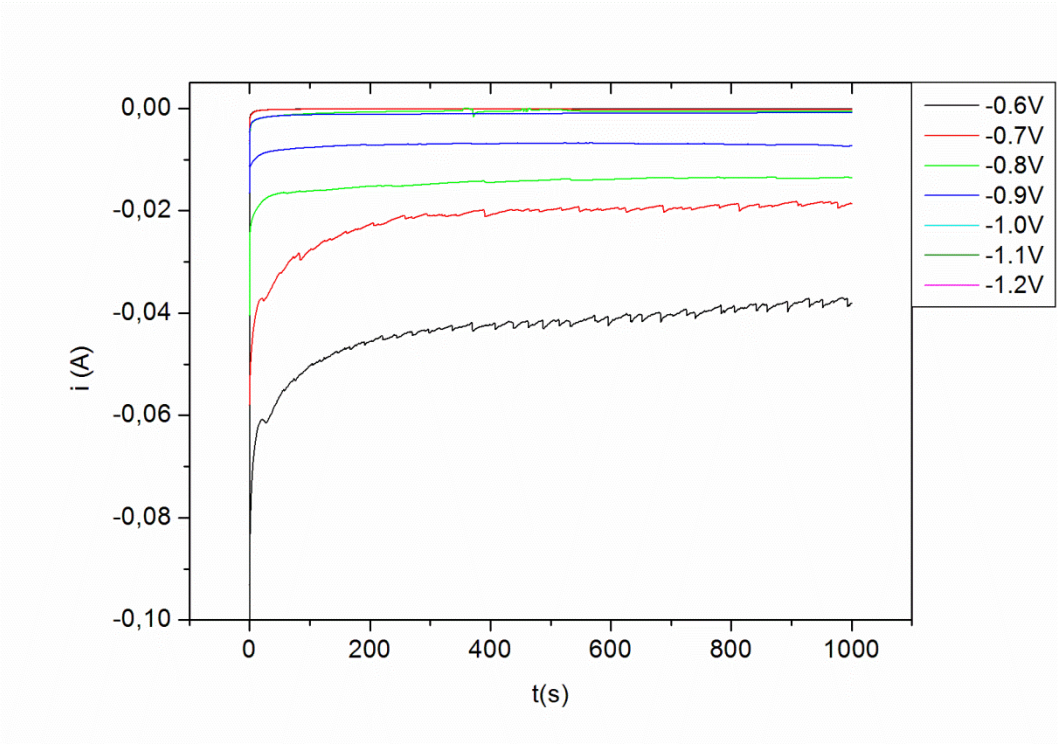

Figure 23: Current observed at different applied potentials during the synthesis of $Mg(OH)_2$

5.3.2.3 LAYERED DOUBLE HYDROXIDES

The same procedure was applied for the study of LDH compounds. NiAl-LDH and MgAl-LDH were studied with M^{2+}:M^{3+} in the molar ratios 2:1 and 3:1. As far as hydrotalcite-like compounds are concerned, the titrations with NaOH showed the presence of two plateaus indicating a sequential precipitation as already reported in literature [62]; the first plateau, at about pH 4, corresponds to the precipitation of $Al(OH)_3$, according to the experiments previously conducted (5.3.1), whereas the one at higher pH is due to the precipitation of the LDH (5.3.2).

$$M^{3+} + 3OH^- \leftrightharpoons M(OH)_3 \qquad [62] \qquad (5.3.1)$$

$$M(OH)_3 + xM^{2+} + (x+1)OH^- + NO_3^- \rightarrow M(III)[M(II)]_x(OH)_{(x+4)}NO_3 \qquad [62] \qquad (5.3.2)$$

The data about the registered currents have not been reported because they do not provide more information than the one obtainable from the comparison between the pH evolution and the titration curves. However in every experiment the trend of the recorded currents was the same showed by pH evolution curves, i.e. more intense currents were obtained when a higher pH was reached as expected.

The study of pH evolution during single hydroxides synthesis shows that the applied potential affects significantly the pH reached at the electrode surface. Therefore, great

differences in the nature and morphology of the deposited LDH compounds should be expected in respect to the synthesis conditions. A complete characterization of the materials was carried out in order to highlight the differences. The morphology and chemical composition of the films were characterized by SEM/EDS, whereas by XRD the presence of crystalline phases was demonstrated after their synthesis on Pt plates.

5.3.2.3.1 NiAl-LDHs

From the titration the interval of precipitation of the HT-like compounds was defined and it resulted within 6.7 < pH < 7.5 and 6.4 < pH < 7.2 ranges for 2:1 and 3:1 molar ratios, respectively (Figure 24). So we can state that a not remarkable difference in precipitation conditions is associated with the stoichiometry of this compound.

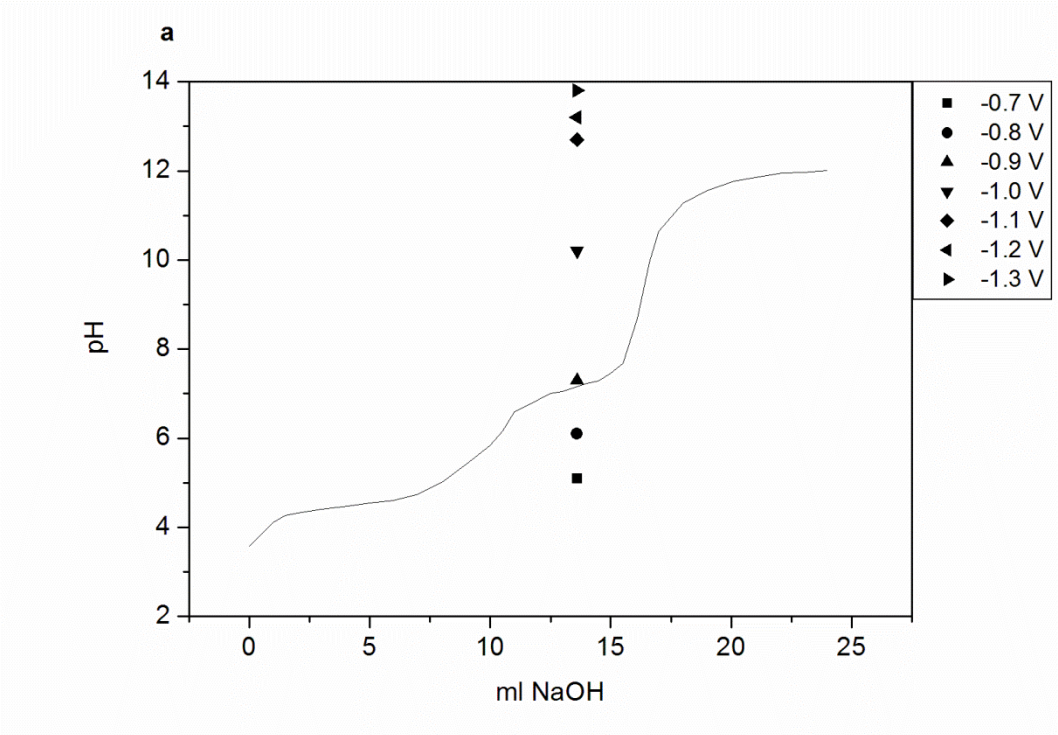

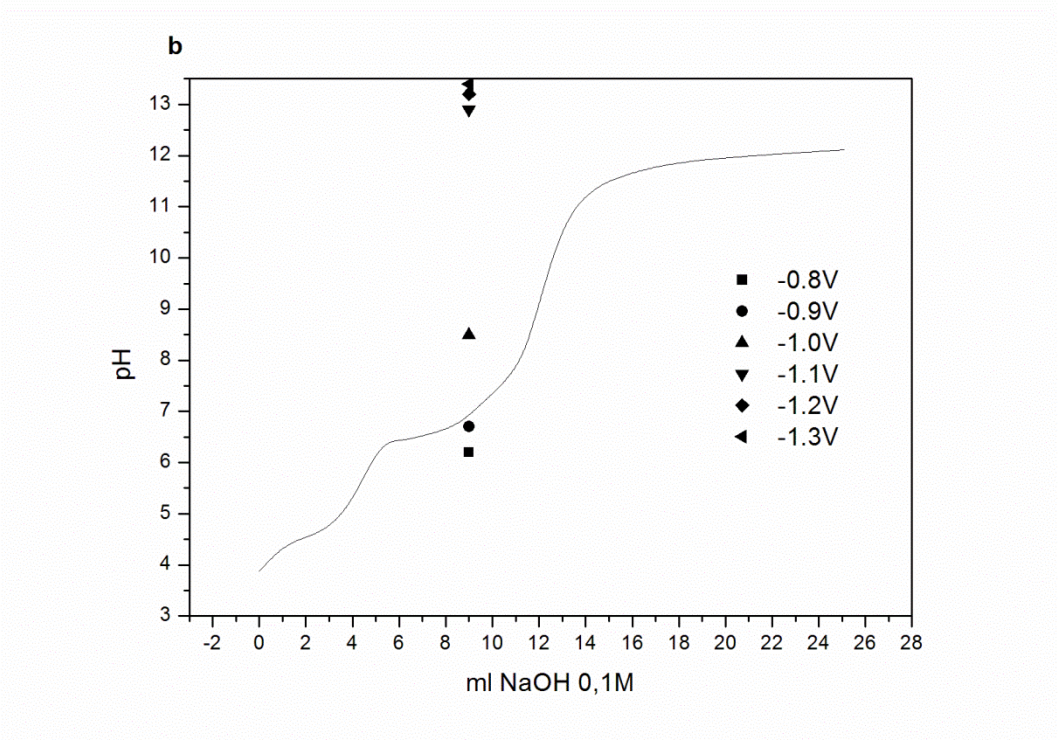

Figura 24: Titration and pH plateau values obtained at different applied potentials of NiAl-LDH with 2:1 (a) and 3:1 (b) molar ratio

On the whole, the pH profiles during electrosynthesis were nearly identical (Figure 25). The time required to reach the stabilization plateau was about 100 s at -0.9 V while it was longer for both higher and lower (≥ 150 s) potentials. The best working potential resulted -0.9 V, regardless of the Ni/Al ratio, and it allowed to attain a pH value of about 7.

For lower potentials it should be remarked that the obtained pH (≤ 6) is too low in respect to the value pointed out by titration (about 6.5-7.5), so they should not be suitable for the synthesis of a pure LDH. For higher potentials (above -1.1 V) the basicity in the electrode-electrolyte interface is strongly increased in every situation similarly to what has been observed during the precipitiation of $Ni(OH)_2$, and pH values are above 12. This probably means the applied potential allows the production of an amount of OH^- higher than the one consumed during the LDH precipitation.

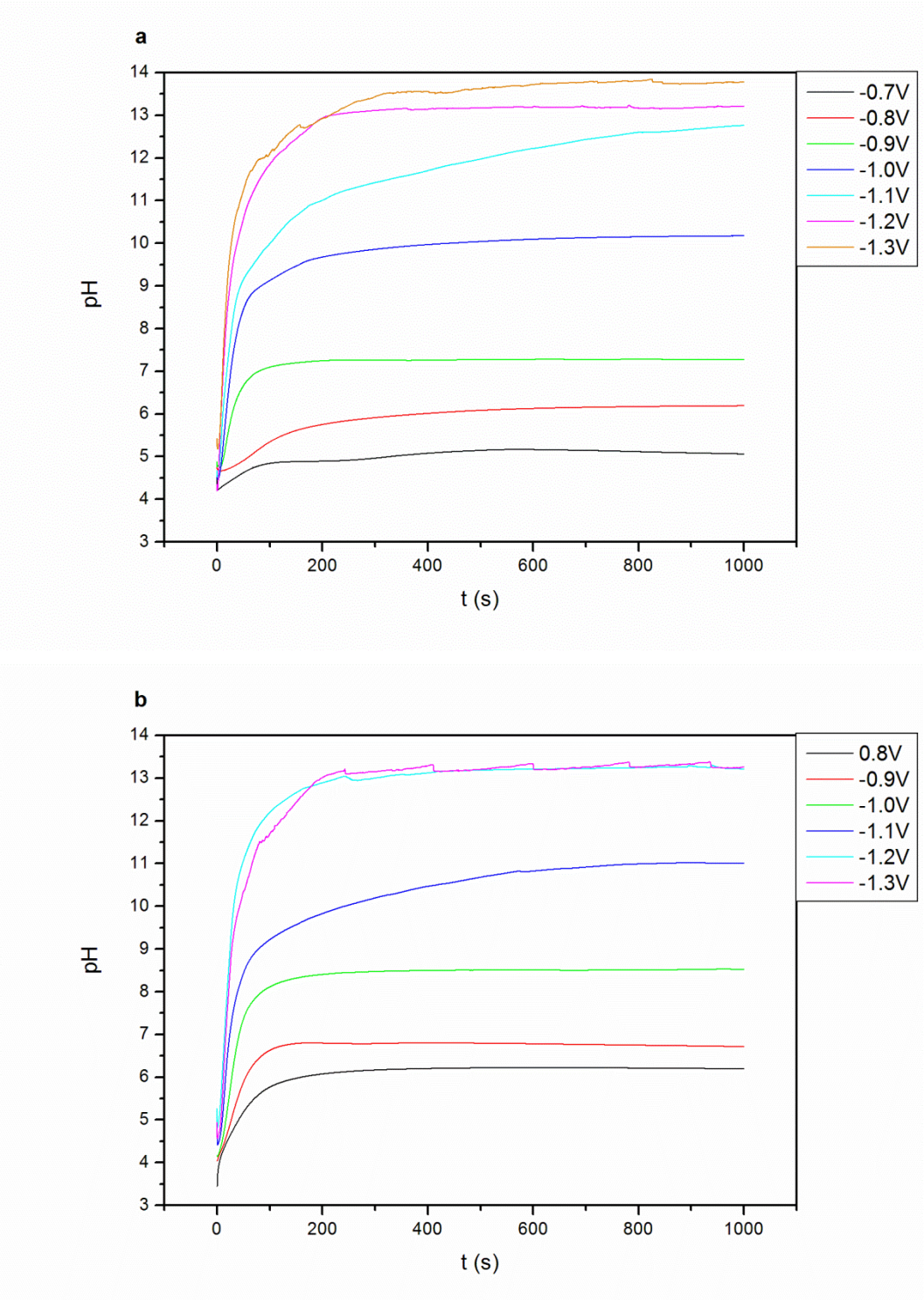

Figura 25: Evolution of pH vs time at different applied potentials of NiAl-LDH with 2:1 (a) and 3:1 (b) molar ratio

As far as the characterization of the compounds deposited at different potentials, morphology and chemical composition are discussed for Ni_2Al_1-LDH considering applied potentials in the interval -0.8 V < E < -1.1 V.

If a potential of -0.8 V is applied to the Pt plate, mainly aluminum precipitates, as expected, since the value of pH is lower than the precipitation plateau of the LDH. A thin film is deposited but some differences in the morphology and composition of the film have been pointed out in some parts of the plate. On less covered areas rounded particles arrays have been noticed and the EDS analysis indicate a Ni:Al molar ratio varying from 1.46 to 2.61 (Figure 26 a and b), although from the pH study discussed before the value reached in this condition (about 5) should not allow the $Ni(OH)_2$ precipitation. In other zones larger agglomerates have been detected, and from the SEM images they seem to have grown on the surface of another layer, that could be the one observed in the less covered areas (Figure 26 c and d). In this case, a Ni:Al molar ratio between 0.15 and 0.26 has been measured by EDS, suggesting that the agglomerates in the top layer are enriched in Al. Moreover, compact zones with cracks development have been also noticed on the Pt plate surface (Figure 26 e), and an underneath layer has been detected inside the cracks (Figure 26 f). In this more compact parts the molar ratio is furthermore decreased, ranging between 0.02 and 0.1.

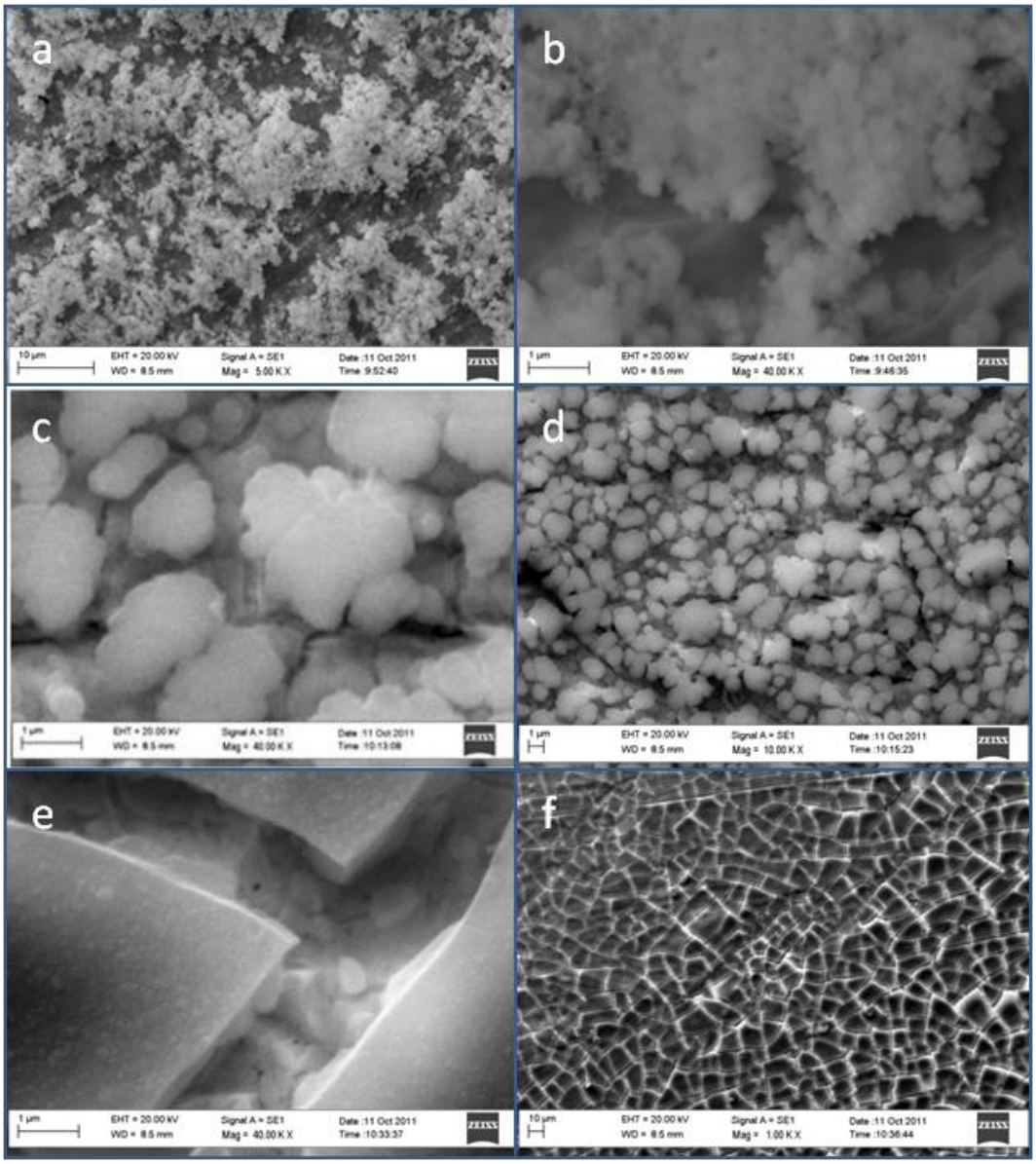

Figure 26: SEM images of the film obtained at -0.8 V for 1000 s from a electrolytic solution containing Ni and Al in 2:1 molar ratio

These observations suggest that a sequential precipitation occurs. Before a mized layer is deposited and then $Al(OH)_3$ precipitates.

The best coverage degree is, however, obtained at -0.9 V, as expected from the pH study results; however, several morphologies have been observed in different points of the plates (Figures 27 a, b and c).

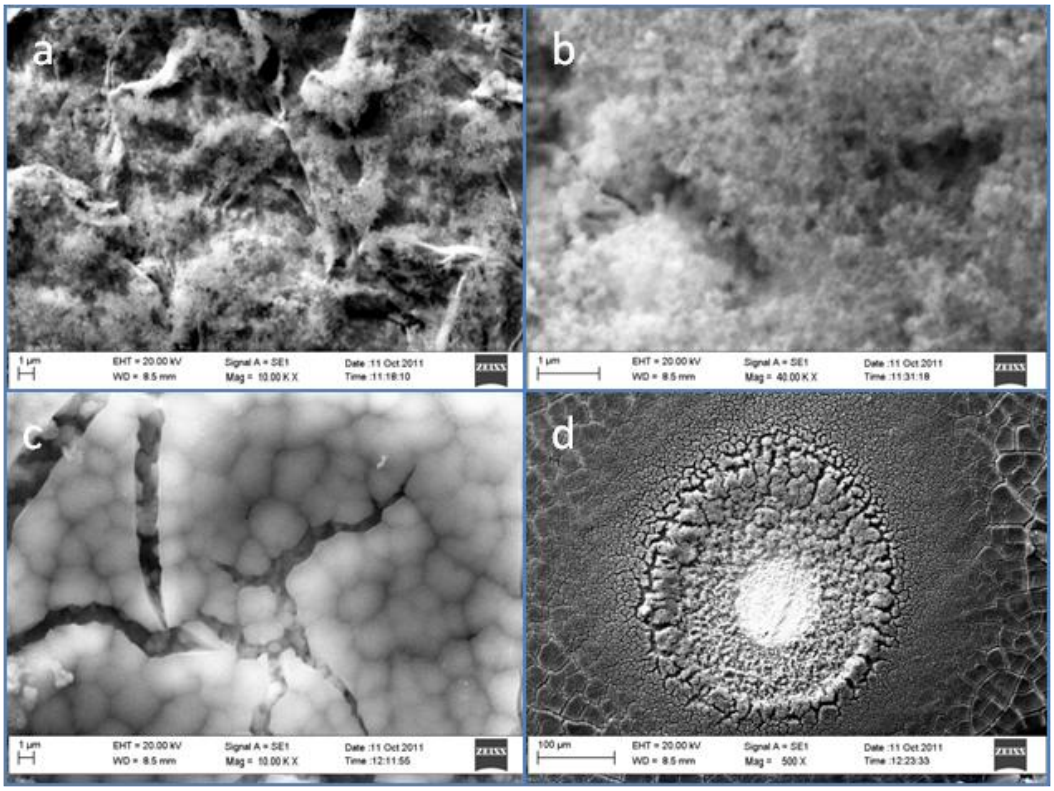

Figure 27: SEM images of the film obtained at -0.9 V for 1000 s from a electrolytic solution containing Ni and Al in 2:1 molar ratio

An aluminum hydroxide layer on the top of a nickel-rich layer is electrosynthesized also in this case. This is confirmed from Figure 27d, for which also EDS measurements suggest the evolution of sequential deposition. The particular structure observed in Figure 27d is probably due to the formation of an hydrogen bubble which is normally undesired, but in this case it allows to evaluate the differences among the observed layers. However when morphologies shown in Figures 27a and 27b are analyzed by EDS the measured molar ratio is just a little below the ideal value of 2, in particular it ranges from 1.52 to 2.17.

After the synthesis at -1.1 V the cracking (Figure 28a) and detaching (Figure 28b) of the film take place together with the deposition of large quantities of potassium. However when a very thin layer is observed (Figure 28c), the EDS analysis gives a Ni:Al molar ratio very next to 2 (1.93-2.05). Probably, it was possible to see the layer due to the detaching of a thicker crust. If no removal of the upper layer occurs the morphology and chemical composition is in according to that observed for other potentials in the outer layer (Figures 28 a and d).

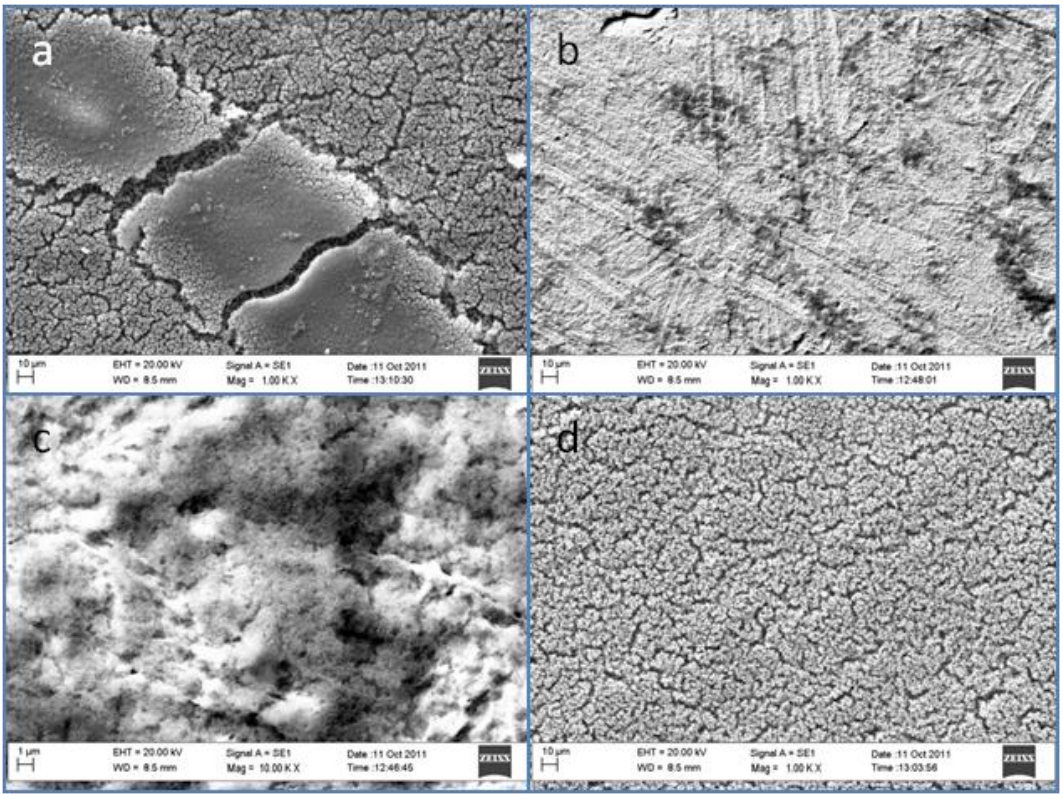

Figure 28: SEM images of the film obtained at -1.1 V for 1000 s from a electrolytic solution containing Ni and Al in 2:1 molar ratio

The modification of the Ni:Al ratio in the plating solution does not largely affect the precipitation sequence. SEM images of the 3:1 NiAl samples electrosynthesised for 1000 s in the cathodic potential range -0.7 V < E < -1.1 V are displayed in following figures (Figure 29).

After the application of the cathodic pulse at -0.7 V, the plate is covered by a thin layer with round particles laying on its surface even if some thicker cracked crusts can be observed too. EDS analyses reveal that the solid is enriched in Al, Ni:Al ratio values ranging from 0.7 to 0.4, according to what observed during the synthesis at a lower Ni:Al molar ratio. Also in this case the study of pH evolution suggests that at this potential Ni deposition should not take place, but only in some zones no nickel has been measured.

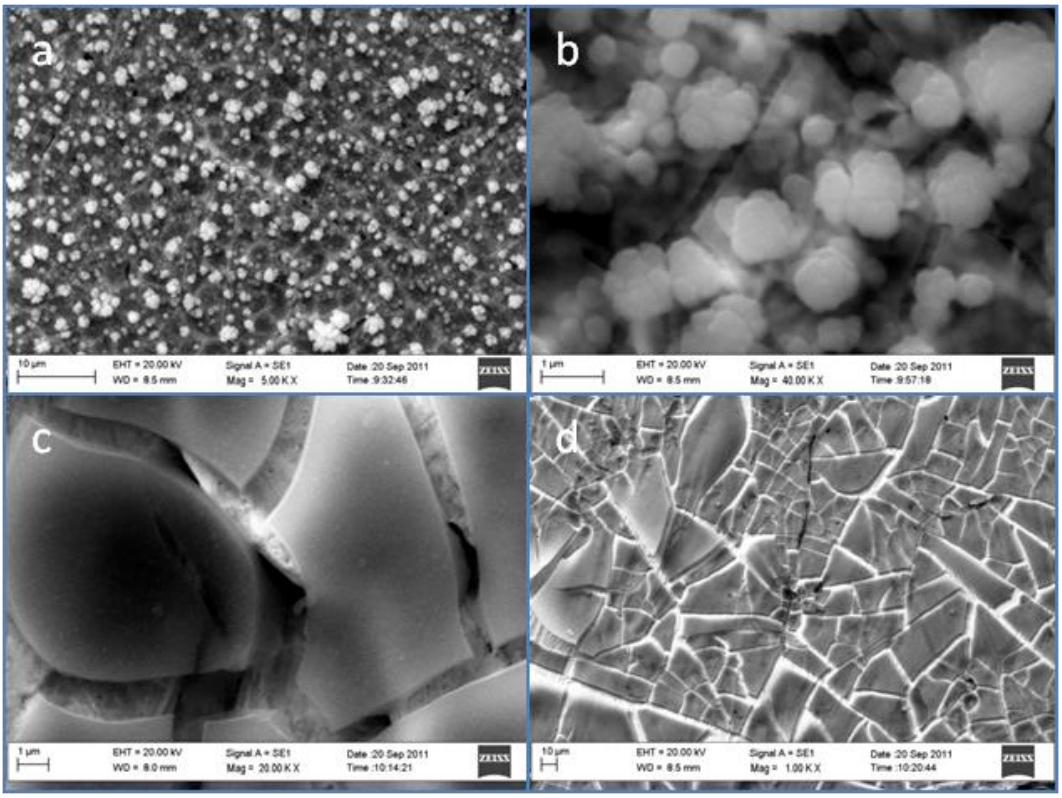

Figure 29: SEM images of the film obtained at -0.7 V for 1000 s from a electrolytic solution containing Ni and Al in 3:1 molar ratio

By increasing the applied potential to -0.9 V, the value selected as the most suitable for performing the Ni/Al LDH electrosynthesis, a thicker film is obtained as for the previous sample. A careful inspection of the surface at high magnification reveals the presence of two layers: that close to the electrode surface is composed by arrays of small particles and contains a larger amount of Ni than Al (Figure 30a); whereas the layer on the top is formed by aggregates of rounded particles, enriched in Al (Figure 30b).

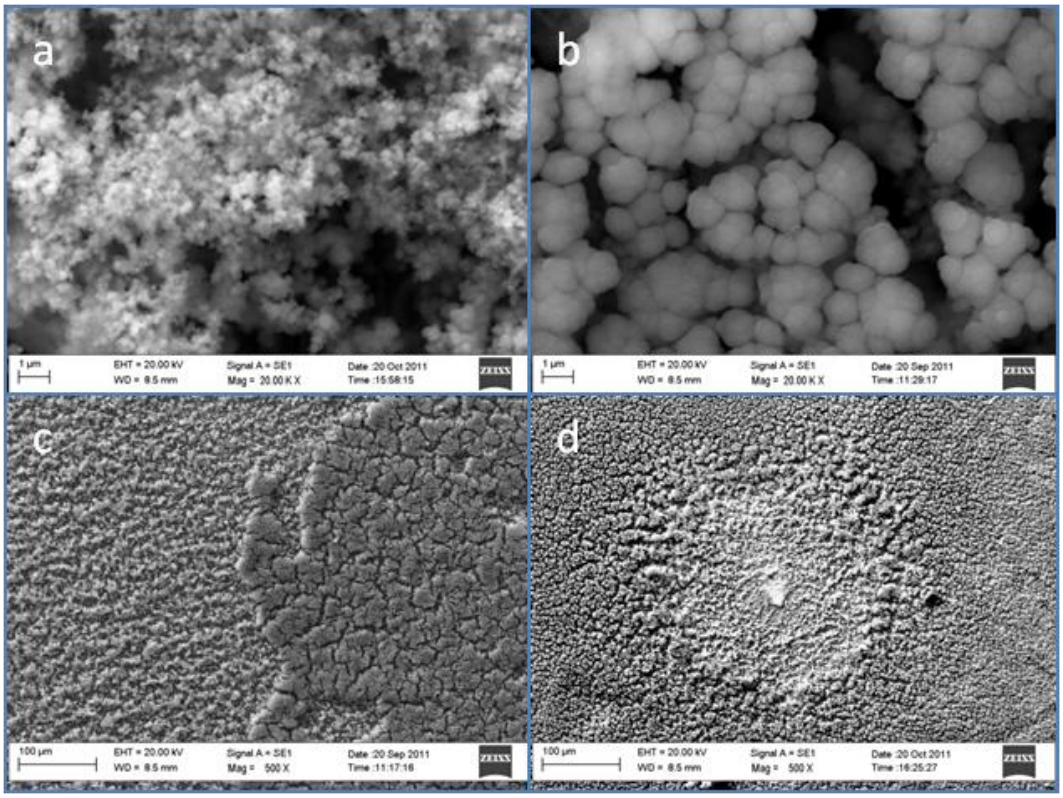

Figure 30: SEM images of the film obtained at -0.9 V for 1000 s from a electrolytic solution containing Ni and Al in 3:1 molar ratio

Also at higher Ni:Al molar ratio, the results confirm a sequential precipitation that can be clearly observed in Figure 30c, where two different layers are effectively distinguished. The particular conformation shown in Figure 30d is again the result of the evolution of a hydrogen bubble. The EDS analyses of several points from the central point of the crater, where a very small amount of material has been found, to the external part show the change of the composition that confirms the hypothesis of the sequential precipitation.

No damage of the layer was observed indicating that no H_2 formation occurs. Although the same deposition sequence is observed for a more cathodic potential as -1.1 V, the increase of the potential applied has a negative effect on the coverage degree: the film thickness decreases, the solid detaches and a large number of cracks are observed. This behavior may be related to the massive hydrogen evolution at the cathode surface. Moreover, it would appear that at more negative potentials the K deposition is favored.

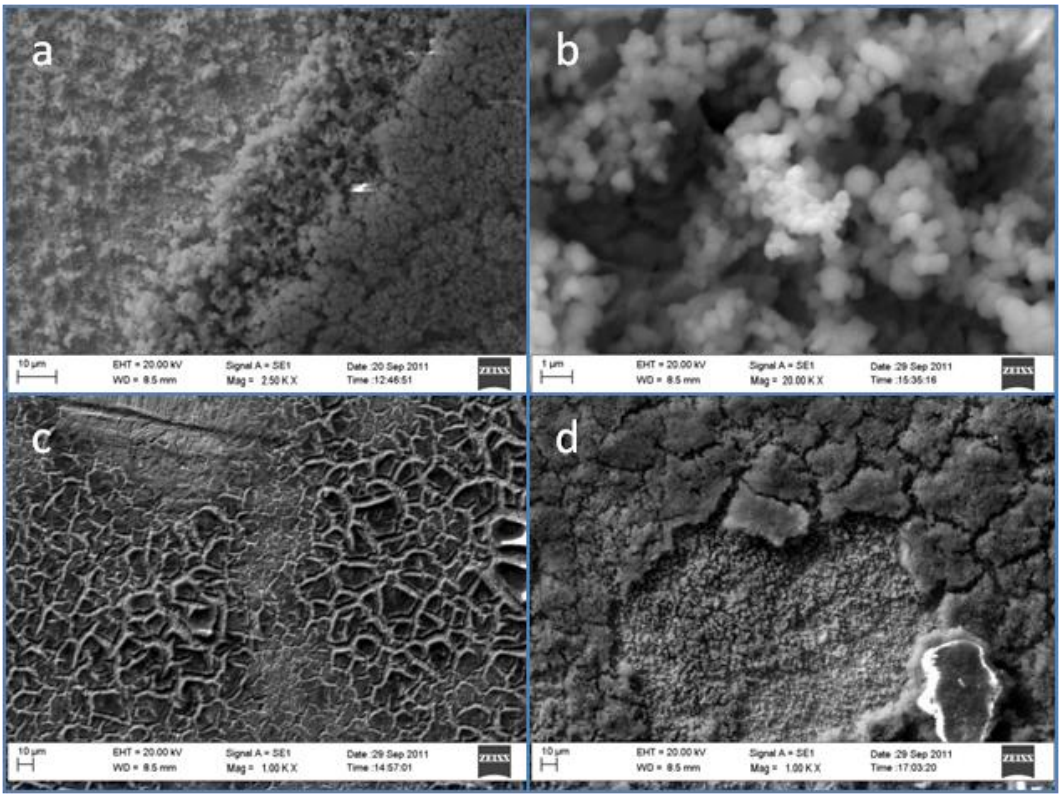

Figure 31: SEM images of the film obtained at -1.1 V for 1000 s from a electrolytic solution containing Ni and Al in 3:1 molar ratio

We can conclude that there is no direct correlation between the composition of electrolytic solution and the composition of the electrosynthesized film. It means that the increase of the Ni^{2+} concentration in the solution does not lead to significant differences in the film composition, for long synthesis times, such as 1000 s.

Diffraction patterns of 2:1 and 3:1 NiAl samples are displayed in Figure 32. Regardless of the divalent to trivalent ratio in the samples prepared at -0.9 and -1.1 V it is possible to observe broad diffraction lines of a poorly crystallized hydrotalcite phase. Some not identified peaks can be also observed in the diffraction patterns. The basal spacing depends on the synthesis conditions: it is ca. 8.0 Å for the 2:1 NiAl sample prepared at -0.9 V for 1000 s, suggesting the presence of anions adopting a "flat lying" configuration with the nitrate plane lying parallel to the brucite-type layers [63]; whereas by increasing the potential applied (-1.1 V) the value is close to 7.8 Å, characteristic of carbonate intercalated samples. The higher pH reached during the syntheses at -1.1 V may favor the nitrate exchange by carbonate anions [64].

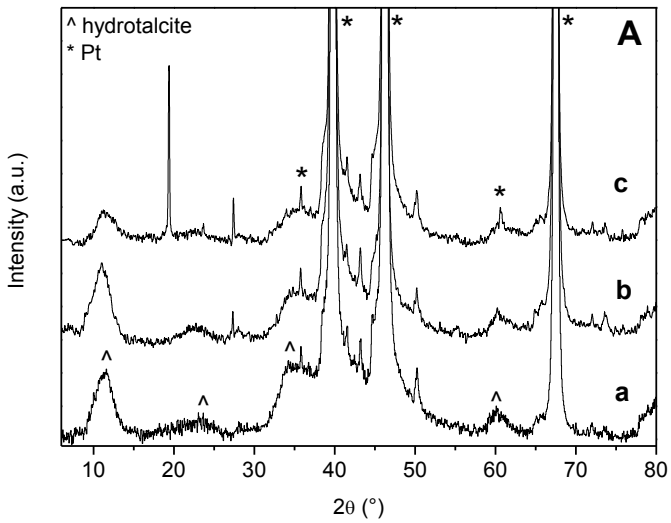

Figure 32: XRD patterns of Ni_3Al_1 synthesized at -0.9V (a), and of Ni_2Al_1 synthesized at -0.9V (b) and -1.1 V (c)

5.3.2.3.2 MgAl-LDHs

Also in the case of MgAl-LDHs the molar ratio does not affect the pH of precipitation obtained by titration that was found to be in the 8.5-9.5 range (Figure 33).

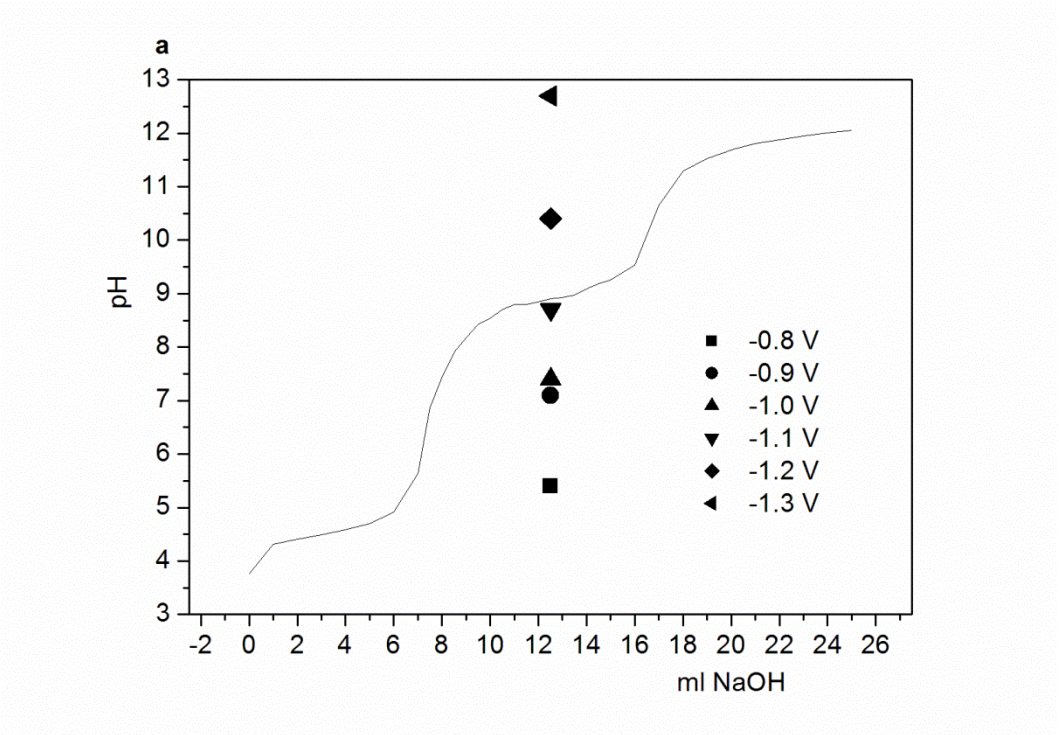

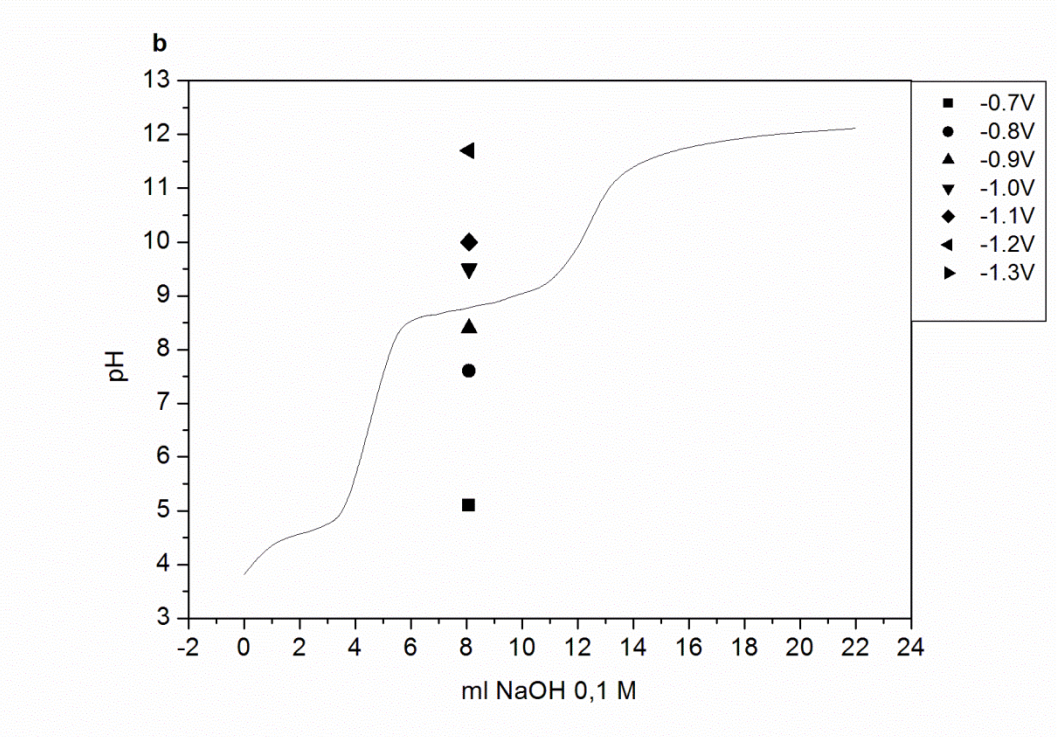

Figure 33: Titration and pH plateau values obtained at different applied potentials of MgAl-LDH with 2:1 (a) and 3:1 (b) molar ratio

However, when Ni is substituted by Mg some differences could be noticed in the pH evolution curves during the electrosynthesis (Figure 34): the time required to reach the steady state is about 100 s for every potential in the case of 2:1 MgAl sample. For 3:1 MgAl sample the time is about 300 s or longer for potential lower than -0.9 V and about 150-200 s for higher potential. Mg^{2+} is the most difficult cation to be precipitated because of its high pH of precipitation, and so the increase in the time required to reach the steady state is probably due to the increase of its concentration that subtracts more OH^- per time unit. The best working conditions are -1.1 V for 2:1 MgAl compounds and in the $-0.9 < E < -1.0$ V range for those for which the molar ration is 3:1. It could be observed that similar pH values are always obtained for 3:1 molar ratio when a potential lower than 0.1 V was applied in respect to the solution where the molar ratio was 2:1. That indicates that the precipitation of the Mg_3Al_1-LDH is favoured, but it has not been possible to give a bright explanation of this behavior.

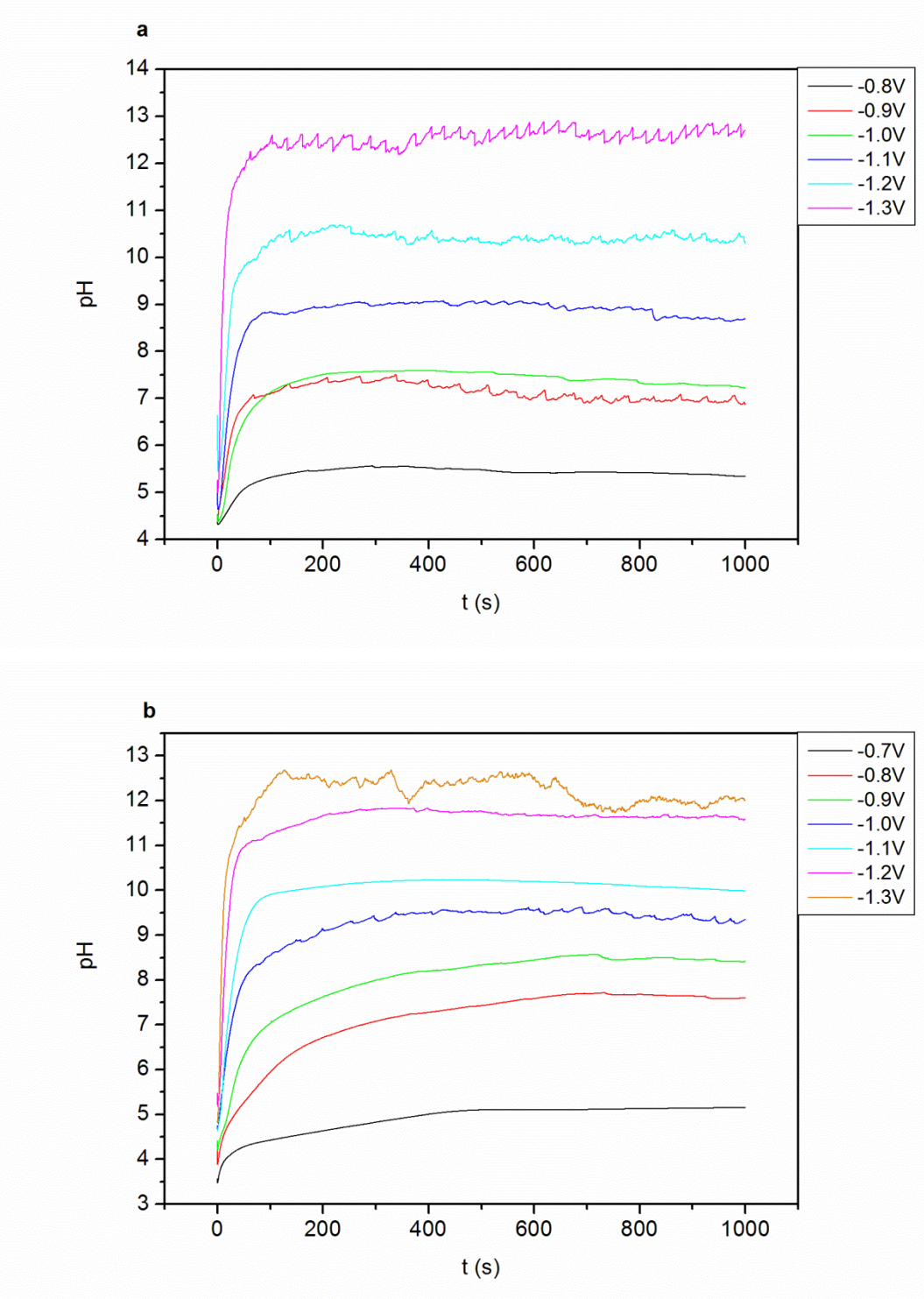

Figura 34: Evolution of pH vs time at different applied potentials of MgAl-LDH with 2:1 (a) and 3:1 (b) molar ratio

The trends observed from SEM and EDS characterization of MgAl-LDHs are similar to those described in the case of NiAl-LDHs.

The analysis of the sample deposited at -0.8 V pointed out the presence of various layers of different morphology and composition: a high amount of Mg is observed for a very thin coating (Figure 35a). The molar ratio MgAl results higher than 3 for both the upper large

aggregates and the smaller round particles. A massive presence of Al when the film is thicker and a noticeable cracks development could be noticed (Figure 35b).

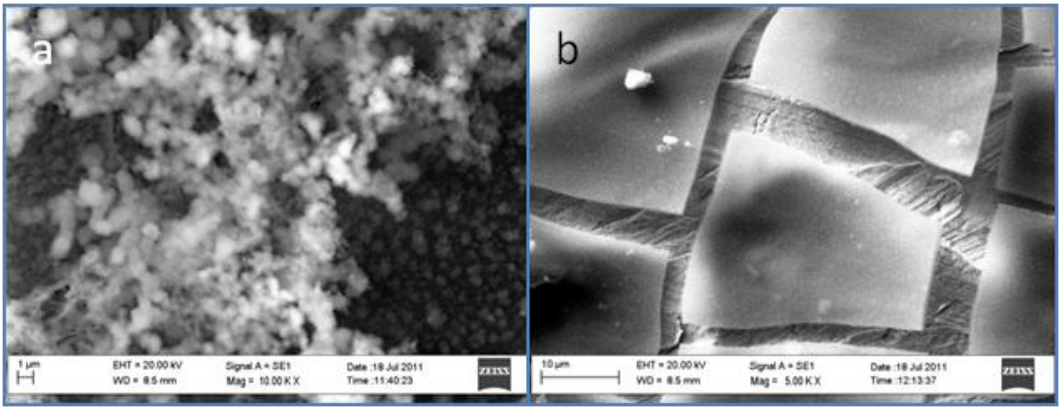

Figure 35: SEM images of the film obtained at -0.8 V for 1000 s from a electrolytic solution containing Mg and Al in 2:1 molar ratio

At a more cathodic potential, such as -0.9 V, a thin layer formed by aggregates of small particles was observed (Figures 36 a and b) with a MgAl molar ratio close to 2. However the coating is not homogeneous and in some zones of the plate very important crack development and crusts detaching were noticed (Figure 36 c and d). In this case also, the phenomena just described make more visible the underlying thin film, which results enriched in Mg^{2+} in respect to the outer layers that display a strong presence of Al^{3+}. The molar ratio is in fact close to 2 also in the adherent layer, while a strong presence of Al has been found in the crusts.

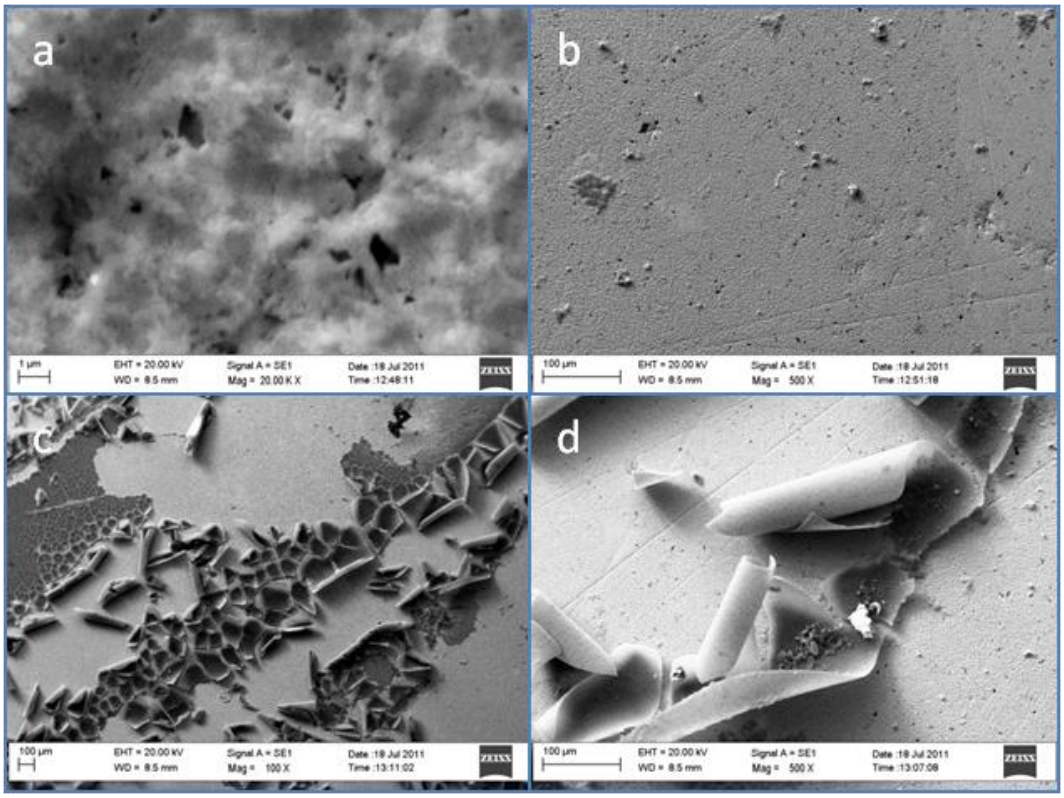

Figura 36: SEM images of the film obtained at -0.9 V for 1000 s from a electrolytic solution containing Mg and Al in 2:1 molar ratio

The film thickness increases and the morphology of the surface changes with the application of a more negative potential, -1.0 V. Several particle morphologies may be observed and as occurring for NiAl electrosynthesized samples the morphology of the coating undergoes a gradual change depending on the region of interest. The morphology shown in Figures 37a and 37b has been found to grow directly on the bare Pt and the EDS analysis indicates a Mg-rich layer (Mg:Al > 3). As far as the film becomes thicker the presence of Al increase (molar ratio < 1) and a compact layer, constituted by round particles aggregates, is observed. Also these observations seem to confirm the hypothesis of a sequential precipitation.

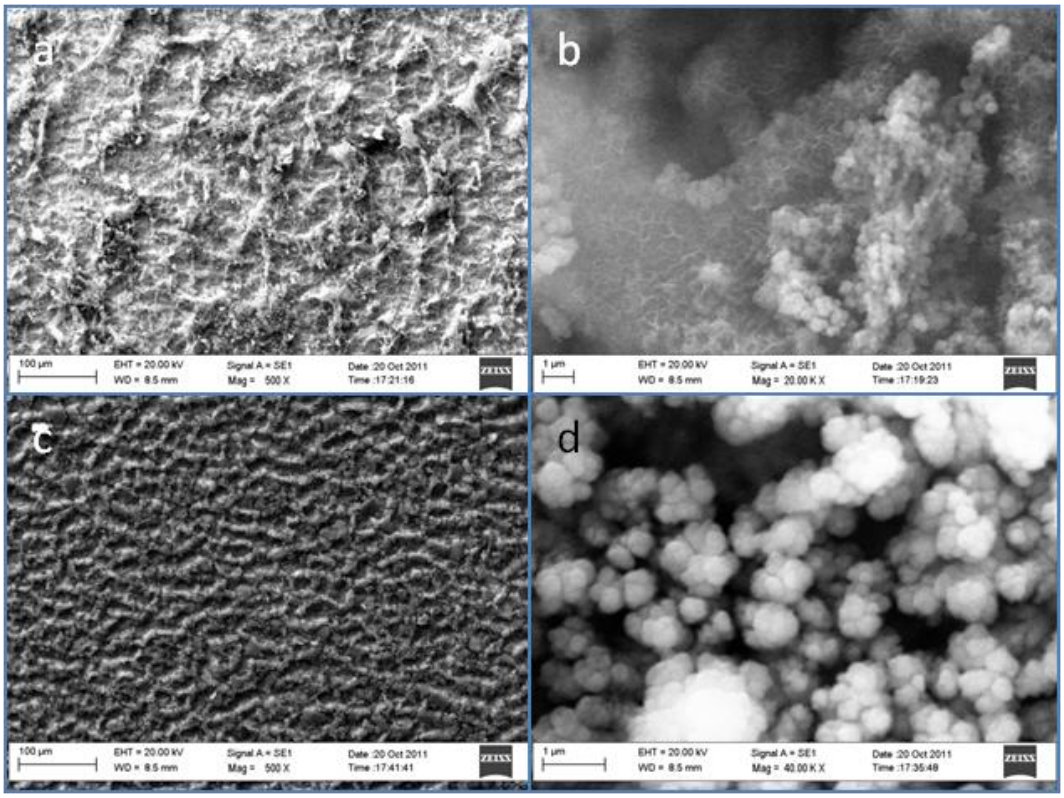

Figure 37:SEM images of the film obtained at -1.0 V for 1000 s from a electrolytic solution containing Mg and Al in 2:1 molar ratio

At -1.1 V the coating is not homogeneous even if this potential was chosen as the best one for the synthesis. In fact the layer growing directly on the bare Pt plate surface is Mg-enriched and it is formed by rounded and platelet-like particles, the latter being characteristic of both $Mg(OH)_2$ and LDH compounds (Figures 38a and 38b); although some uncovered or partially covered zones have been detected (Figure 38c). As already pointed out for the previous described deposition a more compact, thick, and Al enriched layer is found in the uppermost layer (Figure 38d).

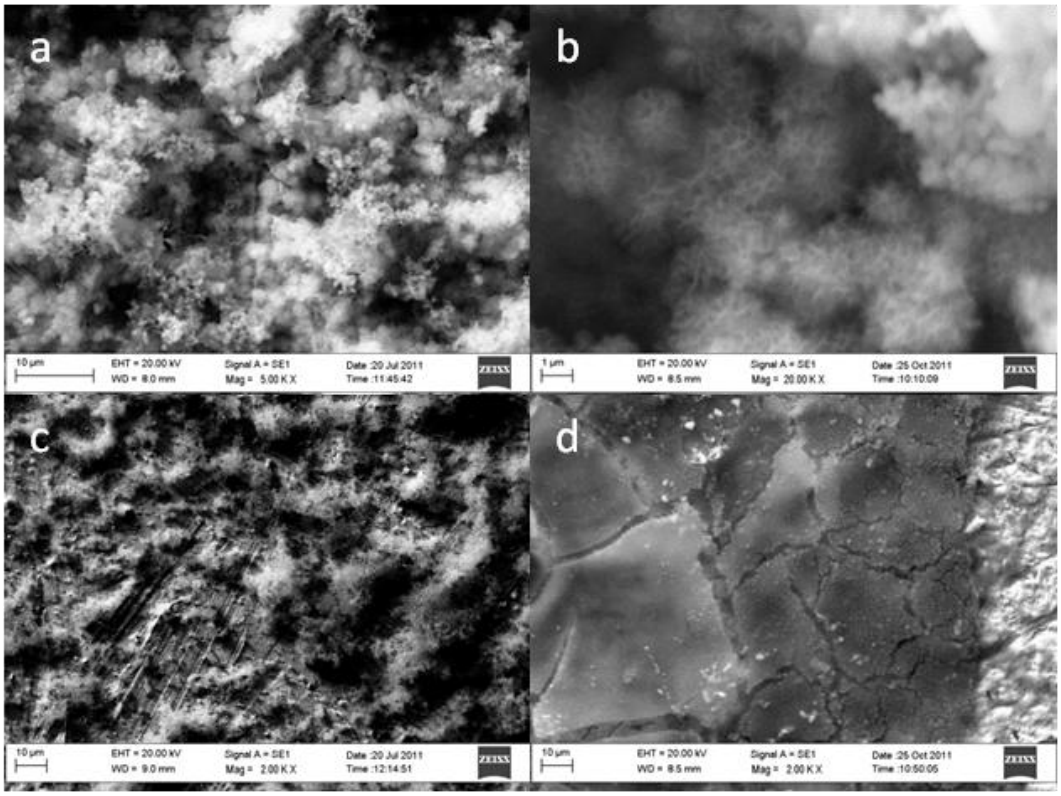

Figure 38:SEM images of the film obtained at -1.1 V for 1000 s from a electrolytic solution containing Mg and Al in 2:1 molar ratio

By applying a more cathodic potential (-1.2 V) the coating becomes less efficient and several uncovered zones are detected (Figures 39a and 39b); however, when a thin film is observed the Mg/Al ratio is generally close the expected one.

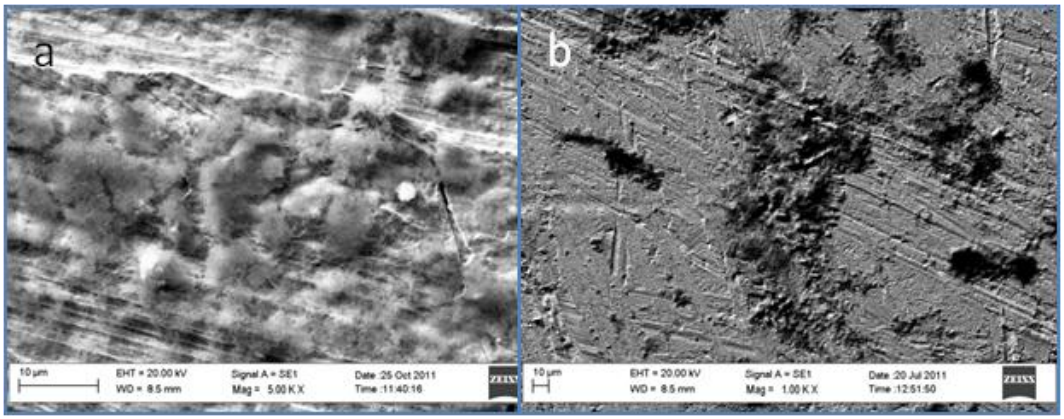

Figure 39:SEM images of the film obtained at -1.2 V for 1000 s from a electrolytic solution containing Mg and Al in 2:1 molar ratio

As far as Mg_3Al_1-LDH is concerned, SEM/EDS analyses of the sample deposited at -0.7 V indicate that no Mg^{2+} precipitates as hydroxide and just a very thin $Al(OH)_3$ layer is formed (Figures 40a and 40b), in agreement with the results obtained during the pH study vs time.

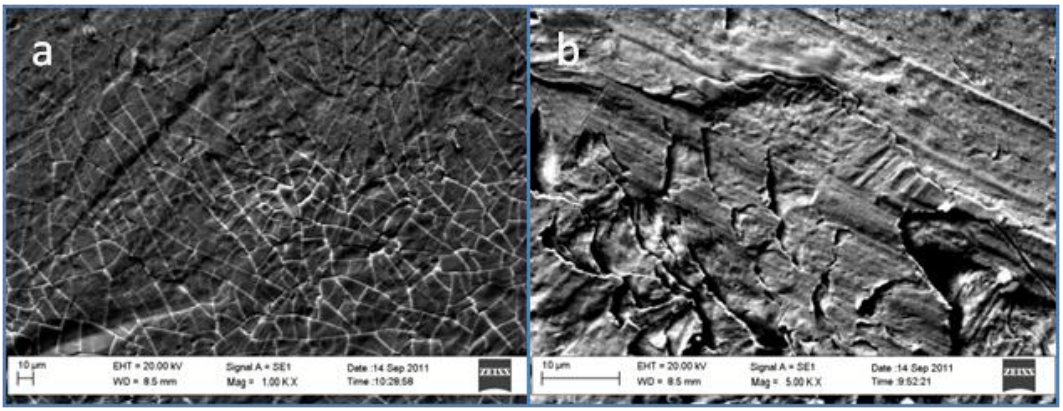

Figure 40:SEM images of the film obtained at -0.7 V for 1000 s from a electrolytic solution containing Mg and Al in 3:1 molar ratio

At a higher deposition potential, i.e. -0.9 V, a thin layer, formed by aggregates of small particles, grows; however the coating is not homogeneous and some zones of the plate remain uncovered. Under these working conditions both Mg^{2+} and Al^{3+} species precipitate and the Mg^{2+}/Al^{3+} average ratio is close to 2 (Figures 41a and 41b). However, as occurring for the molar ratio 2:1, a detaching process of some compact crusts was observed, in particular next to the border of the plate (Figure 41c and 41d). The composition of the crusts is enriched in Al, as expected from the previous observations.

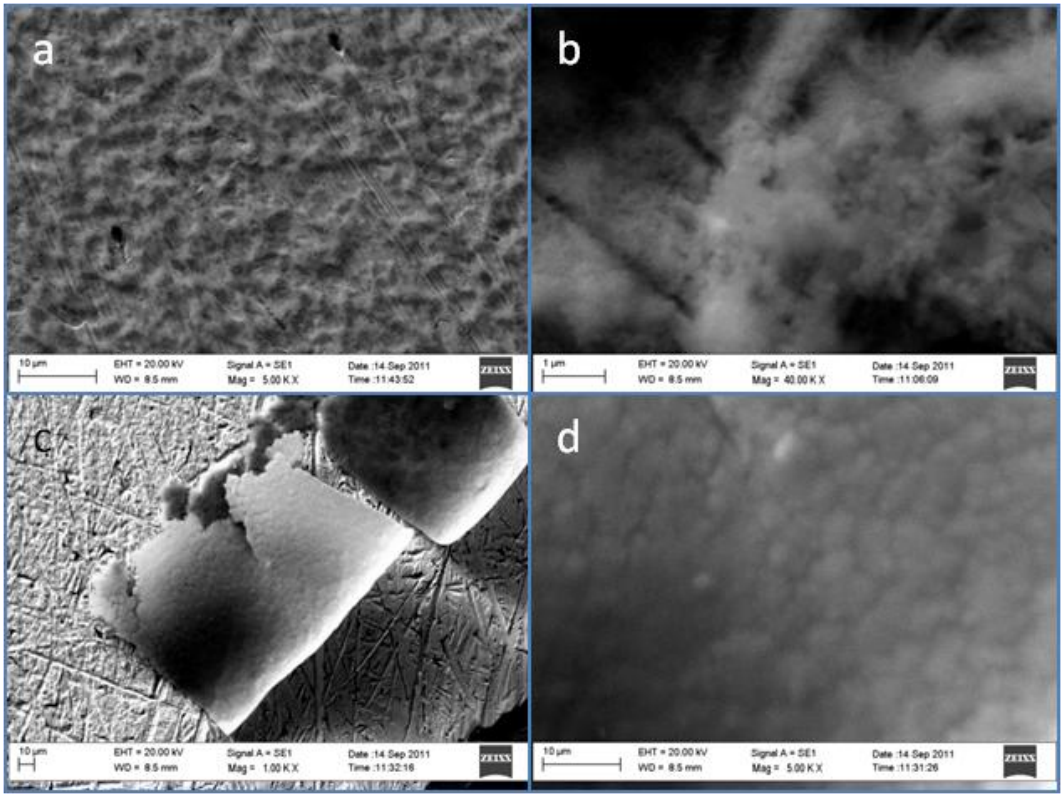

Figure 41:SEM images of the film obtained at -0.9 V for 1000 s from a electrolytic solution containing Mg and Al in 3:1 molar ratio

The film thickness increases and the morphology of the surface changes with the application of a more negative potential than -1.0 V, the one that generates the right pH for the precipitation of the LDH. Several particle morphologies may be observed and, analogously to the NiAl electrosynthesised samples, the morphology of the coating undergoes a gradual change depending on the region of interest and a stratified deposition can be evidenced. As for the previous sample,the layer growing directly on the bare Pt is Mg-enriched and formed by rounded and platelet-like particles (Figure 42a and 42b); the molar ratio MgAl is close to 3 or slightly higher. It would appear that the growing of the aluminium-rich layer occurs by the precipitation of isolated solid islands at the beginning (Figure 42c and 42d), then a net of particles is formed and finally the empty spaces are filled, leading to a compact layer (Figure 42e and 42f). Under these conditions the film seems to be rather homogeneous both in composition and morphology, as observed for the sample synthesized with a lower molar ratio in the same conditions.

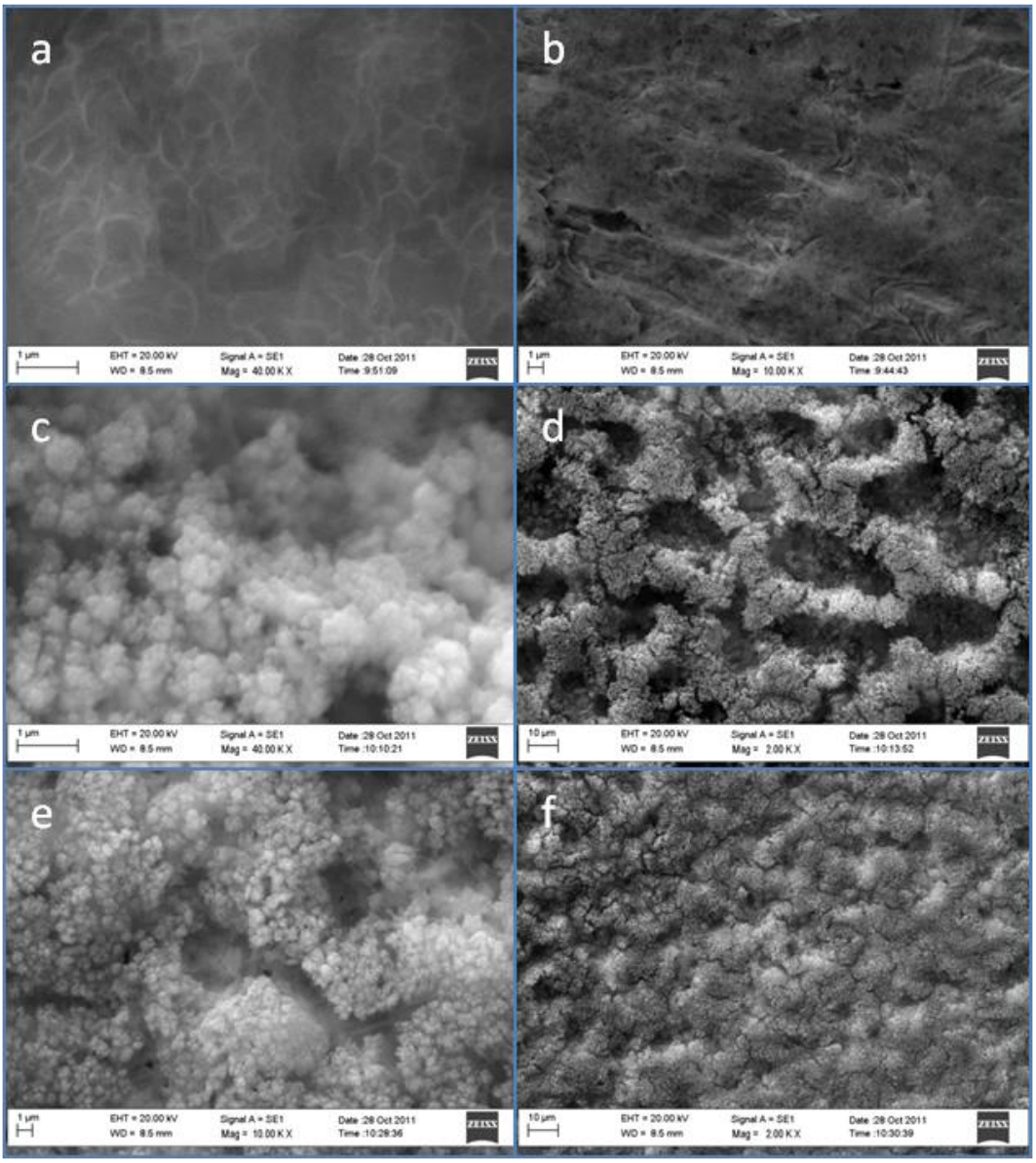

Figure 42:SEM images of the film obtained at -1.0 V for 1000 s from a electrolytic solution containing Mg and Al in 3:1 molar ratio

By applying a more cathodic potential (-1.2 V) the coating more and more uncovered zones, as observed for the sample with a lower Mg content; however, the Mg/Al ratio is closer to the one expected (Figures 43a and 43b).

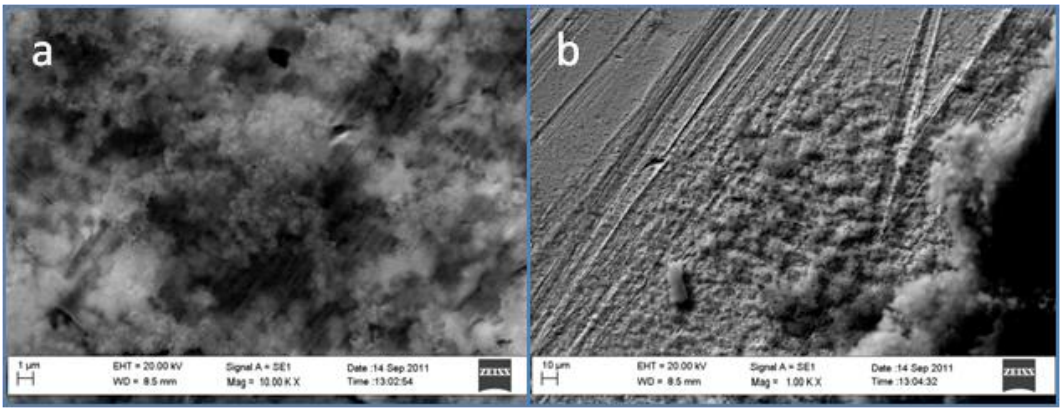

Figure 43:SEM images of the film obtained at -1.2 V for 1000 s from a electrolytic solution containing Mg and Al in 3:1 molar ratio

From the previous observations it seems clear that a sequential deposition occurs in spite of the elemental composition and molar ratio of the plating solution. However, some of the results obtained with SEM and EDS analyses are in contrast with the study of the pH evolution at the WE surface in respect to the applied potential. In order to understand these differences and to obtain more information about the precipitation sequence, the electrosynthesis of 3:1 MgAl LDHs was performed for shorter synthesis times, i.e. 100, 250 and 500 s. At 100 s a very thin film is deposited on the Pt plate, and the Mg:Al ratio has an average value of 2 (Figures 44a and 44b). For this short synthesis time the pH plateau for precipitating the LDH can not be reached, so explaining the low magnesium content. The increase of the synthesis time yielded to both a better coverage and an increase in the Mg/Al ratio, average value was about after 250 s (Figures 44c and 44d). After 500s the Mg:Al ratio overcomes the theoretical value, i.e 4.5 vs 3. Rounded and platelet-like particles are observed in the layer in close contact with the Pt surface, whereas the aluminum hydroxide layer growing over looks like a net of small particles (Figure 44e and 44f).

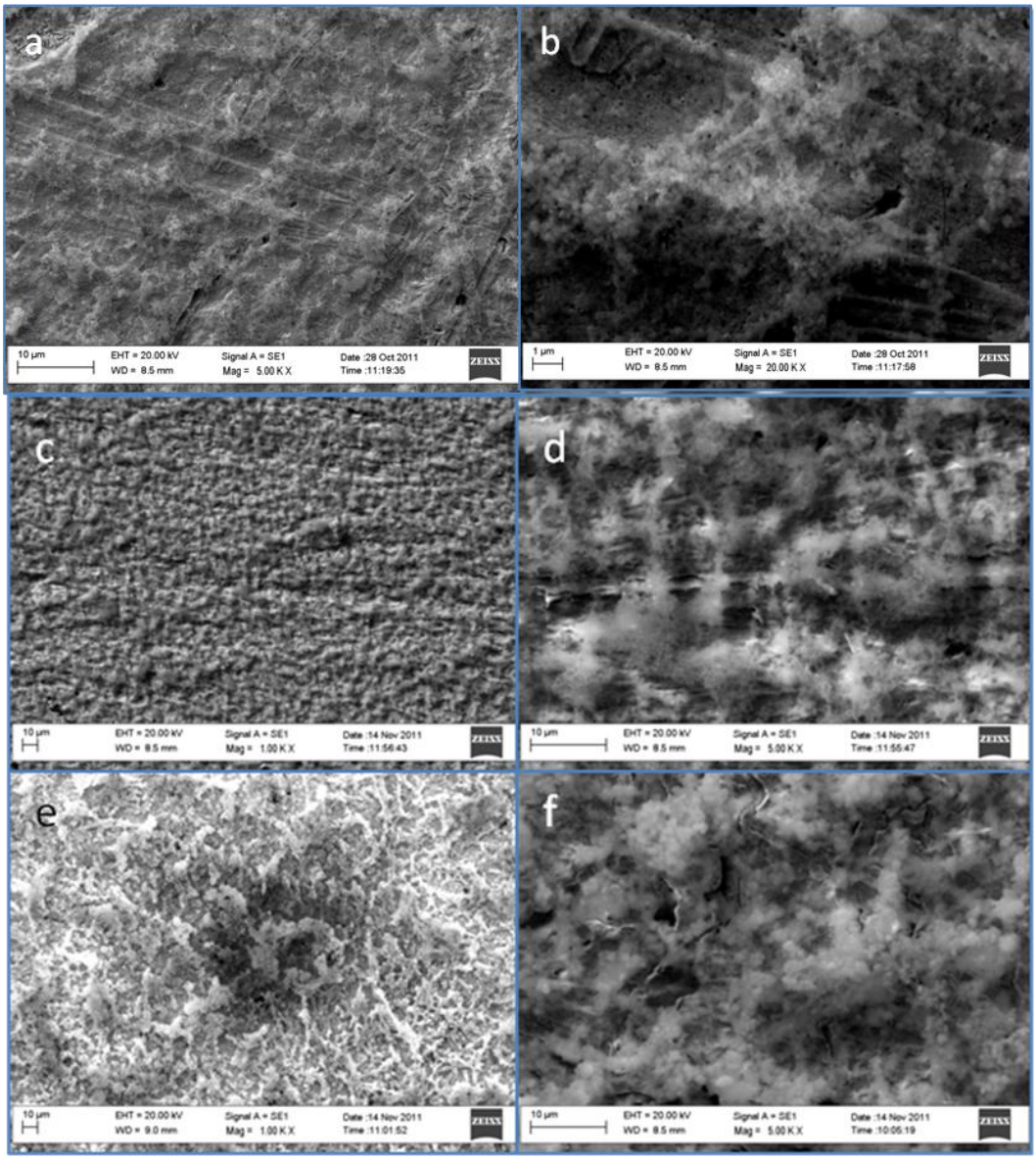

Figure 44: SEM images of the film obtained at -1.0 V for 100 s (a and b), 250 s (c and d) and 500 s (e and f) from a electrolytic solution containing Ni and Al in 3:1 molar ratio

Time seems to be the key parameter to obtain an LDH or mixed hydroxides with a proper molar ratio, although the measured pH, that should be the main parameter affecting LDH precipitation, was shown to be constant for the entire 1000 s synthesis.

Concerning MgAl LDHs (Figure 45), for the 2/1 sample prepared at -1.0 V for 1000 s, the (003) and (006) diffraction lines are splitted, indicating the presence of NO_3^- anions with their main axis tilted ($d_{(003)}$ = 8.7 Å) or parallel ($d_{(003)}$ = 8.0 Å) to the brucite-type layers [Xu]. In the sample prepared at a more cathodic potential, -1.1 V, NO_3^- anions are intercalated giving rise to a basal spacing of 8.0 Å. For 3:1 MgAl samples, even at a very short time such as 100 s, the diffraction lines of the hydrotalcite phase are identified, although they are not intense due to the small amount of solid deposited, as previously observed by SEM. In fact its intensity increases with the synthesis time until reach the maximum at 500 s, then it starts to decrease. Neither $Mg(OH)_2$ nor $Al(OH)_3$ phases are detected.

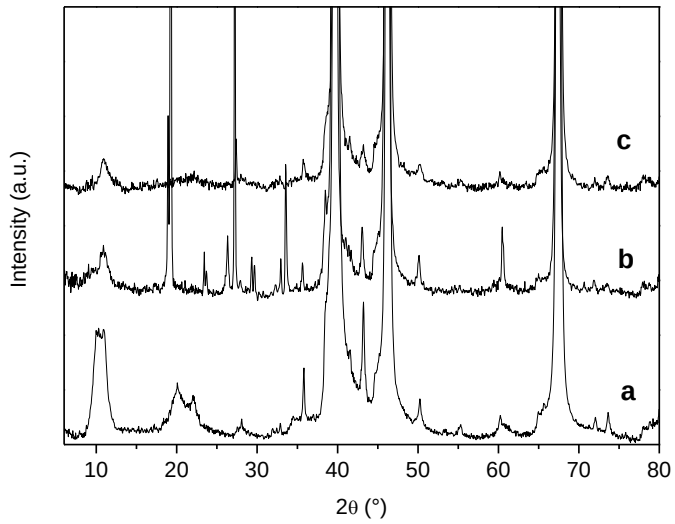

Figure 45: XRD patterns of Mg_2Al_1 synthesized at -0.9 V (a) and -1.1 V (b), and of Mg_3Al_1 synthesized at -1.1V (c)

5.3.2.4 pH IN THE VICINITY OF THE COUNTER ELECTRODE

The evolution of bubbles was observed at both CE and WE. As said before at the working electrode the production of hydrogen bubbles takes place due to the reduction of H^+ (3.5.2), NO_3^- (3.5.3) and H_2O (3.5.5). Their presence at the counter electrode was quite unexpected. A measurement of pH evolution nearby the CE surface has been achieved by positioning the glass electrode in its proximity. It is not a accurate measurement because of the great influence of the bulk solution; however, it could give an idea of what is happening near to the cylindrical Pt gauze. The results are shown in Figure 46.

A decrease of pH is observed for every applied potential with an increasing ΔpH vs time along with the increase of applied potential. A reaction that lead to a consumption of OH^- is supposed to take place. The oxidation of the hydroxide ions to oxygen can explain both the evolution of bubbles on the Pt gauze and the decrease of pH. However, this reaction should just occur next to the counter electrode surface and should not affect the monitoring of the evolution of pH at the WE, and therefore the described electrosyntheses. However, the influence of the bulk solution surely dilutes this acidification effect.

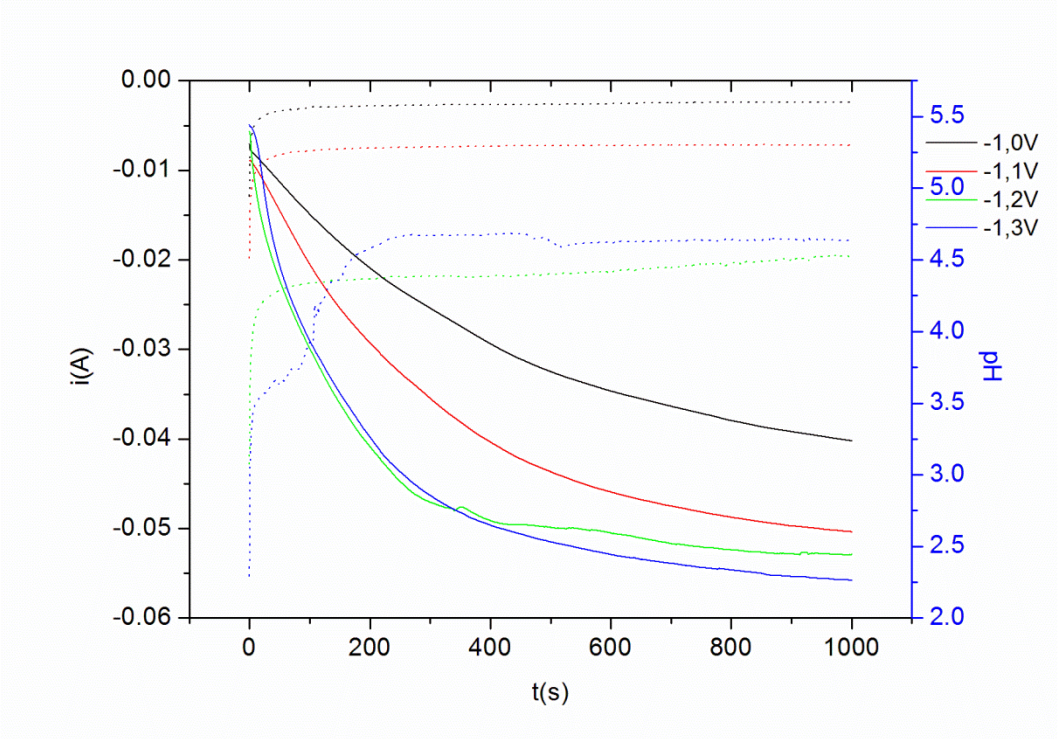

Figure 46: Evolution of pH next to the surface of the CE (solid line) and relative current intensities (dot line)

5.4 ELECTROSYNTHESIS OF LDHs ON FeCrAlY FOAMS

The development of the catalysts as far as the synthesis conditions are concerned was based on the analyses of morphology and composition of the deposited layer obtained by SEM/EDS, as well as on the results of the catalytic tests, performed at the Department of Industrial and Materials Chemistry.

In some cases the characterization by XRD and Temperature Programmed Reduction (TPR) has been performed too.

The data from the EDS analyses for the experiments described below were taken into account just for a qualitative evaluation of the composition of the material deposited on the foam. A precise more analysis, that could be employed for a quantitative evaluation, needs necessary flat surfaces to be analyzed, and this requirement was impossible to be achieved with the just prepared samples, due to the complex geometry of the metallic foams.

The characterization with the porosimeter was tried for the following described samples, but no useful results were obtained due to the low amount of deposited material.

For the same reason, any result was obtained from ultrasonic tests to check the adhesion of the film on the foam. Since the amount of deposited material is very low, no significant difference after the treatment was noticed. Moreover an ultrasonic treatment was seen to damage partially the metallic foam, since it leads to breaking of its microstructures. The SEM and EDS characterizations of the samples were employed also to evaluate the stability of the film after the employment in the reactor.

In carrying out this research work on the foams, different experimental set ups were tested in order to obtain more uniformity and homogeneity of the synthesized films. At first, a classical three electrode cell was employed for the syntheses.

5.4.1 CHARACTERIZATION OF BARE FOAMS

The characterization of a bare foam by SEM and EDS analysis shows a pores dimension between 200 and 800 µm, and a great variability in the composition of the FeCrAlY alloy, depending on the analyzed point. However Fe is the main element of the alloy (52-64%), followed by Cr (17-26%) and Al (12-20%). Y (<1%) was detected in a very low amount and it is not present in all the tested points. This variability could lead to some problems for the electrosynthesis because of the different electrical conductivity of the zones with different composition.

The presence of Al in the foam alloy causes to an overestimation of the Al present in the deposited layer. Some calculations have been tried to subtract the Al signal coming from the support in order to obtain more accurate values for the calculation of the M^{2+}/M^{3+} molar ratio. They are mainly based on the amount of detected Fe and Cr, and the subsequent subtraction of a proportional quantity of Al. However, the considerable variability of the composition of metallic foams did not allow to obtain a good evaluation of the Al signal.

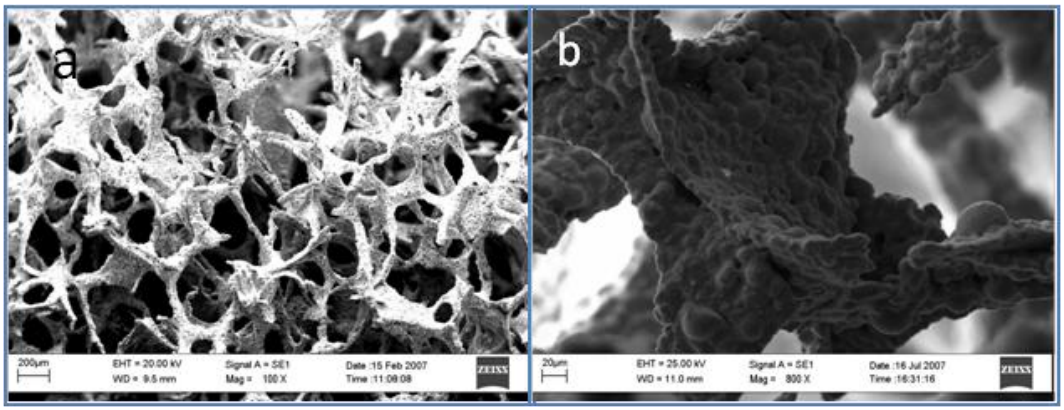

Figure 47: SEM images of a bare FeCrAlY foam

After calcination at 900 °C, a remarkable increase of Al content was observed by EDS. It is due to the typical formation of an alumina layer on FeCrAl surfaces after thermal treatment [65], as also outlined in the 'Introduction' chapter. In fact some needles attributed to alumina are observed in the SEM pictures (Figure 48b). This behavior leads to an overestimation of the Al content obtained by the subsequent EDS analyses of calcined samples.

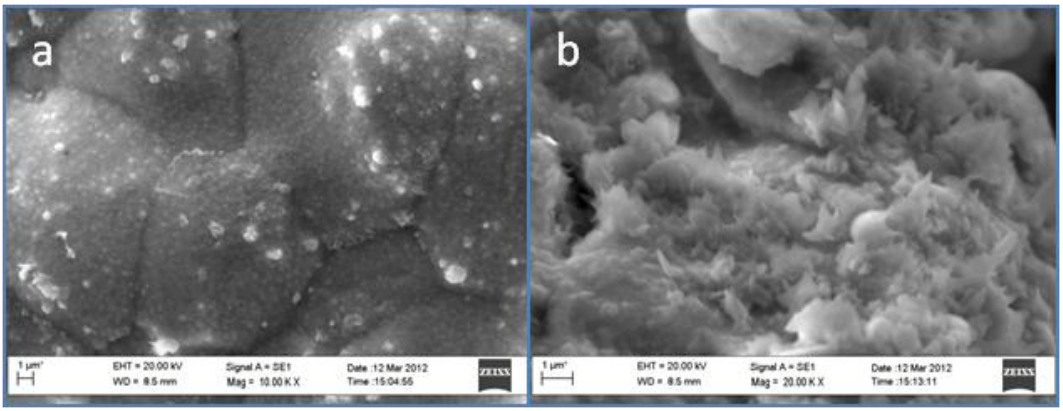

Figure 48: SEM images of a calcined bare foam

5.4.2 SYNTHESIS OF MgAl-LDH ON FOAMS

MgAl samples have been synthesized at -1.2 V for 1000s from a solution containing the nitrates of Mg^{2+} and Al^{3+} at a 3:1 molar ratio. The potential applied was chosen taking into account the data obtained from the study of pH evolution of MgAl-LDH compounds and the evaluation of the overpotantial between a Pt plate and a FeCrAlY foam discussed before.

SEM characterization of the resulting layer shows a not uniform coating, with the deposition of a higher amount of materials on the tips (Figure 49b) in respect to the flat zones (Figure 49a). The morphological analysis of the film shows that it is composed of aggregated small round particles on all the surface and no cracks are evident. However, a difference in composition is observed in the two zones. In the thinner film present on flat areas a low Mg:Al molar ratio (next to 1.5) is recorded. However, it has to be remarked again that the presence of Al in the metallic foam alloy leads to an overestimation of its quantification. Taking into account the high amount of Fe and Cr revealed by EDS, a lower value ofAl can be calculated, thus Mg:Al a molar ratio similar to that of the electrolytic solution could be considered to be achieved in this case. On the tips, instead, the thickness of the film allows a lower influence of the composition of the support to the EDS analysis. In this case a higher amount of Mg is detected and a Mg:Al molar ratio of about 4 (instead of the ideal value of 3), probably because of the formation of a pH gradient. Higher pH would be on the tips, favoring the precipitation of a higher Mg amount. The presence of K was detected in an unexpected level. The reasons for this presence could be the electrostatic attraction of the K^{+} ions towards the negatively polarized WE that leads to the migration and subsequent absorption on the foam surface and for the entrapping of some potassium during the precipitation of the hydroxides on the foams.

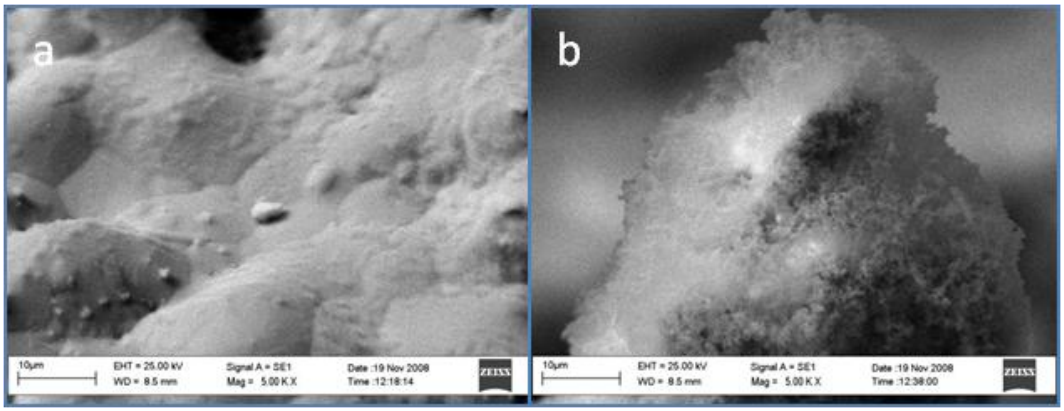

Figure 49: SEM images of a MgAl LDH synthesized at -1.2 V for 1000 s on a FeCrAlY foam

After calcination, crack development is observed, but the differences between tips and flat zones are still present. The processes taking place during calcination should be considered for explaining the crack development. A noticeable weight loss, about 40–50%, is observed for the LDH precursors during the thermal treatment, and it is mainly due to the removal of CO_2, H_2O and NO_2. The formation of compact oxides leads to a great shrinkage of the deposited material, which may be responsible for the formation of cracks. Moreover, the differences in thermal expansion coefficients of the ceramic and metallic materials may be also considered to explain the crack development. Calcination, however, may favour the adhesion of the wash-coat to the support, because of the reaction between alumina from the support and the cations of the mixed oxides layer. In fact the total amount of detected Al is noticeably increased by the growth of an alumina film on the foam surface, coming from the oxidation of the FeCr alloy [65]. Moreover, the amount of K is strongly decreased, probably because of its thermal degradation during the calcination process (900 °C, for 12 h).

Two more syntheses were performed both at a lower (-0.9 V) and a higher (-1.3 V) cathodic potential. The synthesis at -0.9 V resulted in a rather uncovered foam, whereas the application for 1000 s of a more cathodic potential, such as -1.3 V, led to a coverage degree of the foam surface similar to the one obtained at -1.2 V, and the same differences between tips and flat zones were observed (Figures 50a and 50b).

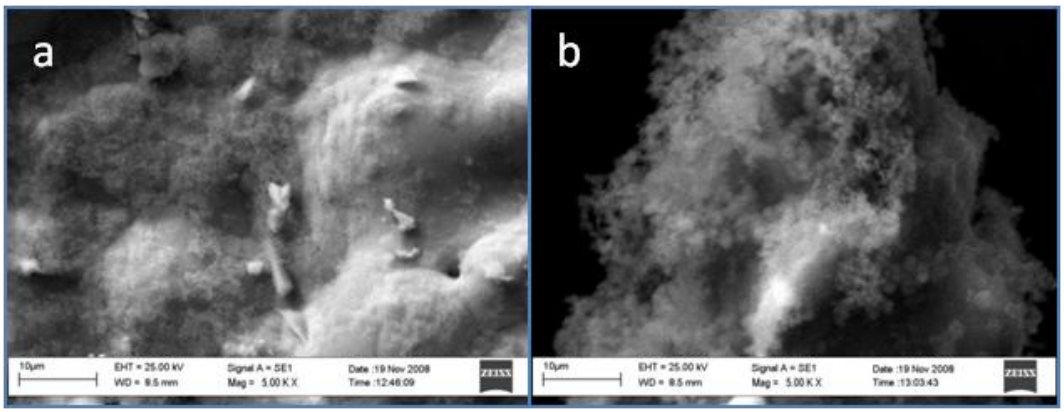

Figura 50: SEM images of a MgAl LDH synthesized at -1.3 V for 1000 s on a FeCrAlY foam

These results are in agreement with the study of pH evolution during MgAl-LDH precipitation on Pt plates, considering the overpotential of about -0.2 V previously measured for the metallic foam vs Pt plates. In fact, by applying a potential of -1.0 V and –1.1 V at the WE, the values of pH reached about 9 after 1000 s were very close to the precipitation interval of the LDH.

Last but not least, it should be remarked that no pore blockage occurred after the syntheses in every working condition reported in this study. This is a really important feature from a catalytic point of view, because a reduction in porosity would limit the performances of metallic foam as catalytic supports, as described in chapter 3.4.

5.4.3 INFLUENCE OF POTENTIAL AND INTIAL pH OF THE ELECTROLYTIC SOLUTION

At first two of the main parameters that have be controlled during the electrosynthesis, i.e. the pH of the solution and the applied potential, were considered. RhMgAl compounds have been electrosynthesized on metallic foams with a diameter of 0.8 cm and a 80 ppi (pore per inch) porosity. These moreover were tested for their activity as the catalysts towards CPO reaction.

As said before, the Pourbaix's diagram of a metal outlines the relation between the electrochemical potential and the pH that allows the formation of a specific phase. The control of the initial pH of the working solution is a main feature when easy reducible metals, such as rhodium, are involved in the electrosynthetic process. Two sets of foams were used for the electrosynthesis at -1.2 V for 1000s in order to check the pH influence, keeping the initial pH of the plating solution at 2.1 and 3.8. The plating solution was a 0.03 M Rh:Mg:Al nitrates solution with a molar ratio 11:70:19 in KNO_3 0.3M, as supporting electrolyte.

The pH of the plating solution containing the nitrates (spontaneous pH) is about 2.1. SEM images after the electrosynthesis are shown in Figure 51. They indicate that the sample is poorly homogeneous, as also observed by a visual inspection of the foams. During the electrosynthesis, the whole or a part of the foam turns black, pointing out the reduction of Rh^{3+}whose characteristic color is yellow, to Rh^0. Moreover, SEM images of some parts of the foam show the formation of arrays of rounded particles and EDS analysis reveals that they are composed of Rh and Al, while no Mg is detected.

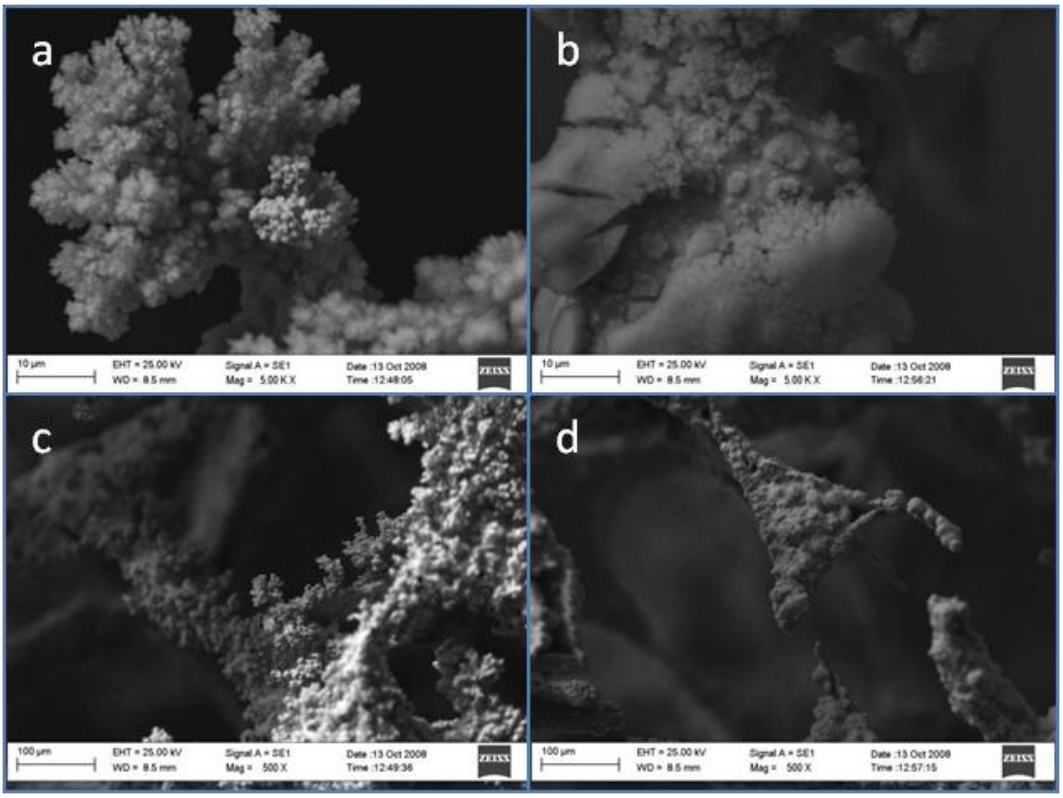

Figure 51: SEM images black (a and c) and yellow (b and d) zones in the sample synthesized at -1.2 V for 1000 s at the spontaneous pH

In other parts of the foam, the coating is made up of small particles containing Rh, Mg and Al. It can, therefore, be hypothesized that the application of a potential of −1.2 V to the plating solution at its spontaneous pH leads to the precipitation of different phases due to the formation of potential gradients, leading to pH gradients, within the foam. In particular, it is clear that these experimental conditions do not ensure, at least in some zones of the foam, a sufficiently basic pH to avoid the precipitation of Rh^0 as weel as of the aluminum hydroxide [66]. In order to suppress the reduction of Rh^{3+} cations, the pH of the solution was adjusted before the electrochemical experiments to of 3.8, which is the highest value avoiding $Al(OH)_3$ bulk precipitation, as demonstrated by titration curves, before discussed.

SEM images of the sample prepared at pH= 3.8 show a coverage that is not uniform: uncoated or partially coated zones are observed on the flat surfaces of the foam and a larger amount of solid is observed on the tips.

Inspection of the sample at higher magnifications reveals that the coating is made up of small particles. The composition of the deposited solid (qualitatively obtained by EDS) is also not homogenous, but the trend in the values is related to the surface coverage. On the flat surfaces of the foam the amounts of Rh and Al (as atomic ratio) are larger than the expected values, while the Mg-content is lower. On the other hand, where the thickness of the solid is higher, the solid appears enriched in Mg with a M^{2+}/M^{3+} atomic ratio >3 (instead of 3.0). These results agree with those obtained during the synthesis of MgAl samples at -1.2 V for 2000 s.

After calcination, the morphology of both samples does not change to a great extent, but some uncovered zones where alumina grows are observed, while crack development is noticed on the covered areas (Figure 52).

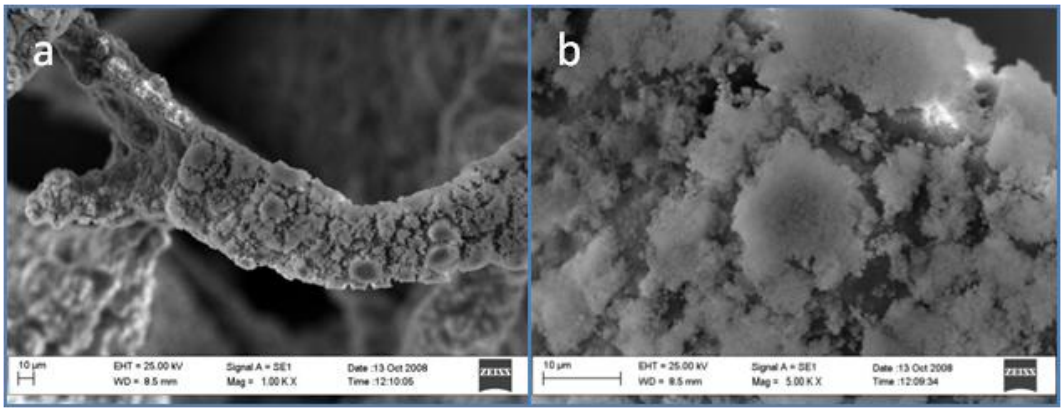

Figure 52: SEM images of a sample synthesized at -1.2 V for 1000s, at pH=3,8, after calcination

To improve the coating quality, some samples were prepared at -1.3 V for 1000 s after the adjustment of the pH of the working solution to 3.8 in order to check the effect of a more cathodic applied potential.

In such conditions the pH increases faster and higher values are obtained, as previously reported in the study of pH evolution. A thick layer is deposited on the surface of the most exposed parts of the foam (Figure 53a) and a thin layer coats the support on the flat surfaces. The chemical composition of the film is closer to that of the plating solution. It should be noted, however, that some cracks are present in the thicker layers (Figure 53a), which may be related to:

- the formation of H_2 bubbles during the synthesis on the foam surface as the applied potential increases;
- the drying of the HT phase;
- the shearing stresses between the support and the deposit [67].

After calcination, coatings exhibit an arrangement of flakes and interconnected surface cracks (Figure 53b) that may be related to a shrinkage mechanism, as previously reported.

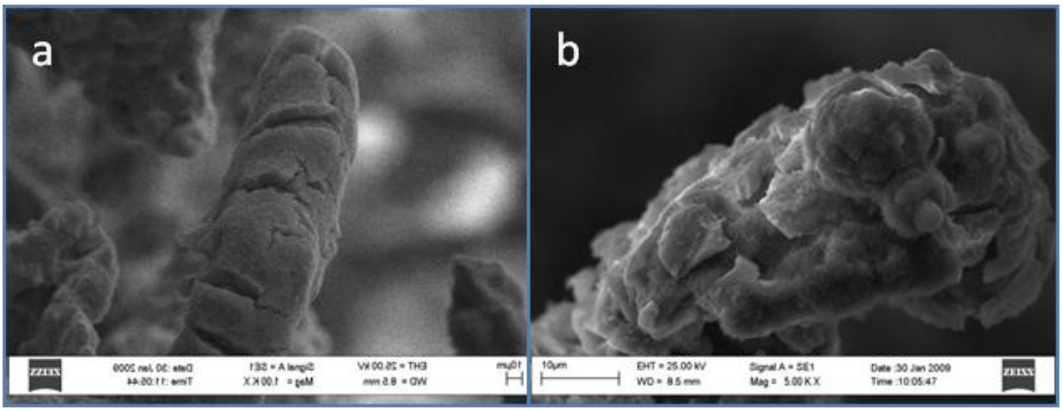

Figure 53: SEM images of a sample synthesized at -1.3 Vfor 1000 s before (a) and after (b) calcination

It should be noted that the morphology and size of the particles are similar regardless of the potential applied (-1.2 V or -1.3 V). In the initial stage, nucleation and particles growth compete each other. The nucleation reaction rate may be high and exceed that of particle growth [67], justifying the similar sizes of the particles. The deposition of small particles would also increase their adhesion to the substrate [68].

To obtain information about the nature of the solid precipitated during the electrodeposition, several syntheses was performed in a FeCrAl plate, immersed in a solution containing the salts of the cations at a corrected pH value, at -1.2 and -1.3 V for 1000 s. The powder was scratched with a lanzet and XRD measurements were carried out (Figure 54).

The hydrotalcite structure was obtained performing the synthesis at both potentials, being more intense the diffraction lines for the sample obtained at a more cathodic potential. Furthermore, the brucite ($Mg(OH)_2$) phase was detected as side-phase. The differences between these results and those obtained in the previous chapter, where no brucite was observed, may be related to the different nature of the support used as working electrode (FeCrAl vs Pt).

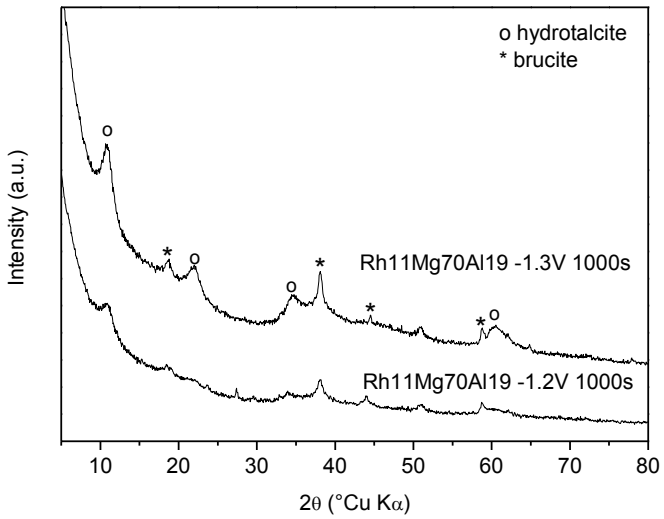

Figure 54: XRD patterns of powders synthesized after the initial pH adjustment

After calcination, MgO and spinel-type ($MgAl_2O_4$ and $MgAlRhO_4$) phases are identified. The formation of the $MgAlRhO_4$ phase, not observed in catalysts obtained from LDH compounds was related to the high content of Rh in the catalysts [69]. However, it should be remarked that the final products from calcination can also results from the possible reaction between the cations of the LDH and the alumina formed during the oxidation of the foam, therefore the actual oxide/spinel ratio may be modified.

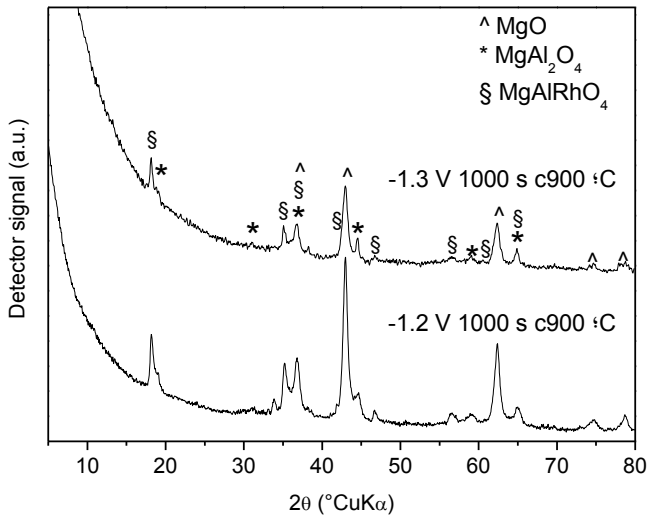

Figure 55: XRD patterns of powders synthesized after the initial pH adjustment after calcination

TPR analyses of the coated foams were performed to show the reducibility of the rhodium species (Figure 56). Two different behaviours were observed in the TPR profiles depending on the pH of the plating solution. The catalyst prepared at a pH value of 2.1 is formed by Rh^{3+} species which are easily reducible. A single H_2 consumption with maximum at approximately 200 ºC is observed. The reduction temperature is similar to that reported for rhodium oxide

species with low interaction with alumina [70] in agreement with EDS data. Conversely, catalysts prepared at −1.2 and −1.3V adjusting to 3.8 the initial pH, show the characteristic profiles of well stabilized Rh-containing particles [69, 71], with a H_2 consumption with maximum at about 550 ºC, and a shoulder at lower temperature, together with a rather complex reduction at temperatures above 700 ºC.

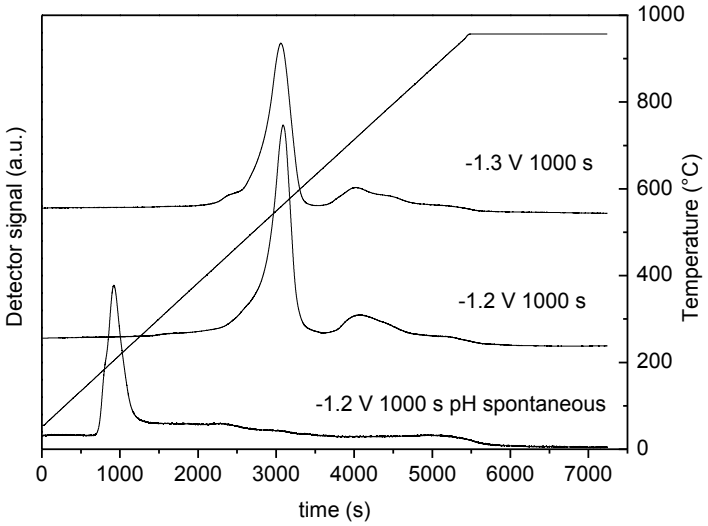

Figure 56: TPR analysis of samples synthesized at -1.2 V and -1.3 V at initial pH=3.8, and at -1.2 V at initial pH=2.1

The effect of feed mixture concentrations (CH_4/O_2/He =2/1/4 and 2/1/20 v/v) on the catalytic performances was also investigated. In Figure 57 the conversion of CH_4 and selectivity to CO and H_2 are plotted. O_2 conversion was complete during all the tests. First of all, blank tests were performed with two bare metal foam pellets, and a low CH_4 conversion to CO, H_2, CO_2 and H_2O was observed during the test with the most concentrated mixture.

Catalytic data indicate that the catalysts prepared at spontaneous pH and at controlled pH at -1.3 V for 1000s are active and stable during catalytic tests. High conversions of methane a and selectivity in syngas are displayed by both catalysts regardless of the concentration of the gas mixture, although the sample prepared at a more cathodic potential shows a slightly higher activity. On the other hand, the catalyst obtained from the LDH precursor synthesized at −1.2V with the initial pH adjustment to 3.8 shows poorer performances with a different trend as a function of the test conditions. An increase of the CH_4 conversion is obtained feeding the concentrated (2/1/4 v/v) mixture since higher temperatures are reached in the catalytic bed.

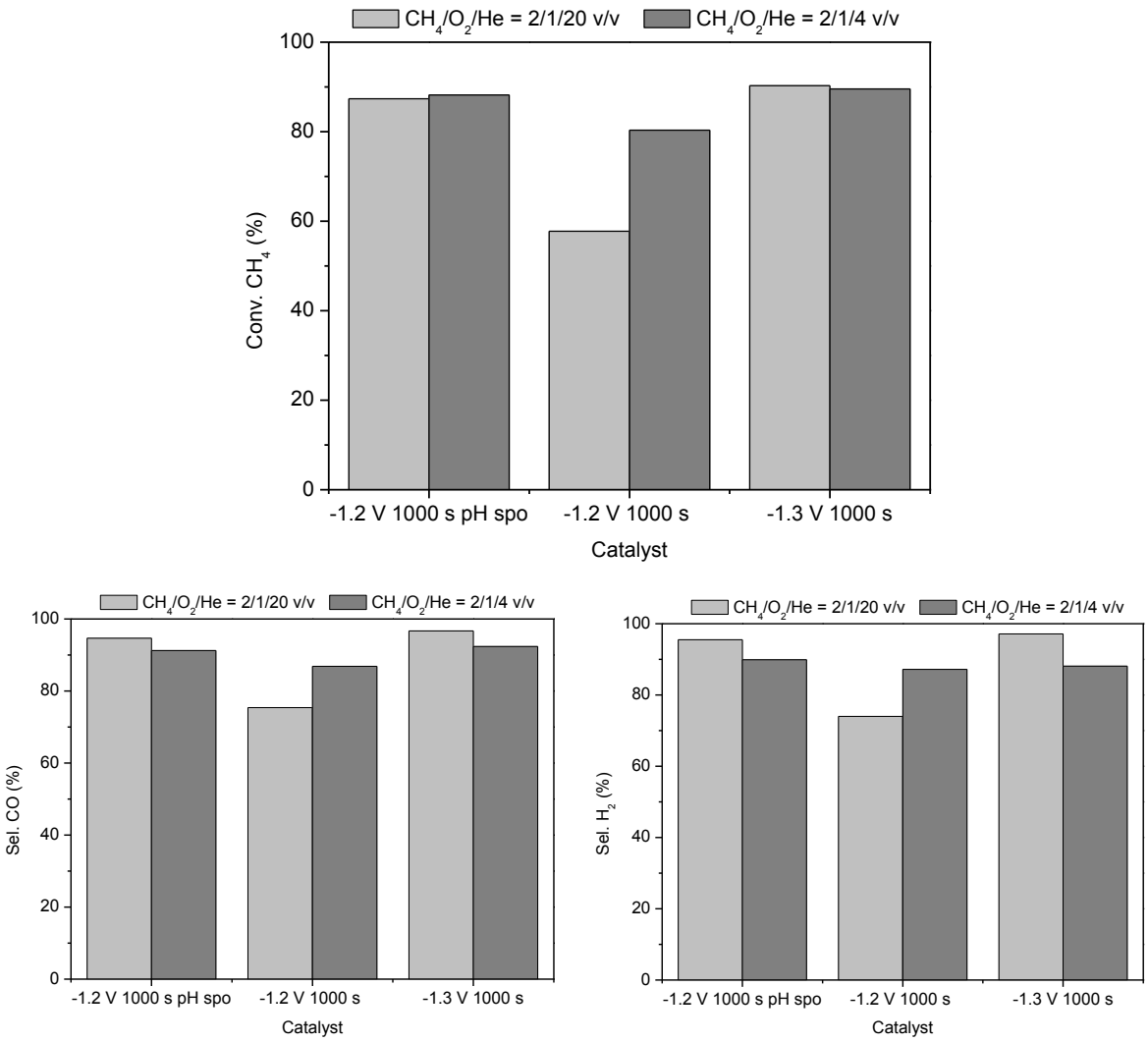

Figure 57: CPO performances of sample synthesized for 1000 s at -1.2 V and -1.3 V at intial pH=3.8, and at -1.2 V at initial pH=2.1

The morphology of the samples after performingcatalytic tests was investigated by SEM and EDS analyses. The one coming from the precursor synthesized at -1.2 V, at the spontaneous pH of the plating solution, is formed by flakes of catalyst and many cracks (Figures 58a and 58b); furthermore, some flakes appeared detached during catalytic tests. They are compact and EDS analyses indicate that they are mainly composed by Al and Rh, with a relatively low content of Mg, as already observed for the fresh catalyst. Small particles are present in the cracks, which may be related to the formation of alumina, although, EDS and backscattering images point out the additional presence of Rh (Figures 58c and 58d). Furthermore, some carbon nanotubes and amorphous carbon (Figures 58e and 58f) are detected both in the catalyst and in a larger amount, on the foam surface. SEM images of the spent catalyst prepared at-1.2 V, after the pH correction, show that the morphology of the original catalyst film is mainly retained (Figures 58g and 58h). In the uncovered zones, already observed in the fresh sample, EDS analyses reveal a small carbon content, but no carbon structures have been detected.

In the case of the samples prepared at-1.3 V, the characterization of the used catalyst shows, the cracks are not propagated, thus indicating a high adhesion of the coating to the surface; furthermore, Rh particles are observed in the catalyst flakes. Some morphological differences, however, are observed in dependence of the analyzed the section of the catalyst, that may be related to their position in the catalytic bed or to differences in the morphology of the catalyst during the preparation. Part of the foam pellets placed in the inlet of the catalytic bed is exposed to high temperatures, leading to the sintering of rhodium particles and to the formation of cracks in the catalytic film. Because of the lower temperatures close to the outlet, the morphology of the film may be retained.

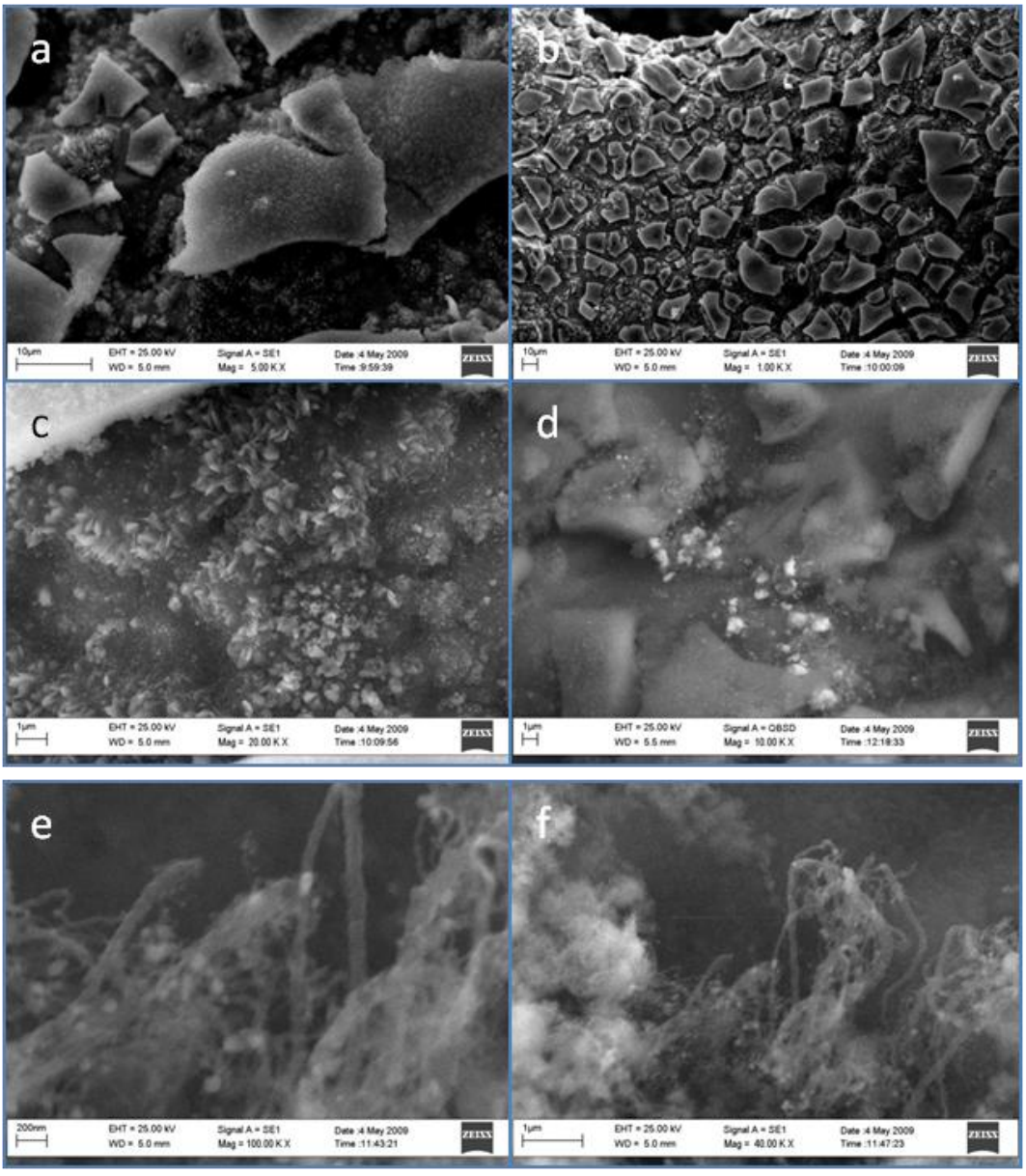

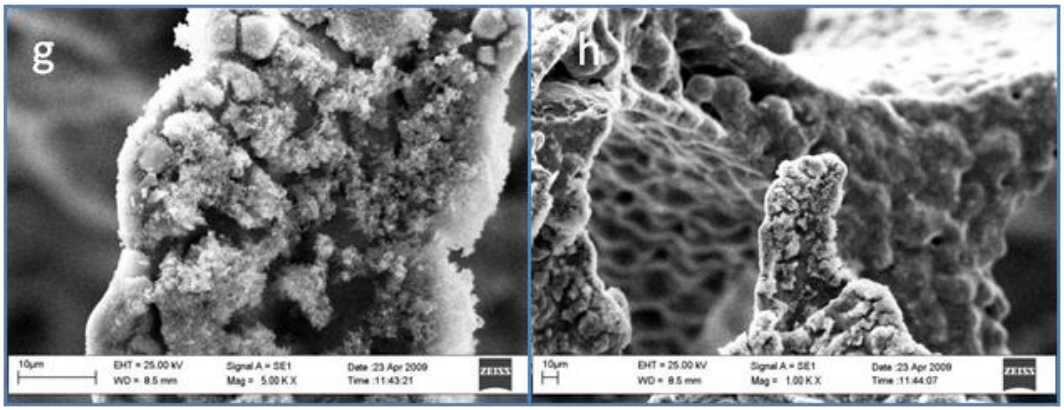

Figure 58: SEM images of a used sample synthesized at -1.2 V for 1000 s at the spontaneous (a-f) and adjusted pH (g and h)

By taking into account the characterization of the catalysts before and after the catalytic tests as well as the catalytic results, it may be stated that the performances of the structured catalysts are strongly related to the amount of active phase, homogeneity and stability of the catalytic coating. The good performance of the catalyst obtained from the LDH precursor, synthesized without controlling the pH, may be ascribed to a large Rh amount, despite of the low stability of the catalytic layer. Likewise, the poor activity of the catalyst prepared under the same synthesis conditions, but adjusting the pH of the plating solution, may be related to both the lower Rh content and to the poor coverage of the foam by the catalyst.

These comparisons confirm that the chemical nature and morphology of the coating, as well as the degree of coverage of the metallic foam, depend on the pH of the electrolytic solution. Consequently, also the catalytic performances (methane conversion and syngas selectivity) are strongly related to the synthesis parameters. The control of the pH of the plating solution (2.1 or 3.8) plays a key role in the formation of LDH phases vs the Rh^{3+} reduction. For these reasons, all the subsequent syntheses were always carried out after the adjustment of the pH at 3.8.

The best performances and stability of the catalyst prepared by applying a higher cathodic potential may be attributed to a larger Rh amount, a better dispersion and higher interaction between support and catalyst as well as between Rh metal particles and the oxide matrix which are present inside the catalyst. The applied potential also affects the nature and the thickness of the layer together with the degree of coverage of the support. However, the catalytic layer obtained in these conditions is more exposed to cracks.

5.4.4 INFLUENCE OF TIME

The synthesis time may influence the characteristics of the deposited film too. Therefore the dependence on the time for which the electrosynthesis is carried out was investigated for the applied potentials-1.2 V and -1.3 V. In these experiments the diameter of the foams was

increased to 1 cm due to technical issues in the catalytic reactor. A higher diameter causes a slightly higher resistance exhibited by the electrode material, that could lead to some differences in respect to the previously described samples electrosynthesized for 1000 s. The catalysts have been tested in SR reaction.

As far as the lower potential is concerned three set of foams were tested by performing the synthesis for 1000, 1500 and 2000 s, respectively, after the adjustment of the pH of the bulk solution to 3.8.

From the SEM images of the precursor samples a clear correlation between the synthesis time and the amount of deposited material can be established. An increase in the thickness of the layer is observed when the synthesis is carried out for longer times on both tips and flat zones, but a better and thicker coverage is still observed on the tips, as showed in Figure 59. Although, the thickening of the deposited layer with the increasing of time induces cracks development also on the precursor samples (Figure 59h), particularly on flat zones. Probably it is caused by the drying in oven, where the loss of water and the shrinkage of the layer,more probable if it is thick, can occur.

A more uniform coating is obtained for higher deposition times as well. However, in the sample synthesized for 2000 s, poorly covered zones were observed inside the cracks (Figure 59i), where the presence of some round particles was also detected.

An evolution in the morphology was noticed on the tips. For low deposition time the film was composed by compact clusters (Figure 59d), that became smaller when the synthesis is going on longer (Figures 59f and 59h).

The composition of the film, evaluated by EDS analyses, is not homogeneous in all the samples, although a better coating seems to be achieved with longer synthesis time. The Mg:Rh molar ratio is always higher than expected, i.e. the value of about 6.4 of the plating solution value of about 6.4. Minor differences in respect to the ideal value (3.7) were observed for the Mg:Al molar ratio, but it must be remarked that Al is also present in the foam alloy and so its amount in the layer composition is always overestimated. Moreover, a strong presence of K is pointed out particularly in the sample synthesized for 1000 s, which decreases for longer times. It is an unexpected behavior, but it could be explained by the higher dilution of the electrostatically adsorbed potassium due to the greater quntity of deposited material.

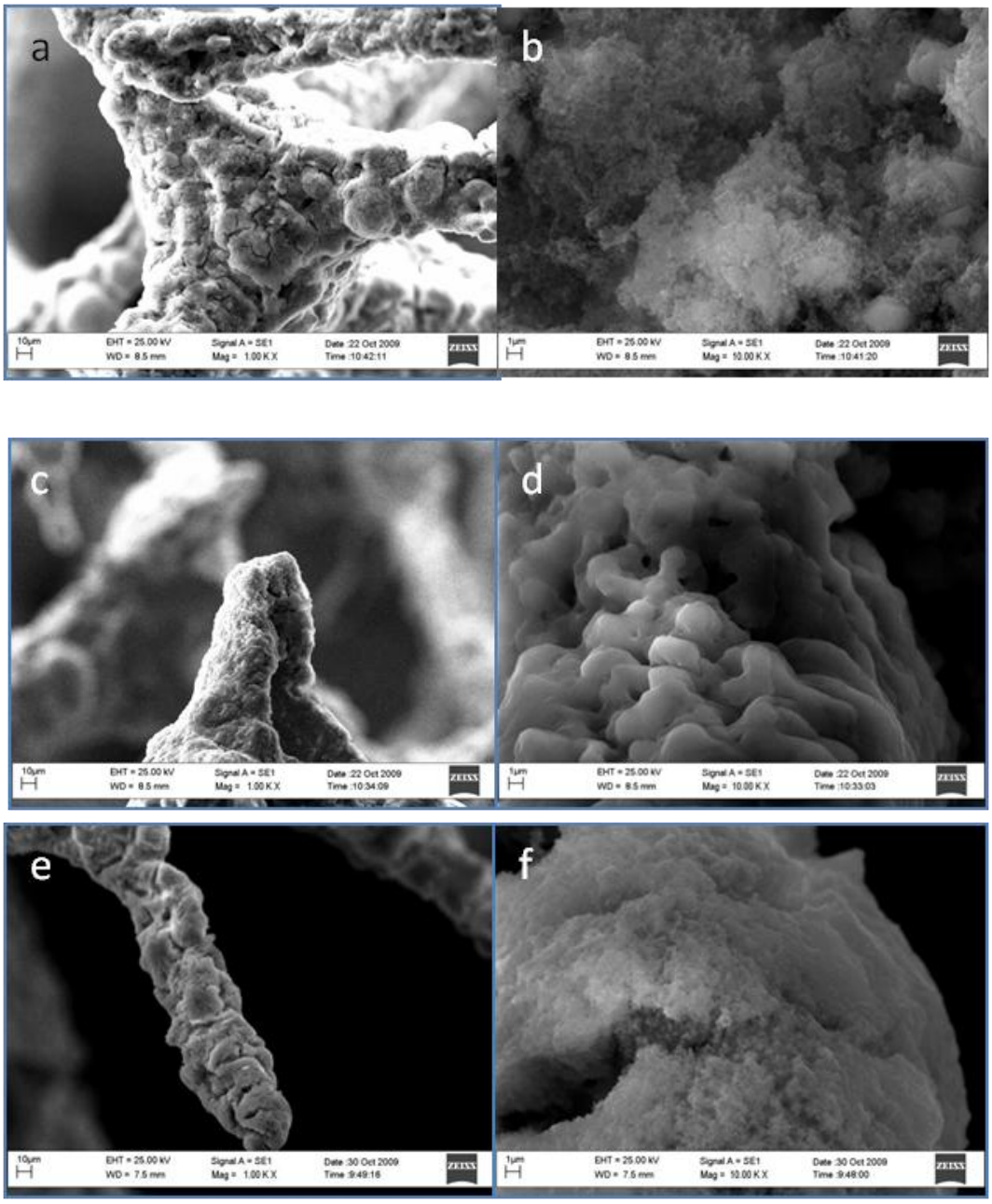
a
10µm
EHT = 25.00 kV
WD = 8.5 mm
Signal A = SE1
Mag = 1.00 K X
Date :22 Oct 2009
Time :10:42:11
b
1µm
EHT = 25.00 kV
WD = 8.5 mm
Signal A = SE1
Mag = 10.00 K X
Date :22 Oct 2009
Time :10:41:20
c
10µm
EHT = 25.00 kV
WD = 8.5 mm
Signal A = SE1
Mag = 1.00 K X
Date :22 Oct 2009
Time :10:34:09
d
1µm
EHT = 25.00 kV
WD = 8.5 mm
Signal A = SE1
Mag = 10.00 K X
Date :22 Oct 2009
Time :10:33:03
e
10µm
EHT = 25.00 kV
WD = 7.5 mm
Signal A = SE1
Mag = 1.00 K X
Date :30 Oct 2009
Time :9:49:16
f
1µm
EHT = 25.00 kV
WD = 7.5 mm
Signal A = SE1
Mag = 10.00 K X
Date :30 Oct 2009
Time :9:48:00

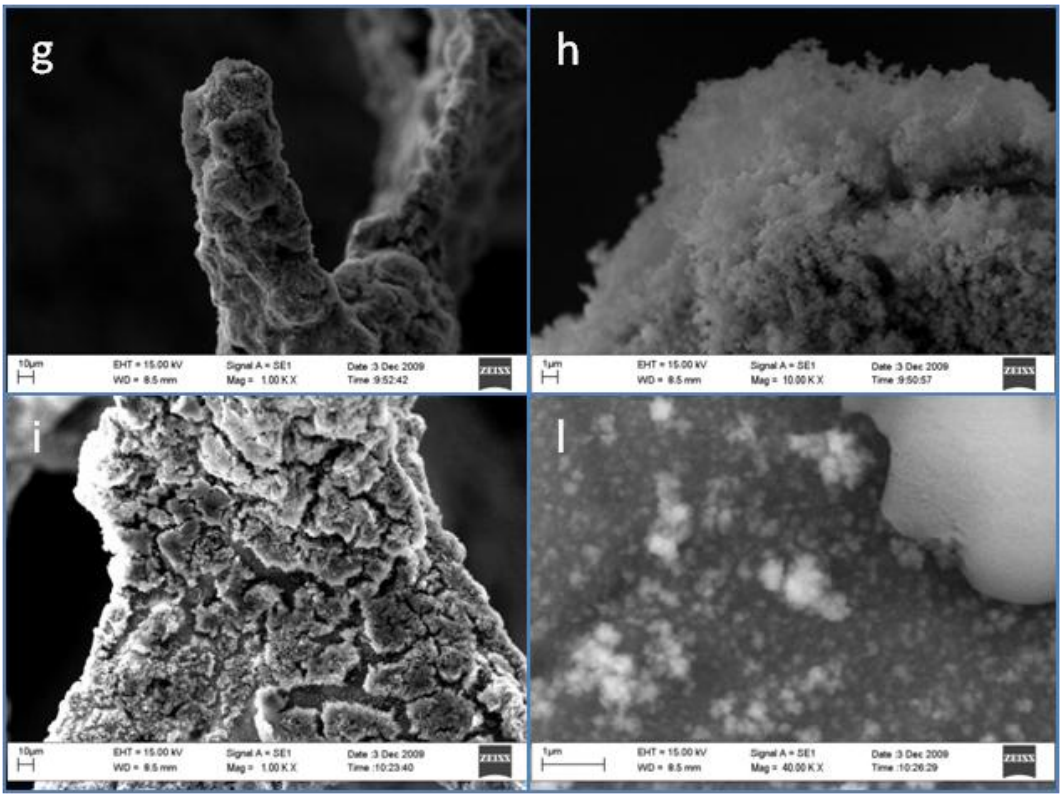

Figure 59: SEM images of samples synthesized at -1.2 V for 1000 s (a-d), 1500 s (e and f) and 2000 s (g-l)

After calcination, the cracks development and the content of aluminum are increased, while K presence is strongly decreased, as expected. A compaction of the small particles is observed, which produces a more compact layer (Figures 60a and 60b) for all the analyzed samples. The main differences observed with the lengthening of the synthesis time are those described for the samples precursors. For higher time, where the deposited layer is thicker, the crack development is more favored because it the film is subjected to a higher shrinkage. The Mg:Rh ratio is still higher than expected, according to the data collected for the precursor samples.

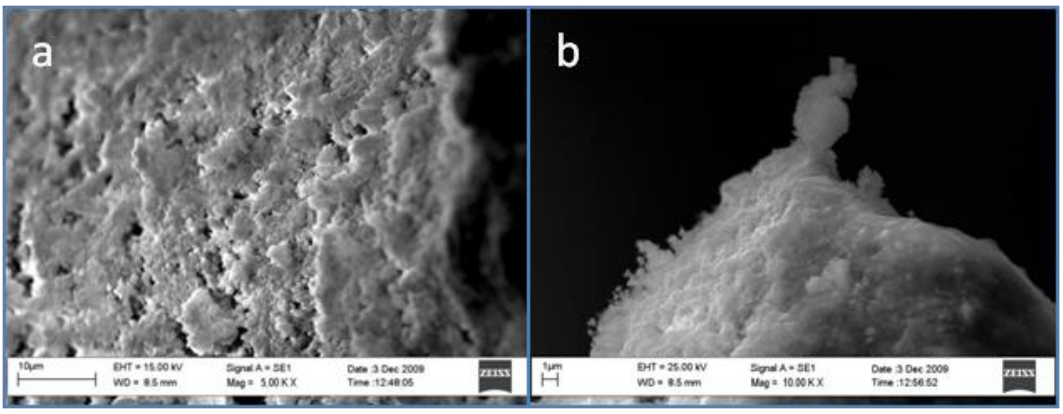

Figure 60:SEM images after calcination of a sample synthesized at -1.2 V for 2000 s

The distribution of the elements in the catalytic coating was obtained by mapping selected zones of the film by EDS. In Figure 61 a map of the elements is displayed: a good dispersion of the element and a good homogeneity of the coating are evident, particularly where the presence of thick film is observed.

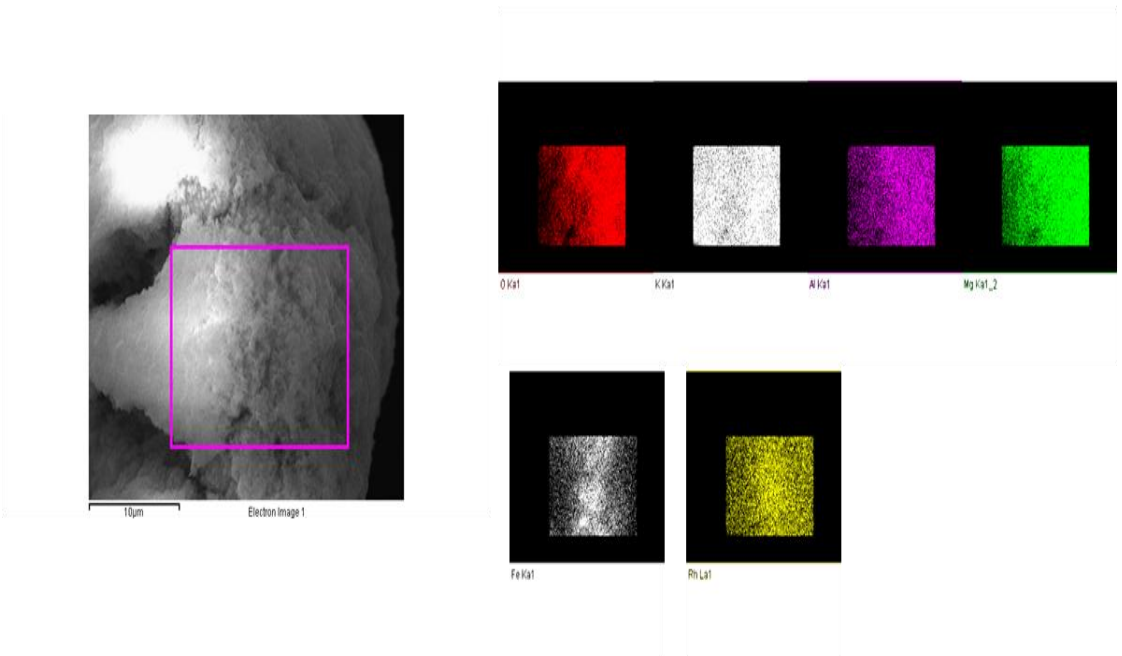

Figure 61: EDS mapping of a thick layer in a calcined sample. In order are shown O, K, Al, Mg, Fe and Rh dispersions

The calcined samples, in the case of the synthesis carried out for 2000 s, has been characterized by µ-XRF/XRD tomography at synchrotron (Figure 62). This analysis is really important to detect the phases present on the sample, because it can be carried out directly on the metallic foam structure, without employing a plate, as for other reported XRD patterns.

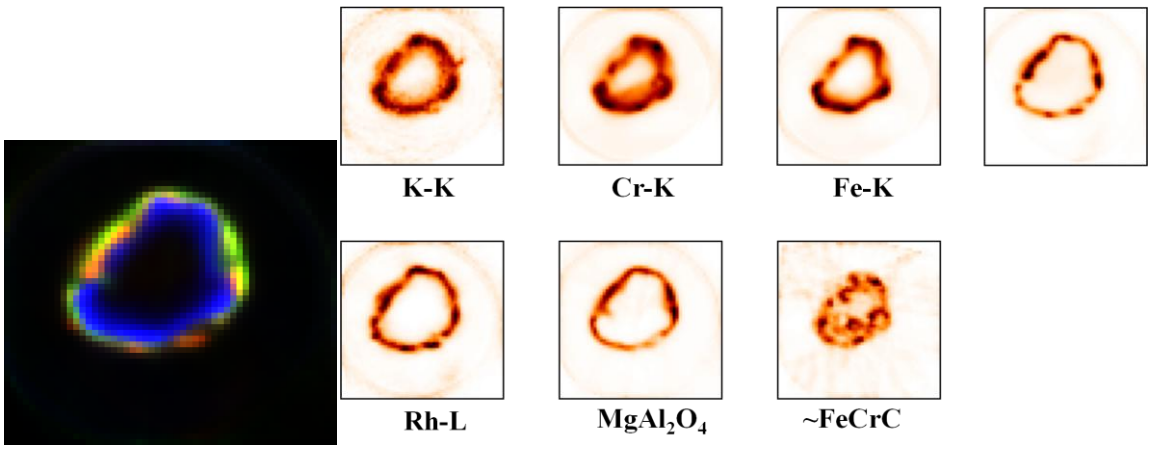

Figure 62: µ-XRD/XRF tomography performed at synchrotron of a calcined sample synthesized at-1.2 V for 2000 s

The XRF gives information about the distribution of the elements, whereas the distribution of the crystalline phase was obtained by µ-XRD. The XRF tomography confirms the presence

of Cr and Fe in the foam. Moreover it is clear the presence of K and Rh in the catalytic coating. The catalyst is composed by $MgAl_2O_4$ and a good correlation between Rh and the spinel phase is observed.

When a more cathodic potential is applied to the foam, the effect of a longer electrosynthesis time are different: a higher coating degree is observed for the sample synthesized for 1000 s in respect to the sample prepared for 1500 s. Several uncoated zones were, however, detected in both samples by back scattering images (Figure 63), and this behavior is probably due to an increase in H_2 bubble evolution at the surface of the foam because of the higher applied potential. This can also induce the detaching of the deposited layer during synthesis (Figure 63c).

Concerning the morphology of the electrosynthesized solid, aggregates of small particles were observed on flat zones (Figure 63a and 63b), while a more compact coating was obtained on the tips, in according with data collected for an applied potential of -1.2 V.

In both samples the Mg:Rh molar ratio is generally higher than expected. However, on some covered tips a value between 6.3 and 6.7 is detemined in the 1500 s sample, that is close to the expected 6.4. It decreases down to 2 if the synthesis time is shorter, pointing to the formation of aggregates of particles rich in Rh. Also the K content decreases for longer synthesis time, confirming the effect of bubbles evolution also on the electrostatic cation adsorption.

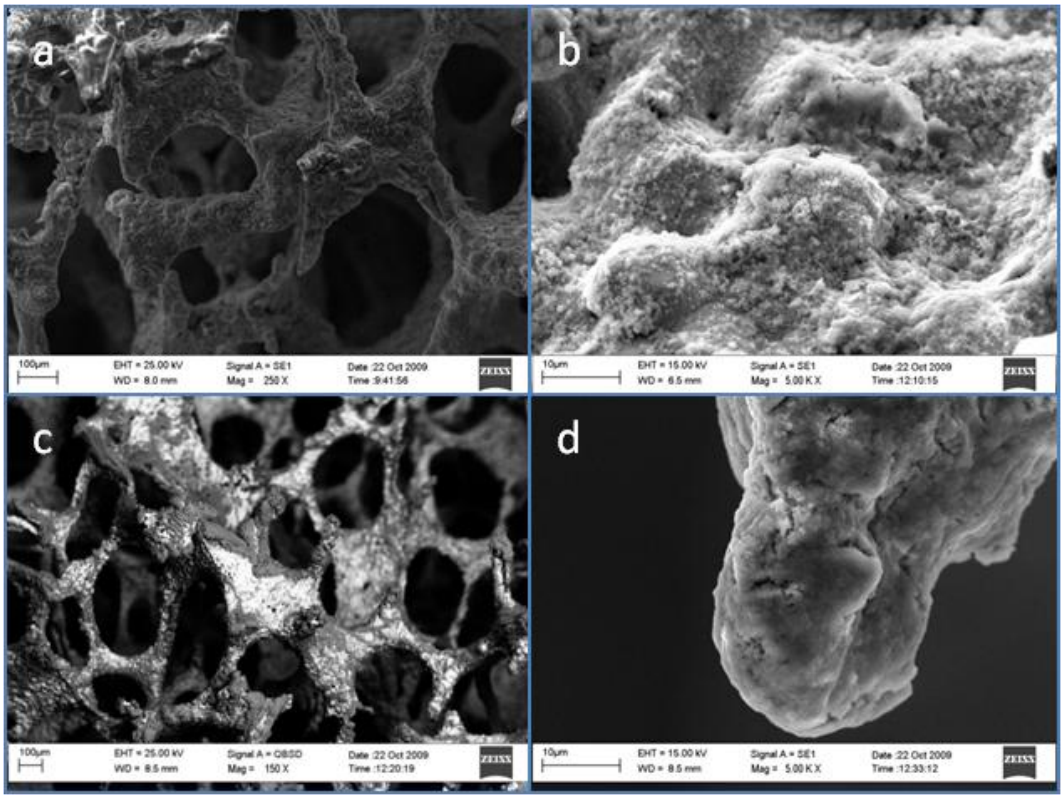

Figure 63: SEM images of sample prepared at -1.3 V for 1000 s (a and b) and 1500 s (c and d)

After calcination, in addition to the expected enhancement of cracks development, some crusts, mostly located on tips, were observed, as shown in Figure 64. This morphology was not so definitely detected in the fresh samples. In these zones, the layer seems to be more compact and uniform, and a low Mg:Rh molar ratio was detected. The lowering of K^+ content and the growth of the alumina layer were observed as well.

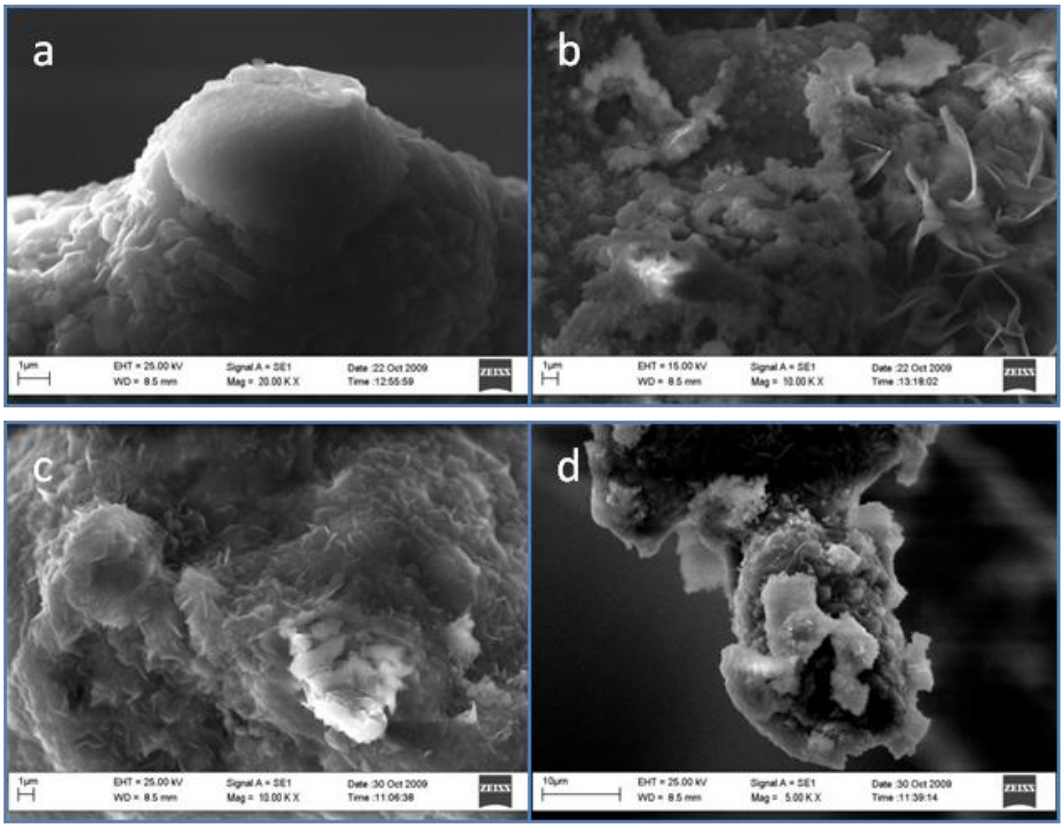

Figure 64: SEM images of calcined samples prepared at -1.3 V for 1000 s (a and b) and 1500 s (c and d)

The catalysts prepared at different potential and synthesis time were tested in the steam reforming of CH_4 under industrial-like conditions. Six foam pellets were used and tests were performed at T_{oven} = 920 ºC, P = 10 bar, S/C = 2.5 and τ = 3 s. The methane conversion and H_2 yield obtained with the different catalysts are displayed in Figure 65.

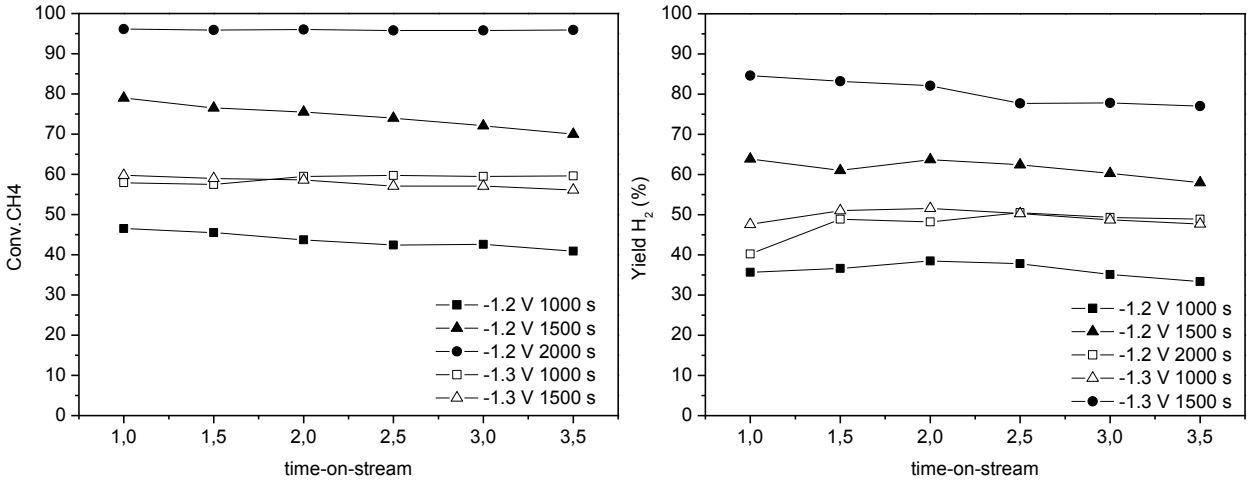

Figure 65: SR performances of catalysts synthesizes at -1.2 V for 1000, 1500 and 2000s, and at -1.3 V for 1000 and 1500 s

The methane conversion and H_2 yield strongly depend on the synthesis conditions and the same trend previously observed during CPO tests is here reported. The increase of the potential applied from -1.2 V to -1.3 V improved the performances; however, 1000 s is a short synthesis time: methane conversion and H_2 yield values are low, and the catalyst prepared at -1.2 V deactivates with time-on-stream. The increase of the synthesis time has two different effects depending on the potential applied. Concerning the catalysts obtained from the samples prepared at -1.2 V the longer the electrosynthesis the better the catalytic performances. The catalysts prepared for 2000 s show a high and stable methane conversion (ca. 95 %); however the H_2 yield decreases during the tests. On the other hand, for the samples prepared at -1.3 V, it would appear that performing the syntheses for longer times does not improve the performances but decrease them.

SEM and EDS analyses of the used samples show that the morphology of the deposited films is retained in respect to the relevant analyses carried out after calcination for the conditions of synthesis. Round Rh particles are better detected on the film surface from back scattering images. However, the dispersion of the particles is different depending on the synthesis conditions. In agreement to the higher activity found out in the catalytic test, more and better dispersed Rh particles were detected in the samples synthesized at -1.2 V with respect to -1.3 V (Figures 66b, 66d and 66f), with an increase in number and dimension in the sample synthesized for 2000 s in comparison to the one deposited for 1500 s. A low number of particles is instead observed for a synthesis time of 1000 s, according to the lower amount of deposited material detected in the analysis of the precursor sample. When a more cathodic potential is applied a lower number of particles with a higher agglomeration is obtained (Figure 66f), resulting in a less active catalyst. However, the number of Rh particles increases when longer syntheses are carried out. The hydrogen evolution that leads to a less covered surface, as described before, may be responsible for the not increased activity of the catalyst synthesized for 1500 s.

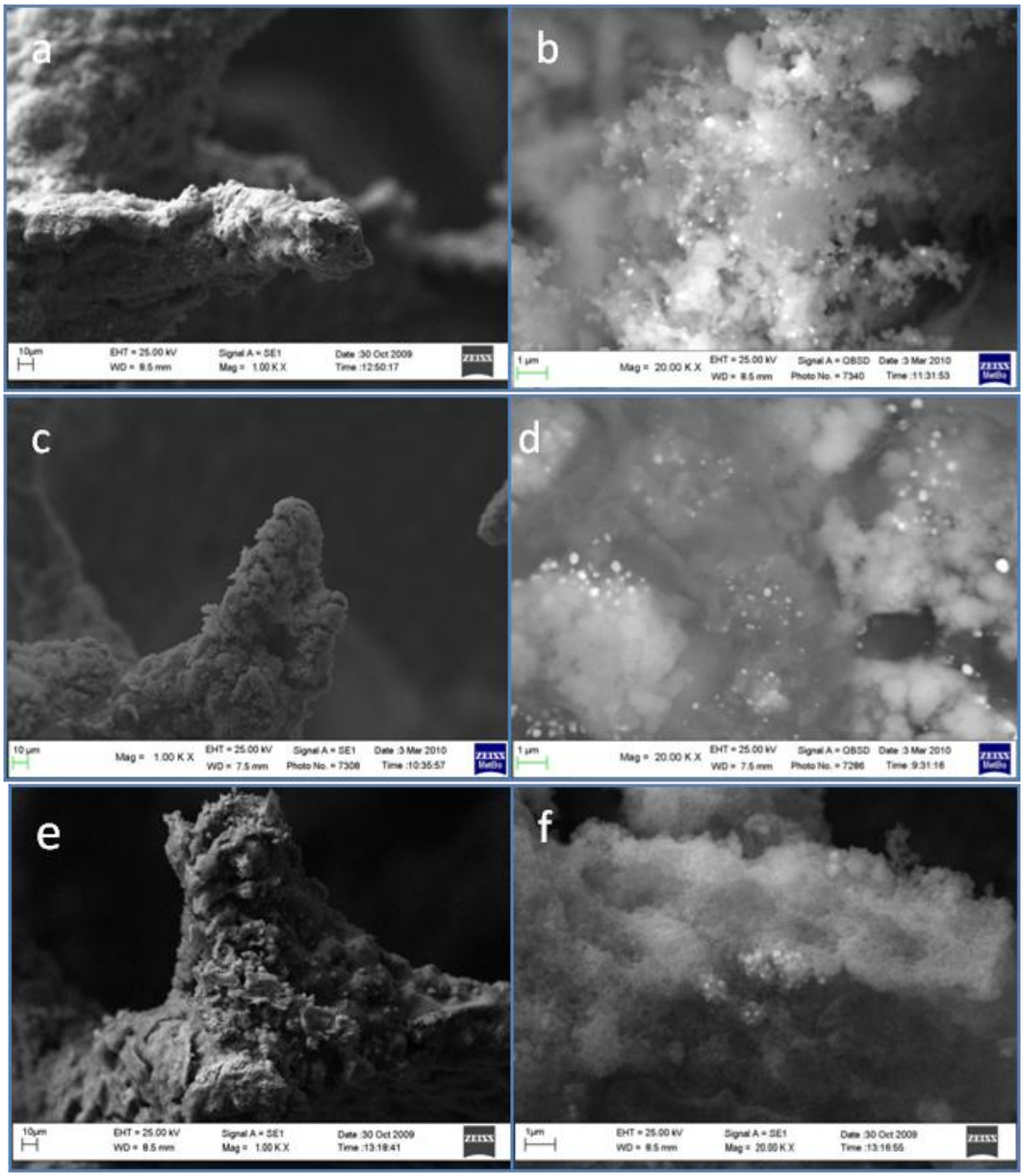

Figura 66: SEM images of a calcined sample prepared at -1.2 V for 1000 s(a and b), 2000 s (c and d), and at -1.3V for 1000 s (e and f)

The characterization by µ-XRD analysis has been carried out also on the catalyst after the use in the reactor (Figure 67). It shows the presence of all the phases found in the calcined catalyst, suggesting that no loss of catalyst occurs during the use in the reactor. In this case the presence of α-Al_2O_3 coming from the oxidation of the foam is observed.

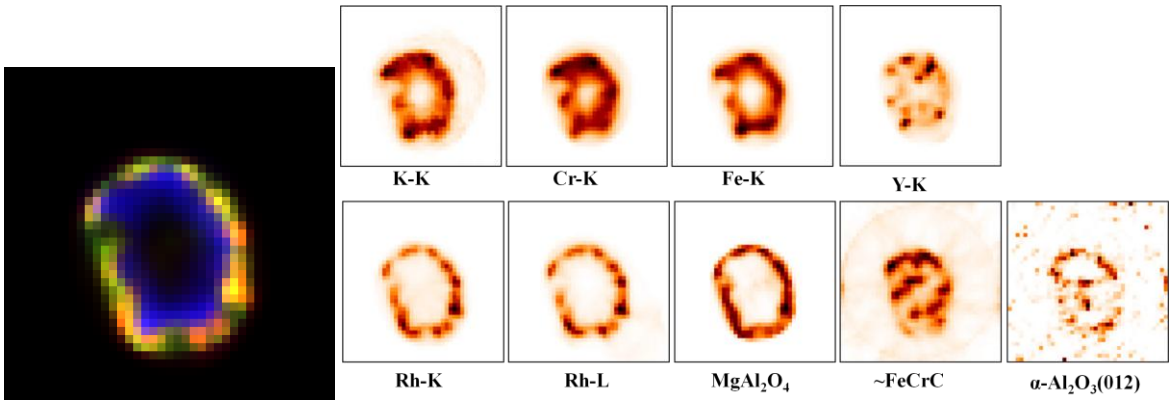

Figure 67: µ-XRD/XRF tomography performed at synchrotron of a used sample prepared at-1.2 V for 2000 s

5.4.5 USE OF THE CELL WITH A CYLINDRICAL CE

The previous syntheses were carried out in a common three-electrode electrochemical cell. However, a not homogeneous covering of whole foam was always observed. This could be due to the cell geometry (Figure 10) that does not allow the same charge exchange in every point of the cylindrical foam. To overcome these drawbacks, the electrochemical cell with a cylindrical Pt counter electrode (Figure 11) is employed for all the subsequently described experiments. It allows a better ratio between the surface area of the foam (WE) and that of the CE, leading to a better charge exchange and to a more uniform application potential, which should results in a more uniform coating on the whole foam surface.

Samples prepared at -1.2 V for 2000 s demonstrated that a more homogeneous coating of the outer surface of the foams was obtained. Apart from the higher homogeneity, the characteristics of both fresh and calcined films were the same as described previously for the sample synthesized in the same conditions.

Other samples were synthesized applying a potential of -1.1 V for 2000 s employing the same plating solution already utilized for the syntheses at more cathodic potential. A good coverage degree and a higher amount of material than in the sample synthesized at -1.2 V were detected on the whole foam surface. Also in this case the SEM and EDS analyses do not reveal any unexpected behavior in both the fresh and the calcined samples.

Catalytic tests have been carried out in order to check the activity of these samples over the CPO reaction (Figure 68). The catalyst prepared at -1.1 V showed slightly better performances (CH_4 conversion, selectivity to CO and selectivity to H_2) than the sample prepared at -1.2 V, both by feeding the diluter (2/1/20 v/v) or concentrated gas mixture. The increase of the activity by concentrating the gas mixture is related to an increase of the temperature within the catalytic bed. However, it should be remarked that the performances are still far from those of the thermodynamic equilibrium. The differences among the catalyst may be related not only to the quality of the coating but also to the amount of potassium that can block some active sites.

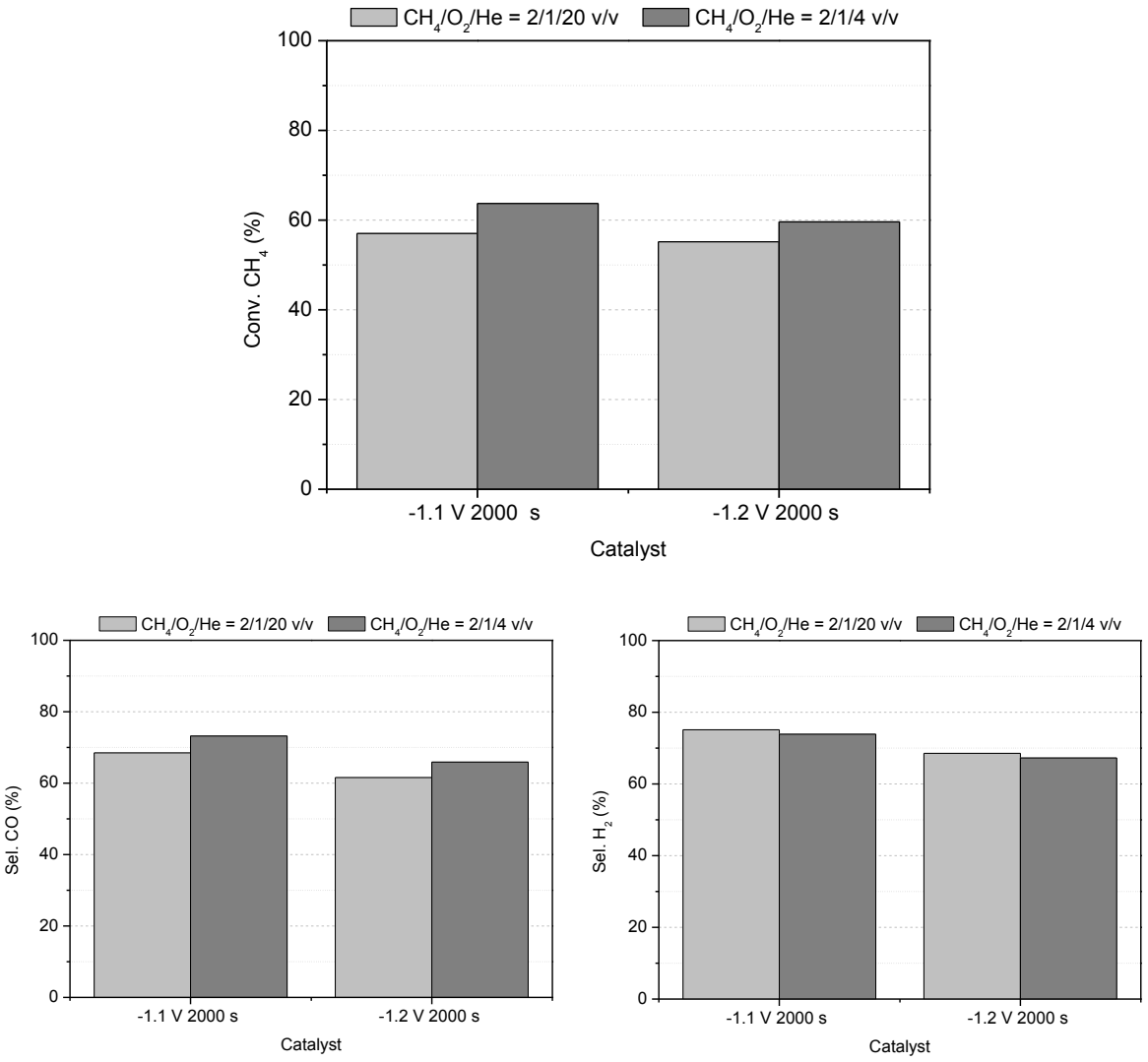

Figure 68: CPO performances of catalyst prepared with the round-CE cell at -1.1 V and -1.2 V for 2000s

5.4.6 DIFFUSION OF THE SOLUTION INSIDE THE FOAM

Despite the better results obtained with the employment of an electrochemical cell with a round counter electrode, EDS analyses of some cross-sections of the just described samples showed a very low amount of deposited material in the inner part of the foams, regardless of the working conditions. It seems that the diffusion of the solution into the pores of the foam hardly occurs, limiting the presence of material only to the outer part. To understand if the problem could be really ascribed to diffusion limitations, several synthesis of Ni_2Al_1-LDH were carried out with an applied potential of -1.2 V for 600 s on foam with different diameter, in order to verify if different % gain of weight were achieved. Since all the foams had the same porosity, the movement of the solution into the foams is expected to be equal. If the permeation is supposed to occur at least in the outer part of the foams, a higher percentage gain should be expected in smaller foams because a larger outer surface to molar ratio. Four groups of foams (A-D) were employed, which differs from each others in the diameter of the

foam (Table 5). Moreover the group with the higher diameter (1.2 cm) possesses also an inner hole with a diameter of 0.3 cm. Every group was made up of five metallic foams that were weighted before and after the synthesis of the Ni_2Al_1-LDH in order to calculate the gain of weigh for each foam.

	A	B	C	D
Outer diameter (mm)	12	10	7	5
Inner diameter (mm)	3	-	-	-

Table 5: Outer and inner, if present, diameter of each foams group

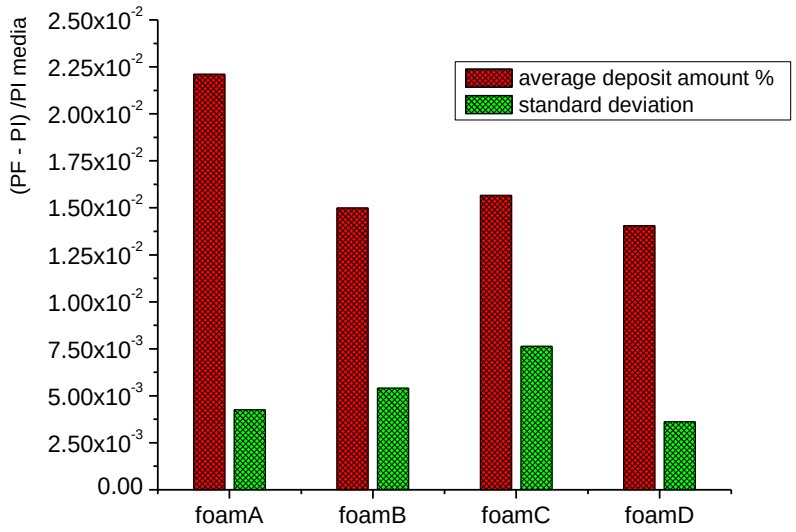

Figure 69: % weight gain and relative standard deviation for each group of foams

The collected data (Figure 69) show that practically no differences in % weight gain were observed changing the diameter of the foams, while there is a difference when a central hole is present. We can conclude that the % gain of weight only depends on the external area of the foam and that no permeation of the solution inside the foams occurs, in agreement with the data collected by EDS analyses.

5.4.7 SAMPLES SINTHESIZED UNDER STIRRING

Besides the problem of the permeation of the solution inside the foam, variable composition far from that of the plating solution were detected on the deposited layer, pointing to the segregation of different phases. This behavior could be due to a different diffusion rate of the

metal cations to the electrode surface caused by a different concentration after their consumption in the first stages of the precipitation.

Some syntheses were carried out under stirring for 2000 s at different applied potential (-1.1, -1.2, and -1.3) in order to solve the problems above cited.

The SEM and EDS characterization of the fresh samples when a potential of -1.2 V is applied showed that the deposited layer is not homogeneous, with a higher coverage degree on irregular regions, as observed for the previously described samples synthesized in the same conditions (Figures 70a and 70b), although a low amount of material seemed to be deposited. Moreover some uncovered zones were observed (Figure 70a). Probably the stirring mixes the composition both in bulk solution and at electrode/solution interface. Therefore, the migration of the generated OH^-, generated in the closeness of the electrode, may take place before they were consumed before the precipitation of hydroxide, resulting in a lowering of pH. However, the presence of Mg increases where a thicker layer is detected, reaching a molar ratio M^{2+}/M^{3+} higher than 3. Moreover the EDS analysis allows to distinguish the formation of some particles enriched in Rh on larger $Al(OH)_3$ aggregates.

Also this phenomenon is probably the result of the formation of potential gradients on the foam surface that lead to the precipitation of aluminum hydroxide and metallic rhodium instead of the desired LDH phase.

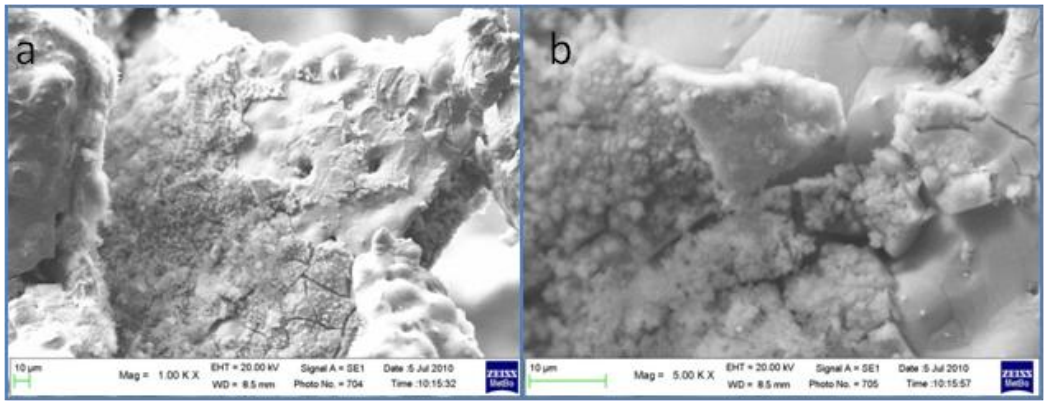

Figure 70: SEM images of a precursor prepared at -1.2 V for 2000 s under stirring

If a more cathodic potential (-1.3 V) was applied, the SEM analysis showed the presence of a quite homogeneous layer on both planar zones (Figure 71a) and tips (Figure 71b). The elemental distributions were more uniform, although a strong presence of potassium were noticed (Figure 71c). The M^{2+}/M^{3+} ratio was close to that of the plating solution, however also in this case Rh particles were detected (Figure 71d).

These results are not in agreement with those obtained at the same potential for 1000 s and 1500 s without stirring. In these samples a decrease of coating degree had been observed for longer synthesis times. The differences in the coating morphology are probably due to the beneficial role of the stirring under these conditions: the use of a non static system probably

removes the little hydrogen bubbles, avoiding their growth, that can cause the detaching of the deposited layer in several zones, as observed before.

However, during the electrosynthesis the bulk solution turns darker, and this is probably due to the reduction of Rh in bulk solution. It was shown (paragraph 5.3.2.4) that in proximity of the CE the pH becomes more acid during the measurement. Therefore, part of Rh present in the plating solution could be reduced in such conditions. Stirring probably enhanced this behavior, dispersed the metal particles and led to a darkening of the plating solution.

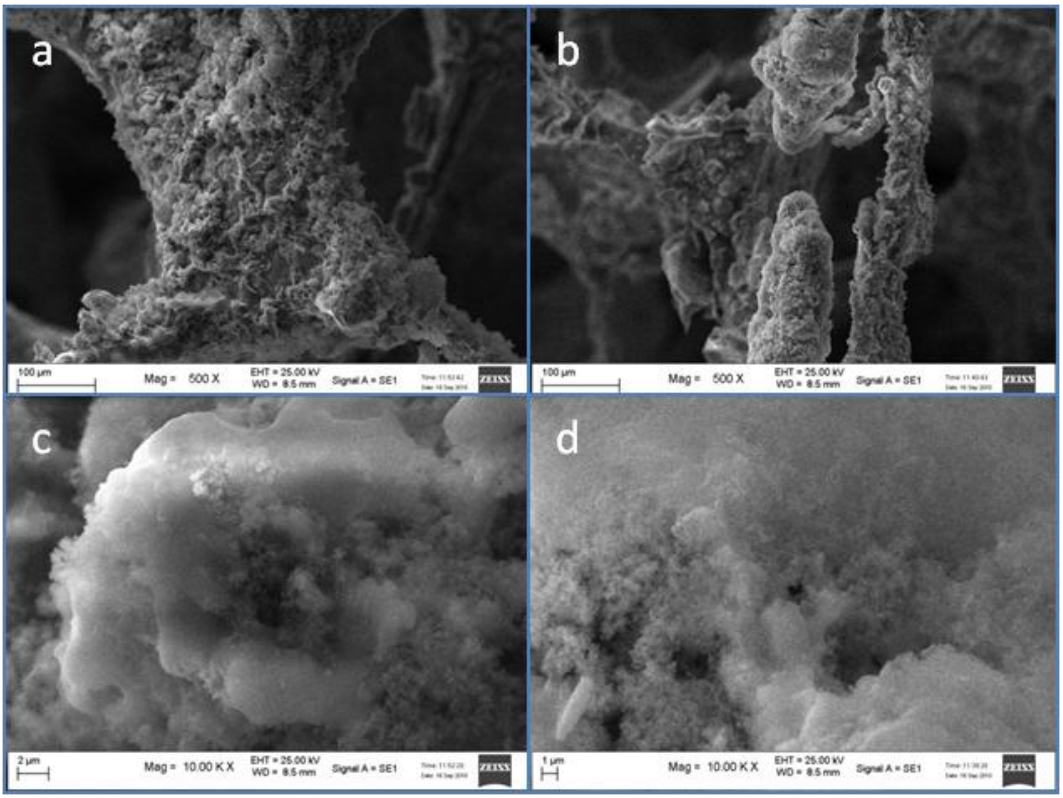

Figure 71: SEM images of a precursor prepared at -1.3 V for 2000 s under stirring

Finally, the influence of a lower potential, such as -1.1 V, was also investigated. From the morphologic analysis by the SEM, the surface of the foam appears to be covered homogeneously on the flat zones (Figure 72a) while there is a higher amount of deposited material on the tips (Figure 72b), in according to the behavior observed for most of the samples synthesized at -1.2 V. On the tips the EDS analysis reveals a higher presence of Mg that could be ascribed to the presence of the LDH phase. On the flat areas round metallic Rh particles were detected (Figure 72c). This could be one of the consequences of the low applied potential. From the discussion about the pH evolution nearby the electrode surface it comes that for this potential a pH of about 5.5-6 can be achieved. Such a low value does not avoid the precipitation of metallic rhodium on the flat areas. On the contrary, this doesnot occurs on the tips, because of the potential gradient that leads to a more basic pH at which the reduction of Rh does not take place. This is also confirmed by the higher amount of $Al(OH)_3$ detected when the surface is planar.

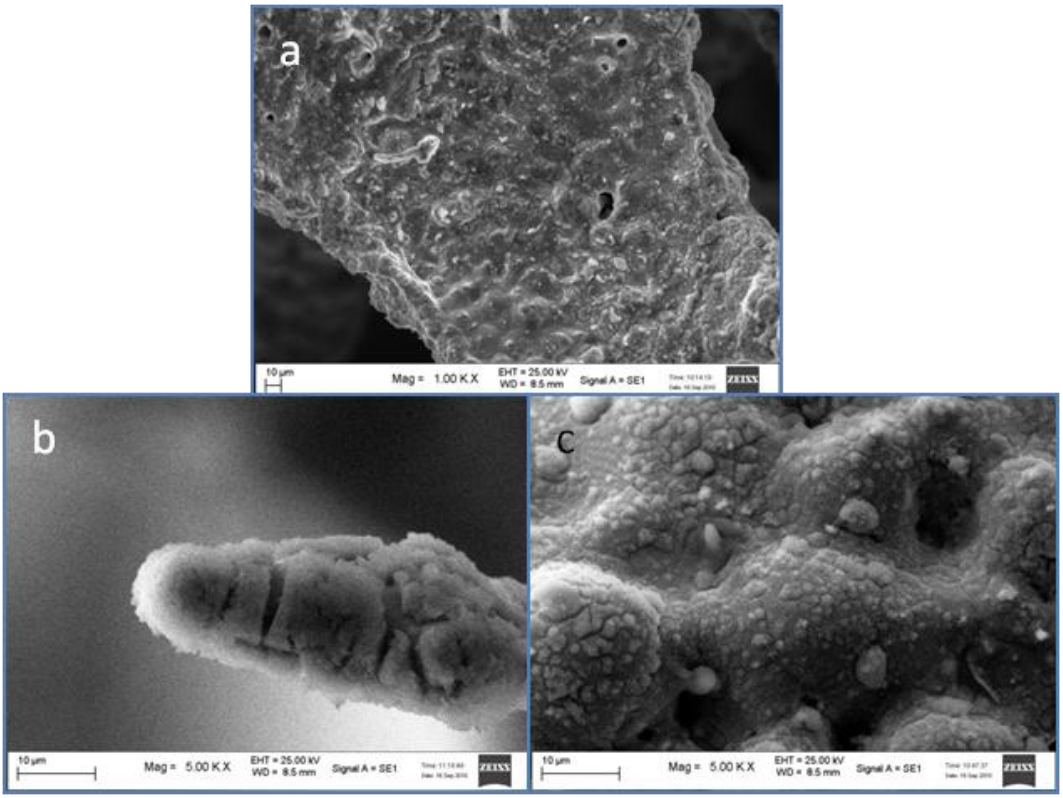

Figure 72: SEM images of a precursor prepared at -1.1 V for 2000 s under stirring

As expected, after the calcination process the main difference in the morphology is the enhancement of cracks formation for all the three samples that is provoked the phenomena explained before, such as CO_2, H_2O and NO_2 loss and difference between the thermal expansion coefficient of the foam and that of the deposited layer (Figure 73a). The formation of an Al_2O_3 layer is observed on not covered areas as the results of the oxidation of the FeCrAlY alloy as well as the Rh particles (Figure 73b).

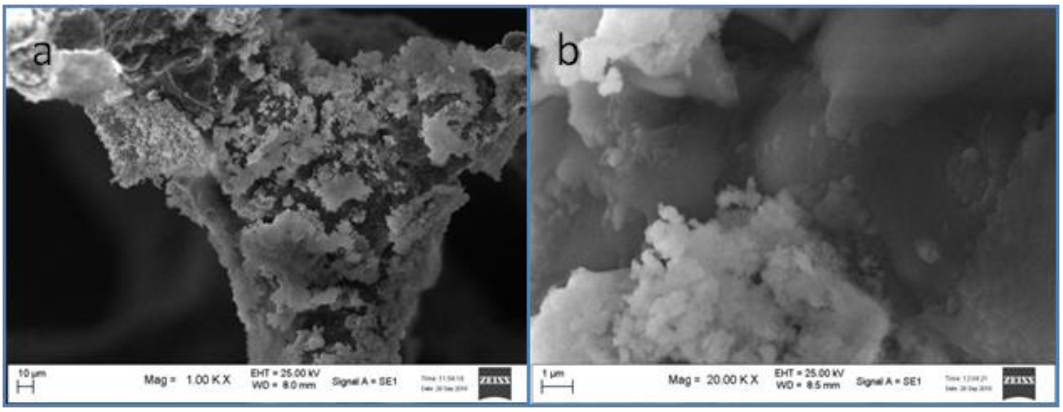

Figure 73: SEM images of a used catalyst prepared at -1.1 V for 2000 s under stirring

The catalytic activity of the samples obtained by calcination of the samples prepared under stirring at different potentials are shown in Figure 74. It can be observed that the activity increases when the potential is increased from -1.1 V to -1.2 V, it may be related to the thicker

coating and to the differences in the chemical composition. The negative effect observed by further applying a more cathodic potential may be explained in terms of potassium deposition, the large amount of potassium may block the accessibility of the reactants to the rhodium metallic active sites.

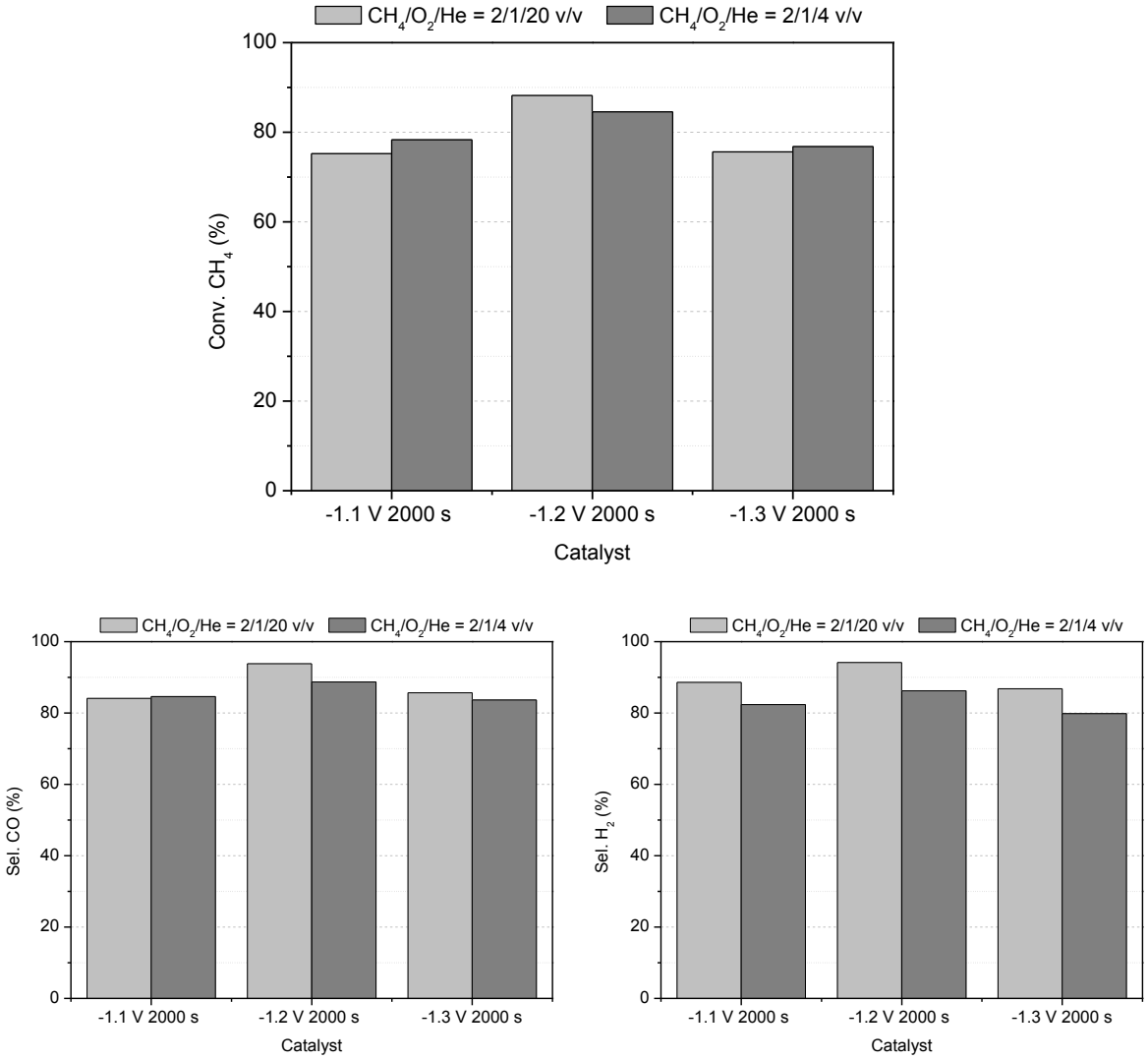

Figure 74: CPO performances of catalyst prepared at -1.1 V, -1.2 V and -1.3 V under stirring

By making a comparison between the performances of the catalysts obtained with and without stirring it could be stated that the addition of stirring improves the activity (Figure 75). It may be related both to the improvement of the coating degree and to the presence of a larger amount rhodium metallic particles, which already precipitated during the electrosynthesis. This behaviour is similar to that of the sample described in section 5.4.3. for the catalyst obtained at pH spontaneous of the plating solution.

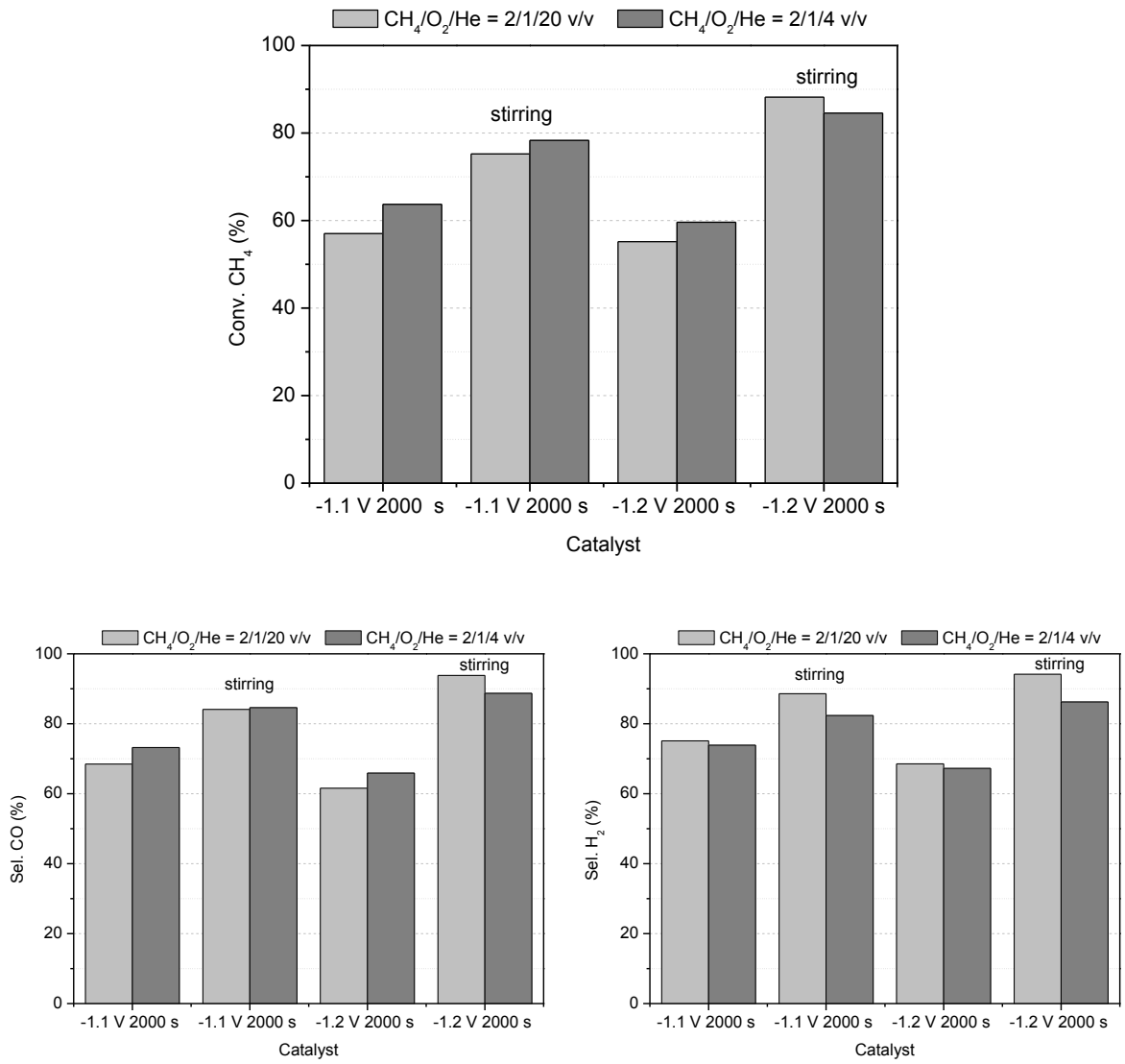

Figure 75: Comparison of catalytic performances for sample prepared at -1.1 V and -1.2 V with and without stirring

The SEM/EDS characterization of the used samples showed that the morphology of the layer were retained and Rh particles were observed in the catalyst flakes (Figures 76a, 76b, and 76c). A good adhesion between the deposited layer and the foam has been obtained, and no loss of catalyst during the catalytic tests seemed to occur. The alumina layer was, however, observed on uncovered zones (Figure 76d).

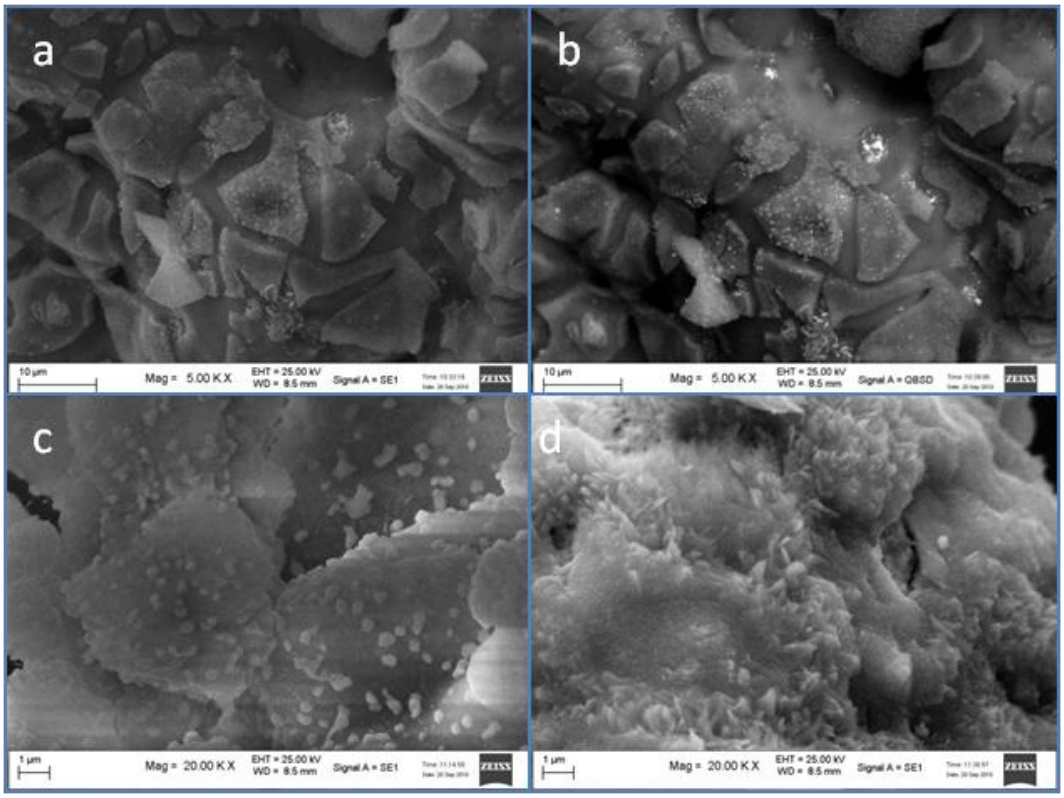

Figure 76: SEM images of a used catalyst prepared at -1.1 V for 2000 s under stirring

A negligible carbon formation was detected on the catalyst surface, and this is probably due to the higher stability and homogeneity of the samples.

Although some good results were obtained, stirring during the synthesis did not solve the diffusion problem and the formation of several phases on the foam surface. Moreover it allowed the precipitation of Rh^0 during the synthesis, so explaining also the observed good catalytic performances. For this reason no stirred conditions were employed for further syntheses. Other modifications of the synthesis parameters were carried out to improve the coating.

5.4.8 MgAl SYNTHESES

Since a better coverage degree of the foam had been observed using the cylindrical CE electrochemical cell, the synthesis of a MgAl-LDH with a molar ratio 3:1 was carried out at -1.2 V for 2000 s by means of such a cell.

SEM characterization of the resulting layer showed a good coating of the foam surface, with the deposition of a strongly higher amount of material in respect to that obtained with a classical electrochemical cell, even if in the latter case the electrosynthesis were for 1000 s. However, a higher deposition rate is still obtained on the tips (Figure 77a) in respect to flat zones (Figure 77b), as far as a high K content. In agreement with the data collected during the synthesis on Pt plates, the obtained film was not homogeneous: different morphologies have

been observed, with a more compact layer grown next to the foam surface and some small particles aggregates deposited on it (Figures 77c and 77d). The EDS analysis suggests that the upper aggregates are mainly composed of Al, while in the underneath layer Mg is also present. The Mg:Al molar ratio is strongly lower (close to 1:1) than expected (3:1), but this result partially is due to the Al contained in the foam alloy, that is detected by the EDS analysis too.

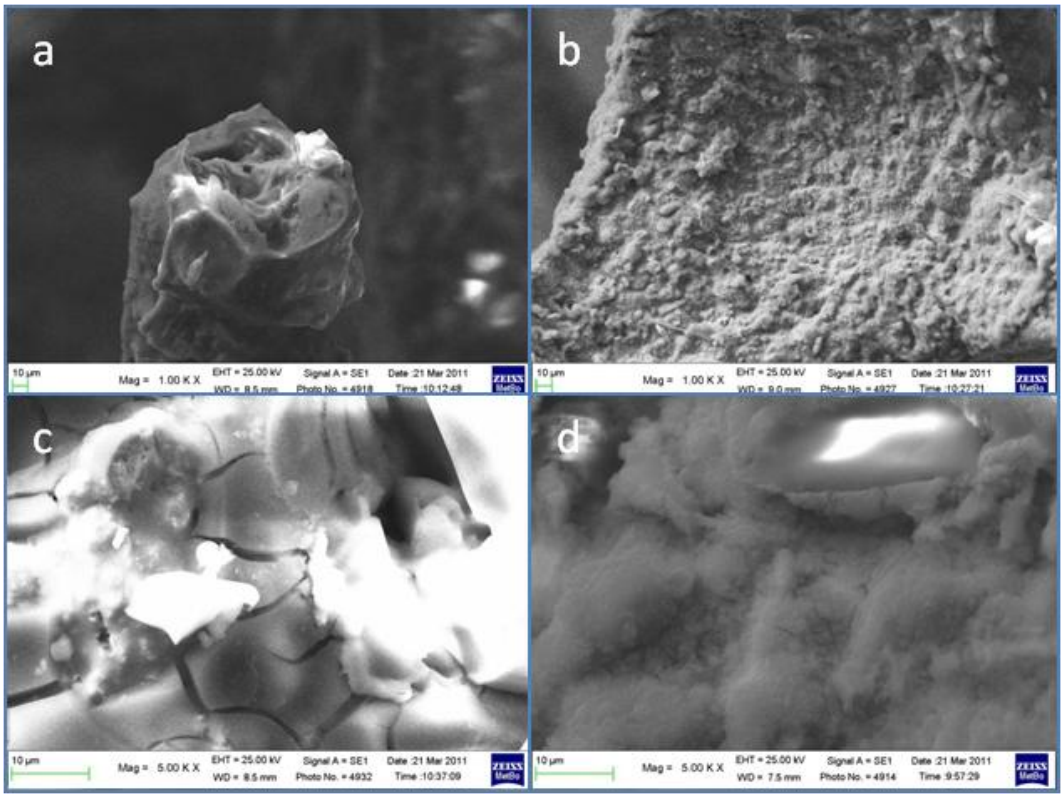

Figure 77: SEM images of a Mg_3Al_1-LDH at -1.2 V for 2000 s

As for all the previous discussed samples, the calcination process induces a stronger crack development and a decrease of the potassium amount.

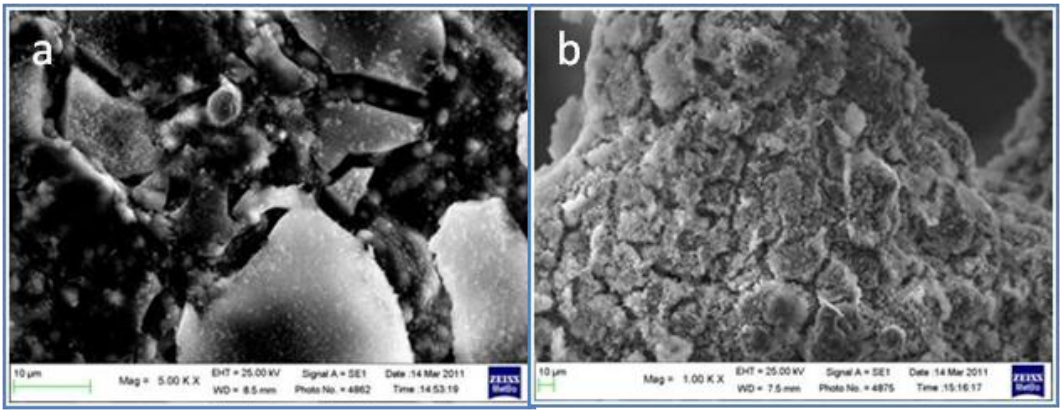

Figure 78: SEM images of calcined MgAL-LDH 3:1 prepared at -1.2 V for 2000 s

5.4.9 CHANGING OF FOAMS POROSITY

In order to solve the diffusion problems, foams with a low ppi (60 ppi), therefore with larger pores, were employed in the further syntheses. The larger pores size should allow a better permeation of the solution, leading to a higher deposition also in the inner part of the foam.

To study this effect, a set of foams was employed and the LDH was synthesized at -1.2 V for 2000 s after the adjustment of the initial pH at 3.8. From the SEM and EDS analyses a thick layer was observed on the surface and differences between flat zones and tips were still evidenced, with a higher amount of deposited material on the latter. Crack development was still observed in the fresh sample, as well as the presence of K and of small aggregates particles, mainly composed of Rh and Al, grown on a more compact layer and inside the cracks. Some uncovered zones were, however, present, and the morphology related to the growth of the alumina layer on the foam surface could be observed in the calcined sample, together with the formation of Cr oxide structures, particularly on the less covered flat zones (Figure 79a). Crack development increased after calcination (Figure 79b), in agreement with all the previous results, and the presence of well dispersed small particles and aggregates was still detected (Figure 79c). As occurred for the samples before described, the thermal treatment highly decreased the amount of potassium.

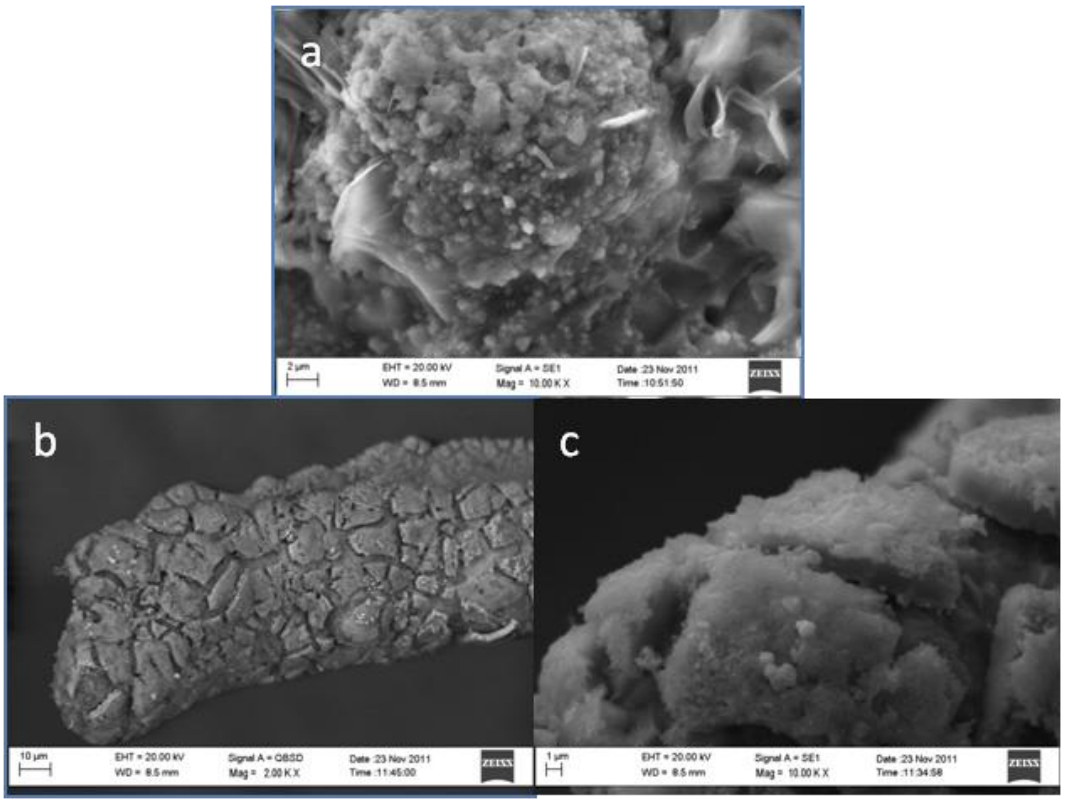

Figure 79: Calcined sample prepared at -1.2 V for 2000 s eployng a 60 ppi foam

The SEM/EDS analyses on some cross-sections of the sample displayed, however, a very poor coating of the inner part of the metallic foam.

The catalyst was tested in CPO reaction using both diluted and concentrated feed mixtures, and a comparison with the sample synthesized in the same working conditions on the 80 ppi foam was carried out. The CH_4 conversion and the selectivity to CO and H_2 are shown in Figure 80.

The sample synthesized on the 60 ppi foams shows a higher methane conversion, as well as an enhanced selectivity to both CO and H_2 in diluted and concentrated conditions. However, they show the same trend as function of the test condition, displaying higher conversion and selectivity to CO when a concentrated mixuture is employed, while a lowerin in the selectivity to H_2 is observed. The increase of the temperature due to the contribution of the oxidation (total and partial) reactions and the lower activity of the catalysts on the reforming of CH_4 may explain these catalytic behaviours.

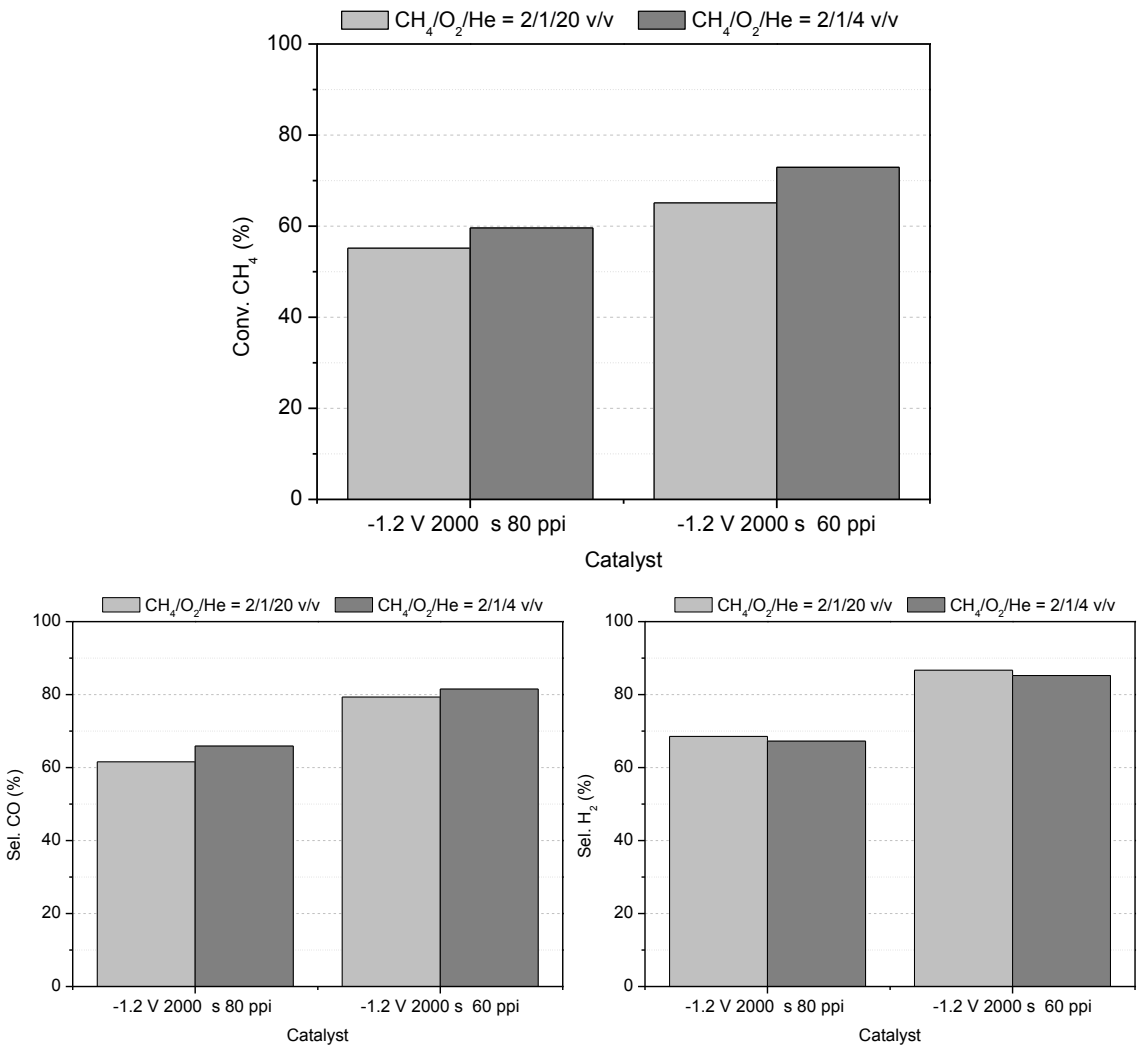

Figura 80: Comparison betwen sample prepared in the same conditions with different porosity

5.4.10 SYNTHESIS CARRIED OUT IN ABSENCE OF KNO_3

A set of foam has been synthesized at -1.2 V for 2000 s in order to check the influence of the absence of KNO_3 on the resulting coating. In this case only the nitrates of the metal salts are available for OH^- production, so no K should be detected in the fresh samples.

However, an unexpected presence of potassium is instead detected in the fresh sample: a little amount was added to the plating solution during the adjustment of the intial pH of the plating solution with KOH. Its presence is probably due to a particular sensibility of K to electrostatic attraction when a negative potential is applied to the foam. The layer however does not present particular differences from the morphologic point of view respect to that obtained in presence of KNO_3 as supporting electrolyte. Only an enhanced presence of particles and aggregates on the more compact layer is observed, confirmed by EDS analyses, that confirm an increase in Al and Rh content. This behavior is probably due to the low nitrates amount in the plating solution, that leads to a slower OH^- production which could favor the precipitation of Al and Rh. After calcination, the presence of a higher amount of aggregates on the compact layer is still detected (Figures 81a and 81b), and, moreover, less uncovered zones are observed. The molar ration Rh:Mg is higher than expected in almost all the analyzed points, with values up to 1 on some crusts.

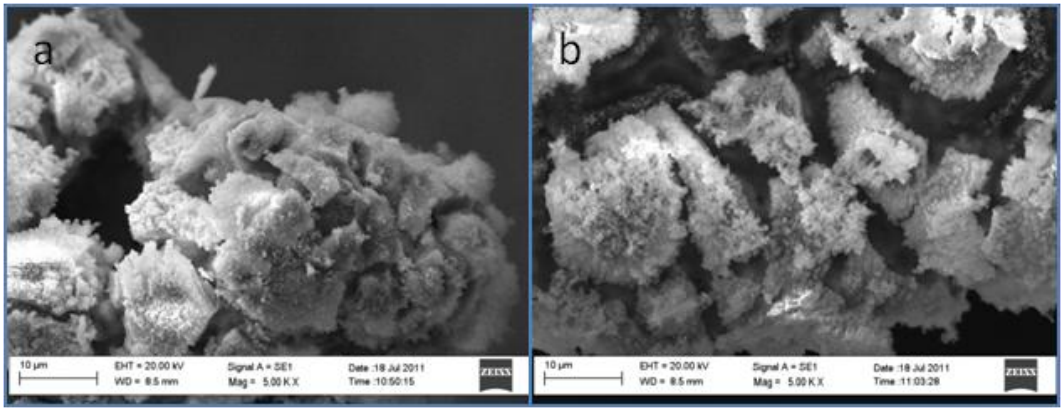

Figure 81: SEM images the calcined sample at -1.2 V for 2000 s in absence of KNO_3

The performances of the catalyst prepared at -1.2 V and 1.1 V for 2000 s, with an without KNO3 are displayed in Figures 82. An important enhancement of the activity in CH_4 conversion and selectivity in syngas is observed by removing the KNO3 from the plating solution, confirming the poisoning effect of large amounts of potassium previously described. However, it should be noted that during the electrosynthesis without supporting electrolyte a lower increase of the pH may be achieved in the electrode/electrolyte interface so some modifications in the chemical composition of the film may also explain the different catalytic behaviour. In particular, the lower OH^- production would have allowed a higher precipitation of Rh and Al aggregates, that could be deposited at a lower pH than Mg^{2+}. This behavior can

explain the increase in catalytic activity as far as a higher amount of active phase is deposited. For this reasons further synthesis are always carried out in absence of KNO_3.

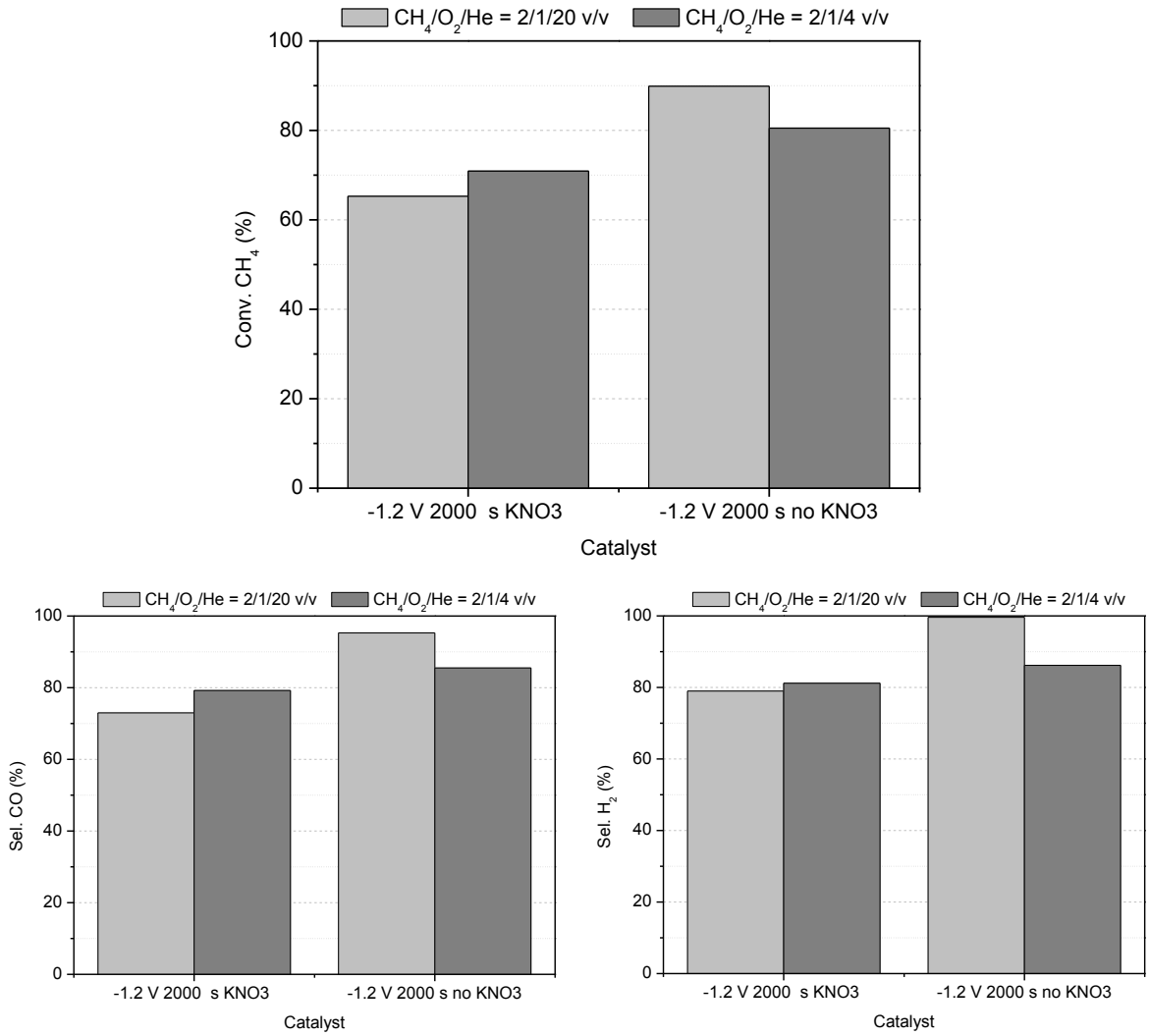

Figure 82: COmparison in CPO performances between samples prepared in presence and in absence of KNO_3

As said, in absence of supporting electrolyte the OH^- production rate is lowered by the decrease of NO_3^- ions in solution, allowing a higher precipitation of Rh and Al aggregates, that could be deposited at a lower pH than Mg^{2+}. This behavior can explain the increase in catalytic activity as far as a higher amount of active phase is deposited. For this reasons further synthesis are always carried out in absence of KNO_3.

5.4.11 IMPROVEMENT OF THE ELECTRIC CONTACT FOAM-POTENTIASTAT

Some samples were synthesized at -1.1 V for 3000 s, after the adjustment of initial pH, in absence of KNO_3 as supporting electrolyte.

The growth of small aggregates and round particles on the top of a more compact film is revealed, although this phenomenon was less evident in comparison with that observed in the sample synthesized at -1.2 V for 2000 s with the same set up. Moreover, few uncovered zones were still detected, although a few rounded particles were detected also in these areas. The EDS analysis shown that the deposited film was mainly composed of Al and a lower presence of Mg than expected was detected. This result was explained by the application to the foam of a less cathodic potential, such as -1.1 V, that generates a lower pH than that reached in the other experiments and does not allow an efficient precipitation of LDH and magnesium. In this way the noticeably low value of the Mg:Rh molar ratio (lower than 1) pointed out in several of the analyzed points on both flat and tip zones can be easily explained.

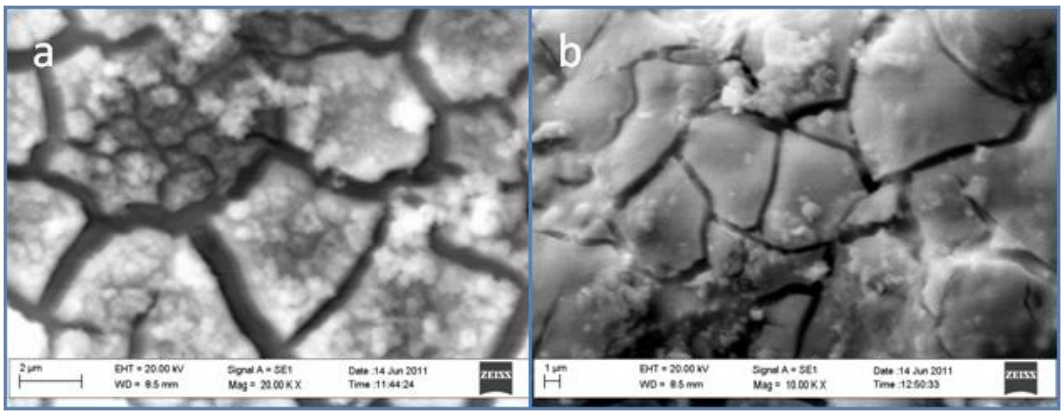

Figure 83: Sample synthesized at -1.1 V for 3000 s with a single point plug

In the calcined sample the crack development increased, and the catalyst was arranged in form of flakes on the surface electrode (Figure 84), as for the majority of previous samples. A good dispersion of round particles could be observed on the flakes (Figure 84). Alumina was revealed in uncoated zones, deriving from the thermal treatment of the foam alloy surface.

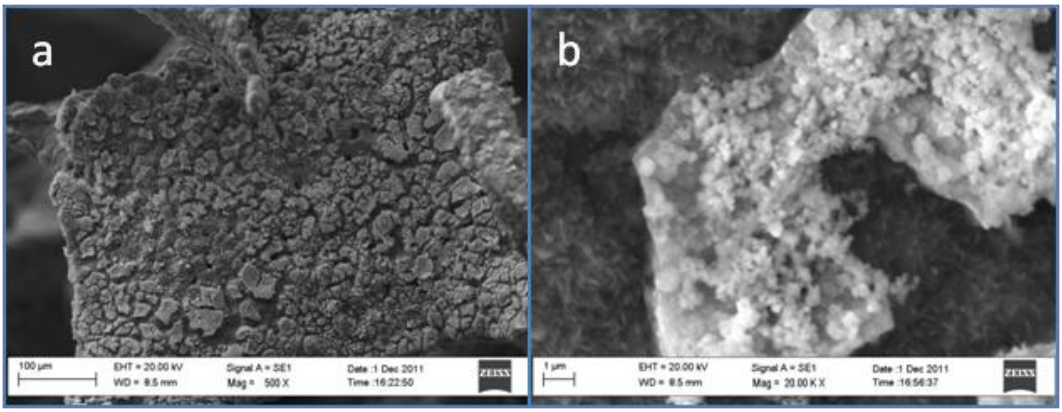

Figure 84: Sample synthesized at -1.1 V for 3000 s with a single point plug after calcination

It has been possible to analyze the calcined sample also performing a µ-XRD analysis at the synchrotron. The results of a XRD/XRF tomography are shown in Figure 85.

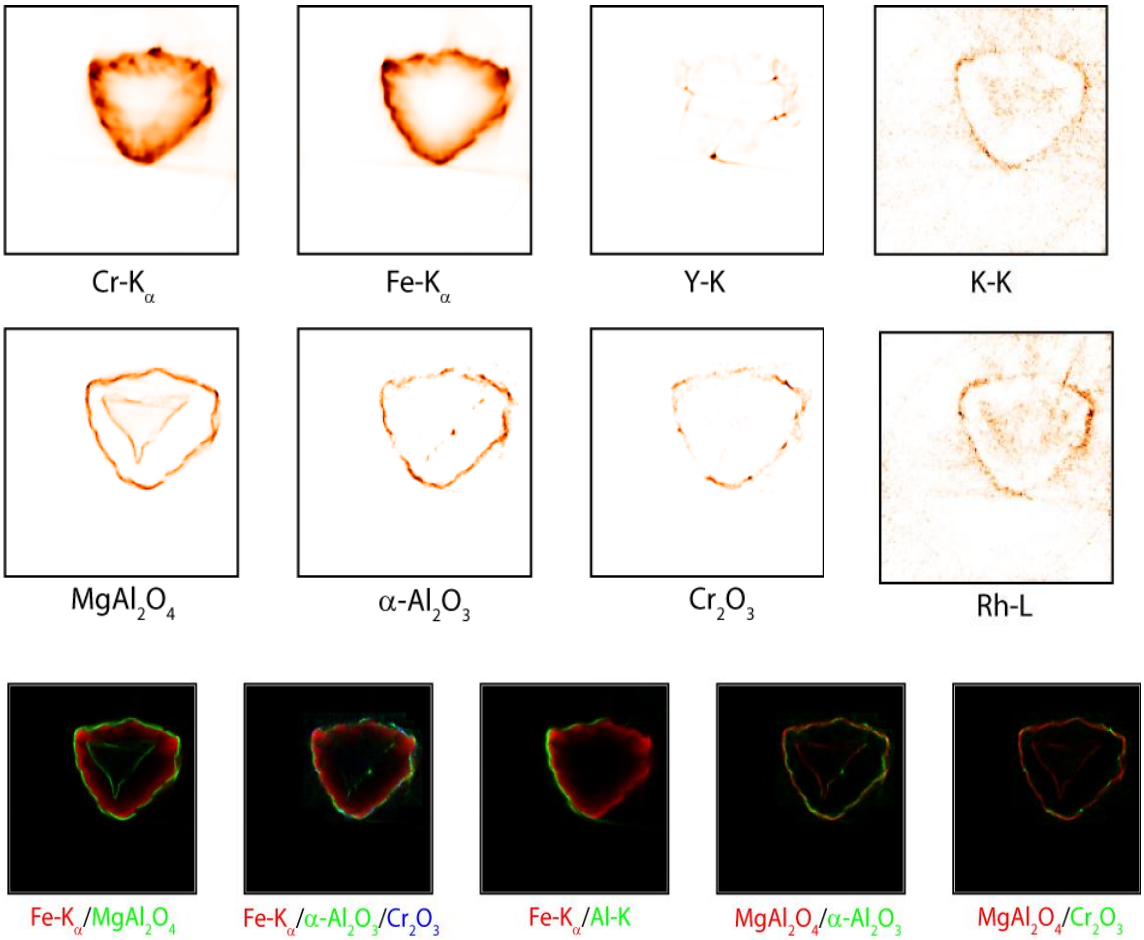

Figure 85: µ-XRF/XRD performed at the synchrotron of a calcined sample prepared at -1.1 V for 3000 s

The catalyst is composed by $MgAl_2O_4$ spinel, a quite good correlation between the spinel and the Rh is obtained, pointing to its inclusion in the spinel phase. Some K is detected dueto the KOH added.

. The presence of alumina, chromium oxide and potassium are detected on the foam surface pointing to the oxidation of the foam, as expected from the previous collected data.

In order to obtain a better surface coating the plug between the metallic foam and the potentiostat has been modified. In the previous syntheses it was obtained by sticking a single Pt wire in the center of the foam. A three Pt wire plug has been achieved by sticking two other Pt wire in the foam laterally (Figure 86) in order to minimize gradients after the application of a potential.

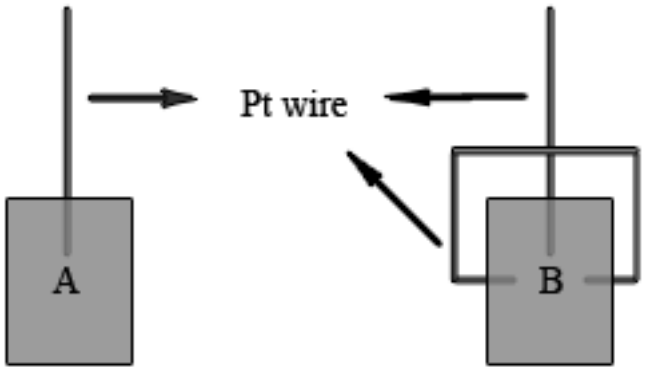

Figure 86: Schematic representation of single point an three points plug

Some syntheses carried out in the same conditions of the sample described before confirmed that the aim has been reached. The coating presents almost the same characteristics observed in the previously described samples, apart from the higher amount of material deposited on the whole foam surfaces. Catalytic tests, performed on CPO, confirmed the increase in efficiency due to the massive presence of catalyst. As expected from observations reported before, a higher methane conversion is obtained for the catalysts synthesized with the three point plug for 2/1/20 and 2/1/4 CH_4/O_2/He feed mixtures. The same behavior is observed as far as the selectivities to CO and H_2 are concerned. However, a different trend in CH_4 conversion is observed for the two samples respect to the reaction conditions. A lowering is in fact observed for the sample synthesized with a three point plug, while an increase is detected for the other. Differently, a lowering in selectivities is observed for both samples when a concentrated feed mixture is employed.

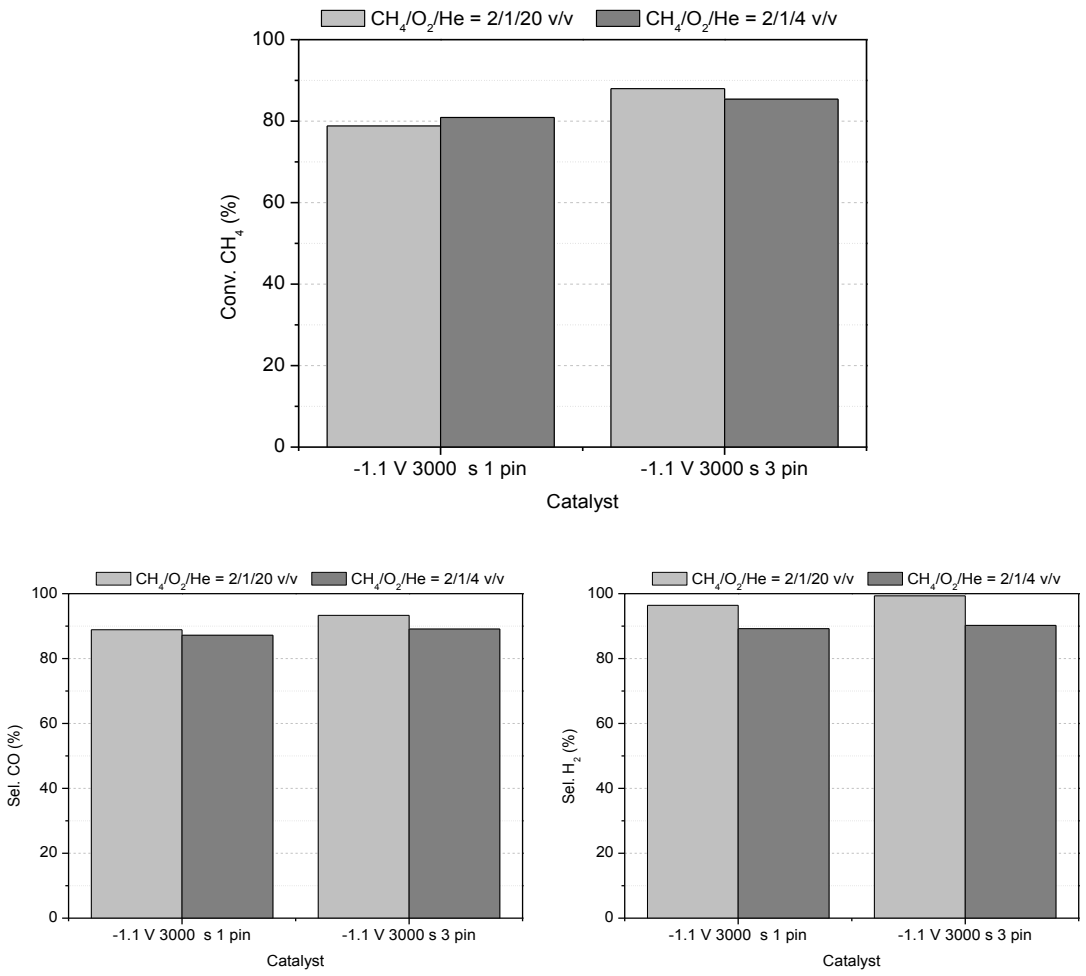

Figura 87: Comparison between the catalytic performances in TPO for prepared at -1.1 V for 3000s changing the number of connection point with the potentiostat

SEM and EDS analyses of the used samples showed that a quite good dispersion of the Rh particles was observed on the top of the layer. However, some larger metal particles were detected respect to those observed in the calcined sample, probably due to the sintering caused by the high temperature reached in the reactor (Figure 88).

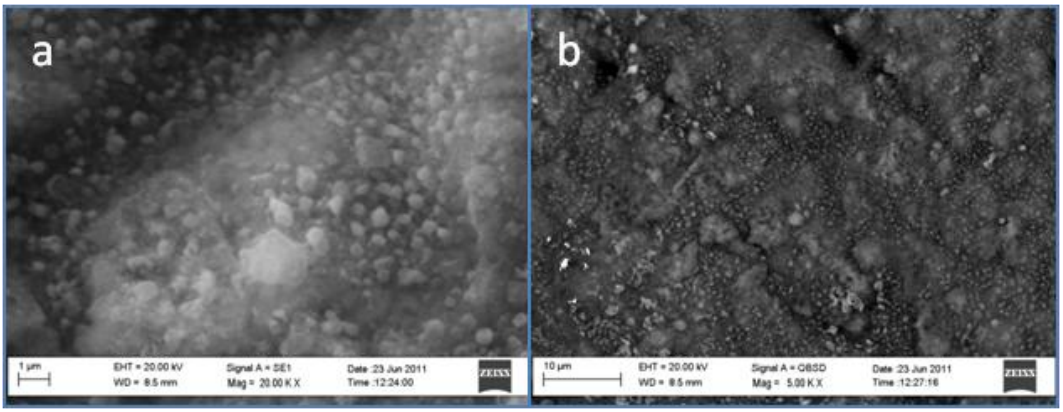

Figure 88: Calcined sample synthesized at -1.1 V for 3000 s with a single point plug after calcination

The µ-XRF/XRD tomography measurements using a synchrotron radiation has been performed also on the used catalyst for the sample synthesized with a one point plug. The presence of the previously detected phases in the calcined sample is detected (Figure 89), pointing to a no loss of catalyst during the employment in the reactor. Moreover, the presence of metallic rhodium is detected, confirming the reduction of Rh during the reaction and its stability during the catalytic tests.

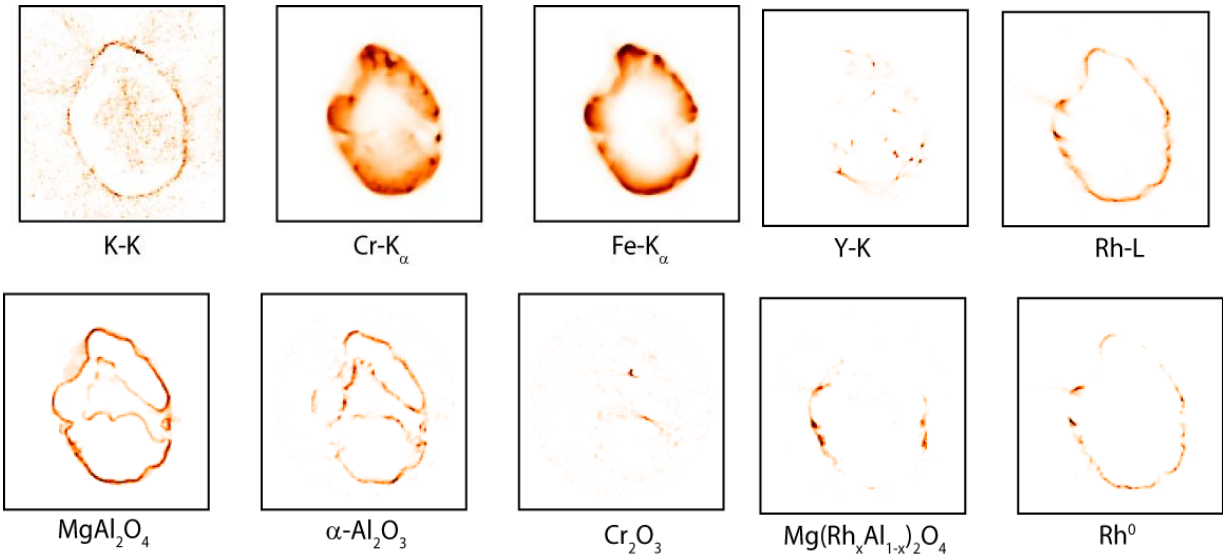

Figura 89: µ-XRF/XRD performed at the synchrotron of a used sample prepared at -1.1 V for 3000 s

The amount of deposited material is then the only difference between the two samples that have been detected in all the previously described analyses, and in this way it is responsible for the better performances of the catalyst. For this reason all the subsequent syntheses have been carried out increasing the number of connections between the metallic foam and the potentiostat.

5.4.12 IMPROVEMENT OF THE SYNTHESIS AT -1.2 V FOR 2000 S

The application of a -1.2 V potential for 2000 s can be considered one of the best working conditions consulting the results of all the previous tests. Another set of foams was used for the electrodeposition employing the three point plugging without adding the KNO_3 to the plating solution and after the adjustment of pH.

A better coating was observed in respect to the sample synthesized under the same conditions, with presented higher thickness (Figures 90a and 90c), and a strong increase of small particles and aggregates mainly composed by Rh and Al over the compact top layer (Figure 90b) and inside the cracks (Figure 90d). This behavior is probably due to the low nitrates amount in the electrolytic solution, that leads to a slower OH^- formation which could favor the precipitation of Al and Rh. It is similar to that previously observed during the synthesis of LDHs on the Pt plates Less covered zones presenting a thinner film are however detected in flat areas. The Rh:Mg molar ratio is in fact higher respect to the plating solution where a thicker film is observed, while it is almost the expected one in the less covered zones. Moreover, cracks development was also observed on both flat and tip zones due to the thickness of the film. A good dispersion of all the elements was obtained, as shown by the maps in Figure 91.

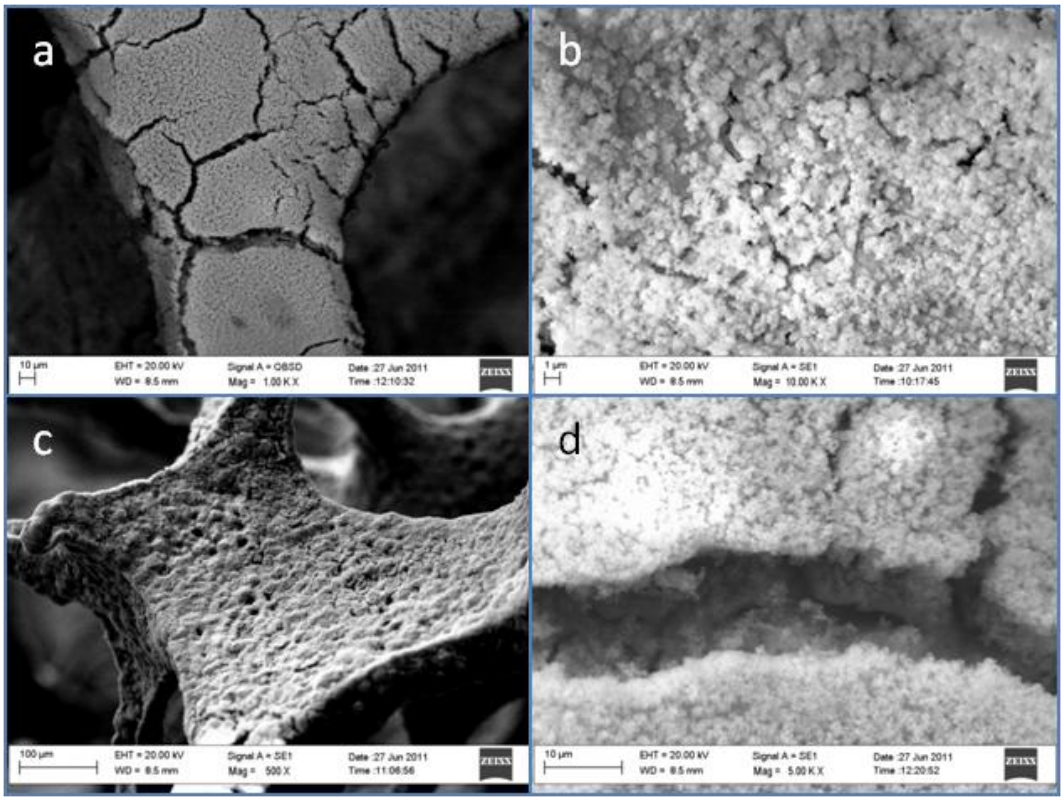

Figure 90: Sample synthesized at -1.2 V for 2000 s with a three points plug in absence of KNO_3

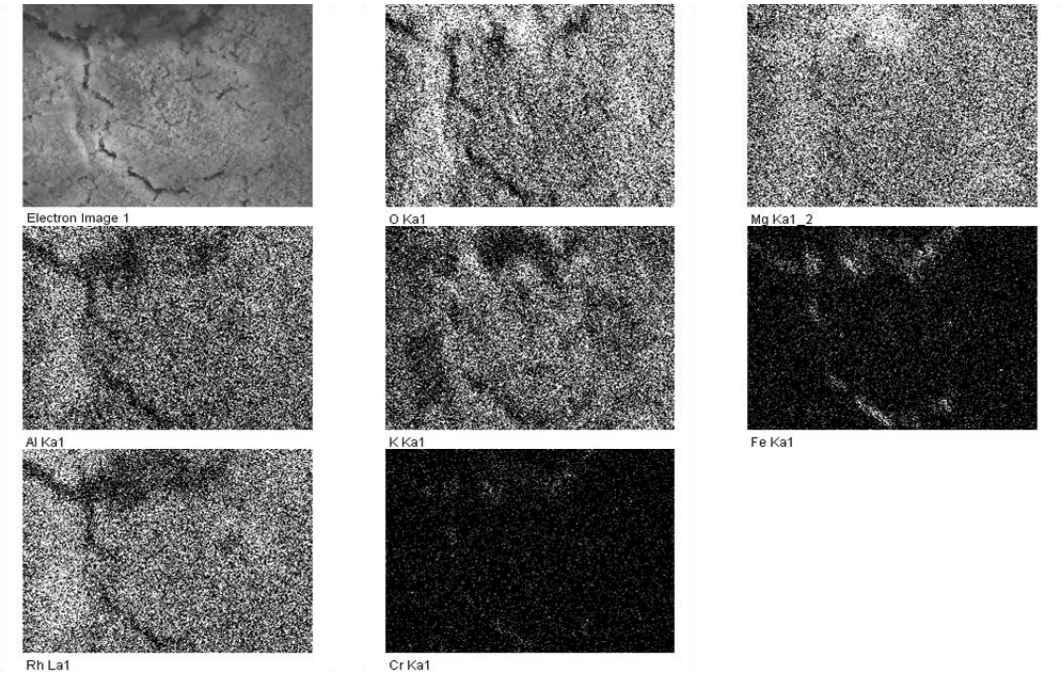

Figure 91: EDS mapping of a sample synthesized at -1.2 V for 2000 s with a three points plug in absence of KNO_3, in order O, Mg, Al, K, Fe, Rh and Cr dispersion have been shown.

After calcination the crack development increased, as expected, and the alumina growth observed among the flakes of catalyst. The presence of well round particles on the top of the flakes have been observed on flat and tip zones.

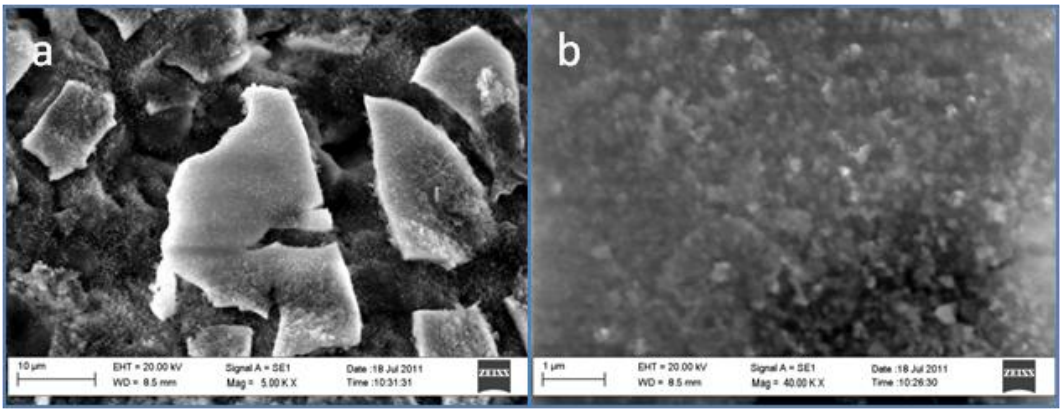

Figure 92: Calcined sample synthesized at -1.2 V for 2000 s with a three points plug in absence of KNO_3

The sample has been tested in catalytic partial oxidation of methane, as the previous samples, in diluted and concentrated conditions. The comparison with the catalytic performances of the sample synthesized in the same conditions but with a single foam-potentiostat connection is displayed in Figure 93. An unexpected decrease of both CH_4 conversion and selectivities are observed, without depending on the conditions of reaction. However the same trend is observed, and a decrease of the methane conversion and the selectivity to CO and H_2 is observed when a feed mixture CH_4/O_2/He 2/1/4 v/v is employed.

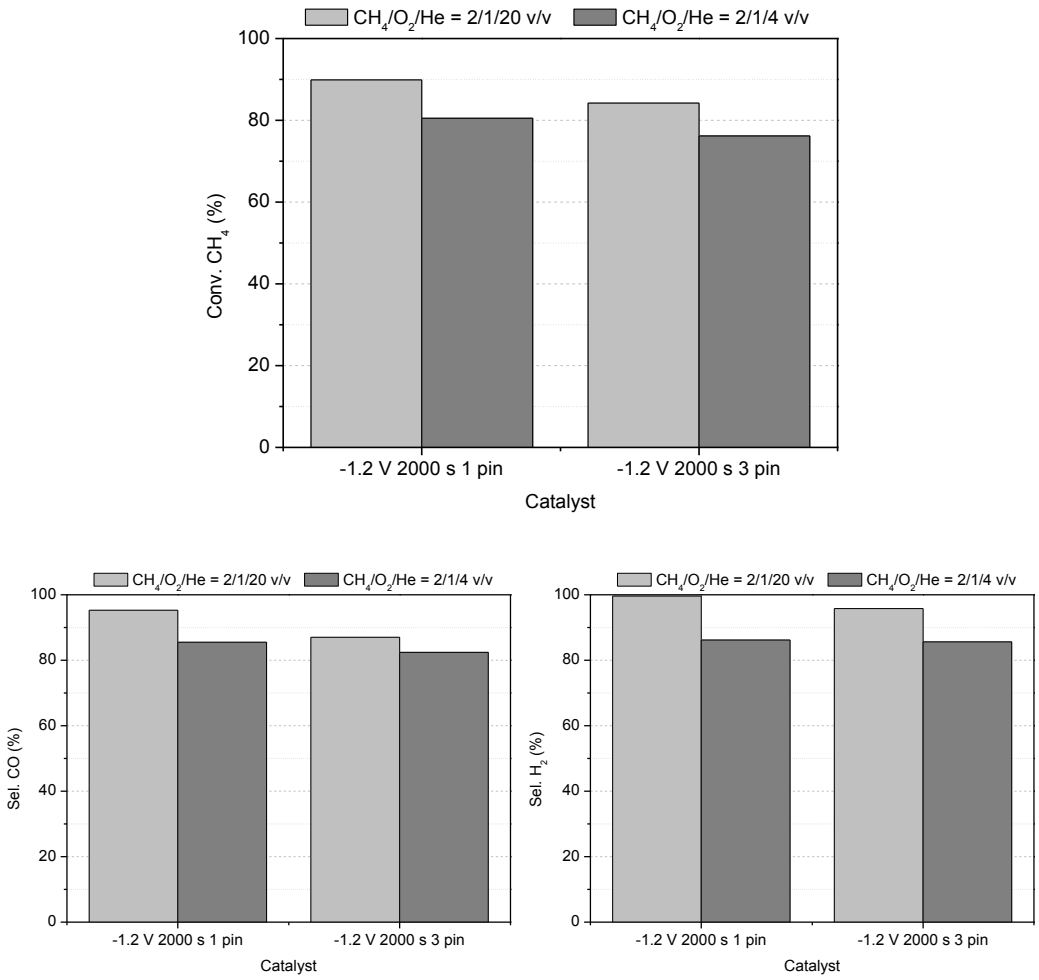

Figure 93: Comparison between the catalytic performances in TPO for prepared at -1.2 V for 2000s changing the number of connection point with the potentiostat in absence of KNO_2

The SEM and EDS analyses of the samples after the use in the reactor showed expected behaviors, and dispersed Rh particles are still detected on the surface of the catalyst flakes. However a lower number of metal particles and aggregates is detected (Figure 94a) respect to the previously discussed sample, explaining the lowering of catalytic performances. Moreover in some zones round metal particles are not detected also by back scattering images (Figure 94b).

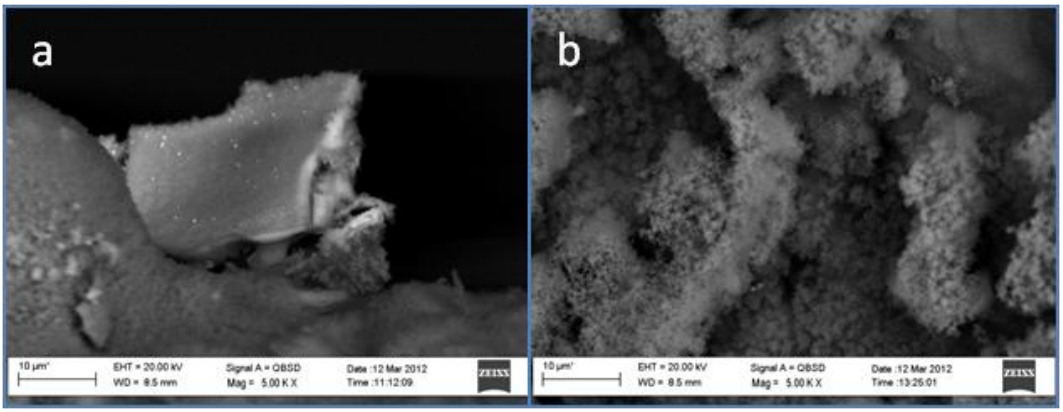

Figura 94: Used sample synthesized at -1.2 V for 2000 s with a three points plug in absence of KNO_3

5.4.13 INFLUENCE OF THE COMPOSITION

Some samples with different molar ratios in the plating solution were synthesized in order to check the catalytic activity in CPO reaction when a lower amount of Rh is present. The electrosyntheses were carried out at -1.2 V for 2000 s, employing the same set up described before for syntheses with a higher Rh amount. Several compositions has been investigated, and a first the influence of lowering of amount of Rh in the electrolytic solution (5:70:25 and 2:70:28 Rh:Mg:Al molar ratios) has been considered. Then the addition of Ni was investigated, employing a working solution with a 5:15:70:25 Rh:Ni:Mg:Al molar ratio.

The SEM and EDS analyses showed expected results whereas employing a plating solution with a Rh:Mg:Al molar ratio 5:75:20. A good covering degree but also the crack development were observed also in the fresh samples. The growth of small particles and aggregates on the Mg enriched layer is, however, reduced in respect to the sample synthesized in same conditions from a electrolytic solution containing a higher amount of Rh (Figure 95). A higher Mg content is found on tips, while a noticeable variability in detected amount of rhodium is observed on both tips and flat zones.

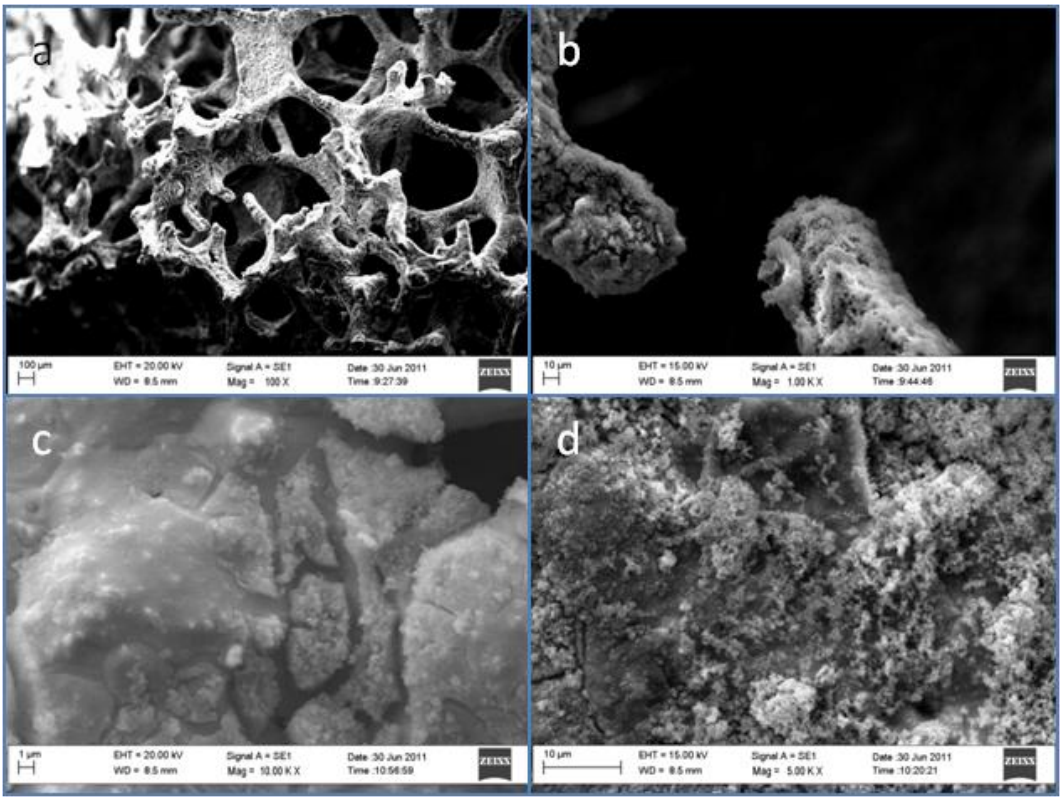

Figure 95: Sample synthesized at -1.2 V for 2000 s with a three points plug in absence of KNO_3 from an electrolytic solution with 5:70:25 Rh:Mg:Al molar ratio

The employment of the electrolytic solution with a Rh:Mg:Al 2:70:28 molar ratio results in a lowering of the presence of particles and aggregates on the more compact layer (Figures 96a and 96b). This observation is in agreement with the trend observed from the comparison of the samples synthesized in the same working condition from 11:70:19 and 5:70:25 Rh:Mg:Al molar ratios electrolytic solutions. It is also in according with the data collected for MgAl-LDH synthesis carried out at -1.2 V for 2000 s, where a lower amount of particles aggregates was detected in the upper part of the coating. In this way the presence of Rh seems to promote the deposition of particles and aggregates, although Al was also detected in these zones by EDS analysis. Some more covered flat zones are however detected (Figures 96c and 96d).

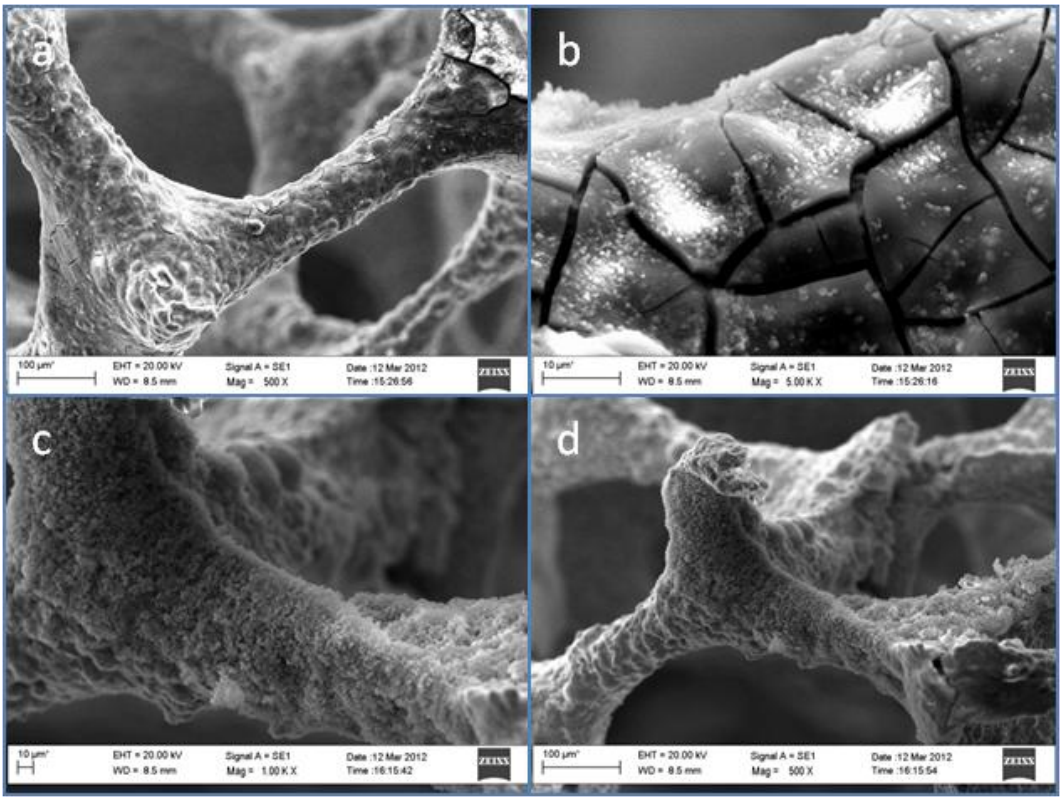

Figure 96: Sample synthesized at -1.2 V for 2000 s with a three points plug in absence of KNO_3 froman electrolytic solution with 2:70:25 Rh:Mg:Al molar ratio

Furthermore, the calcined samples did not show unexpected behaviors: a stronger crack development, the growth of an alumina layer from the foam surface, and round Rh particles dispersed on the upper layer are observed.

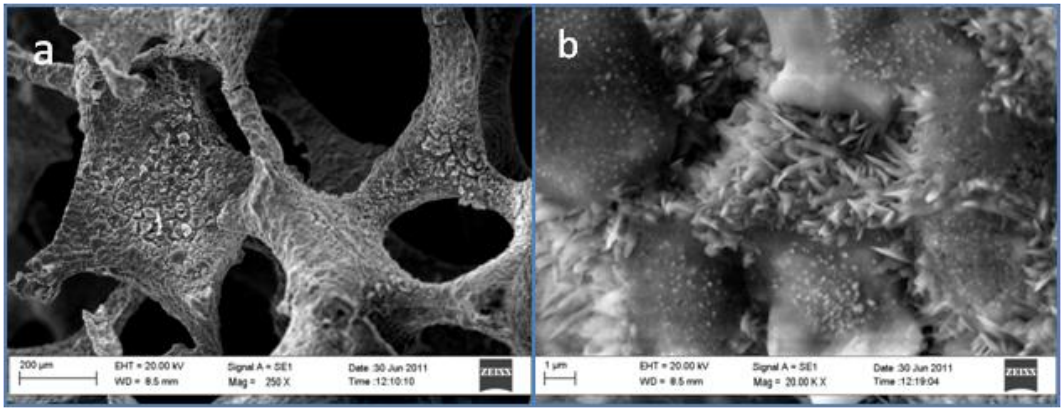

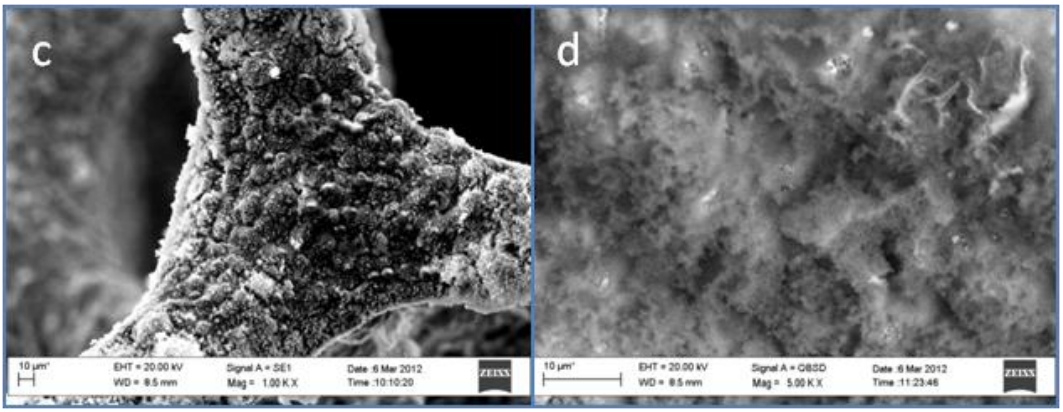

Figure 97: Calcined samples synthesized at -1.2 V for 2000 s with a three points plug in absence of KNO_3 from an electrolytic solution with 5:70:25 (a and b) and 2:70:25 (c and d) Rh:Mg:Al molar ratios

As done for the previous samples, the influence of changing the composition were tested in CPO with different feed mixtures (2/1/20 and 2/1/4 v/v CH_4/O_2/He). A comparison of results obtained for the samples prepared with a different of Rh loading has been carried out (Figure 98). The three samples display the same trend, with a slightly lowering of CH_4 conversion and selectivities when a concentrated feed mixture is used. As far as the sample with a 5:70:25 Rh:Mg:Al molar ratio is concerned almost no differences have been detected in catalytic performances respect to the catalyst with a higher Rh amount. A decrease is instead observed in the case of 2:70:28 Rh:Mg:Al molar ratio catalyst.

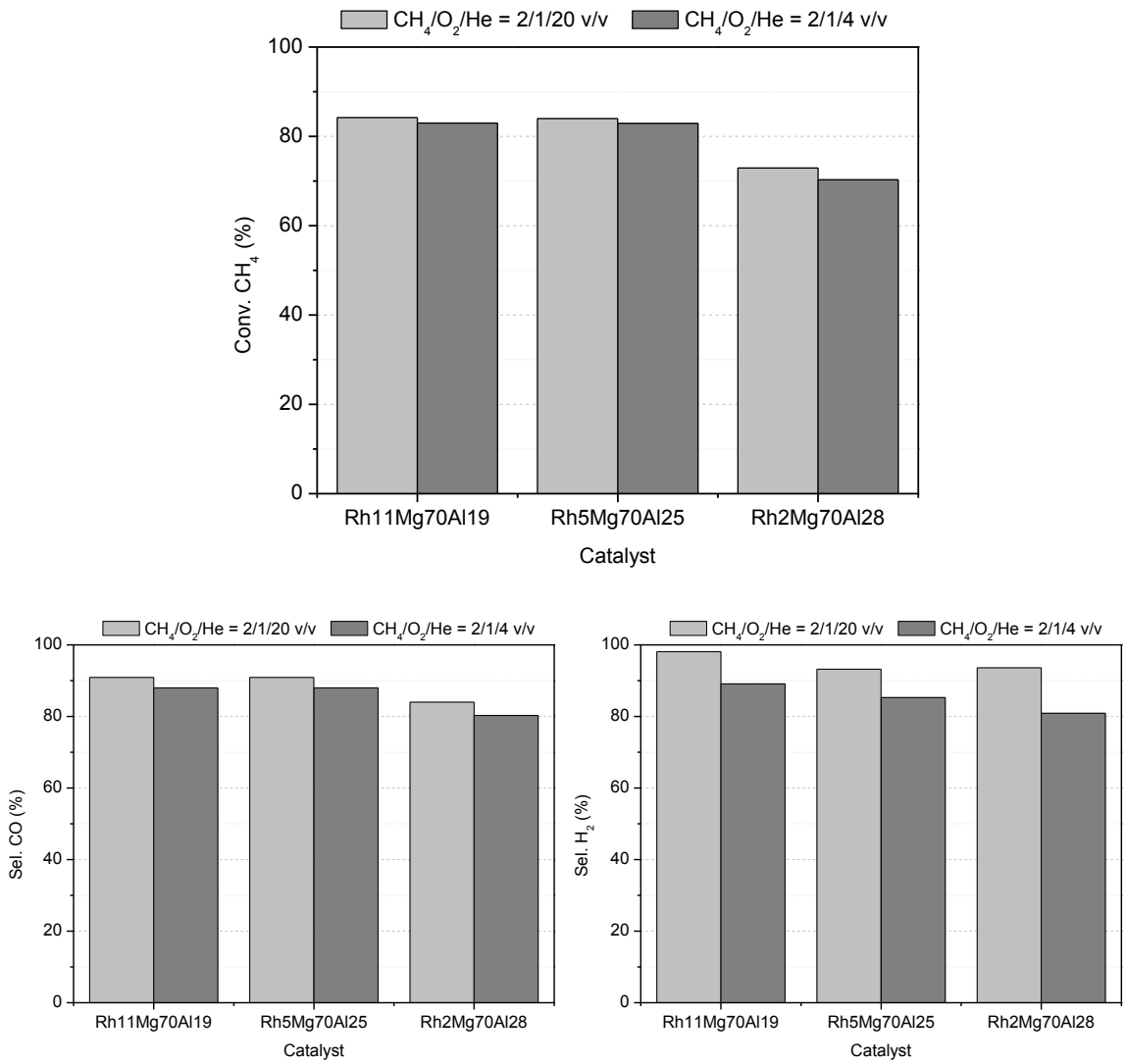

Figure 98: Comparison between the catalytic activities for sample synthesized synthesized at -1.2 V for 2000 s with a three points plug in absence of KNO_3 from electrolytic solutions containing with 11:70:19, 5:70:25 and 2:70:28 Rh:Mg:Al molar ratios

SEM and EDS analyses of the sample synthesized from plating solutions with 5:70:25 and 2:70:28 Rh:Mg:Al molar ratios do not display any unexpected behavior. In the first case, a good coverage degree is still detected and small round Rh particles and aggregates have been detected by back scattering images on the coating surface (Figure 99a and 99b). The same behavior has been found also in the sample prepared from a 2:70:28 Rh:Mg:Al molar ratio plating solution, although less and smaller Rh particles have been detected during the analyses (Figure 99c and 99d), according to the low metal amount employed in the synthesis.

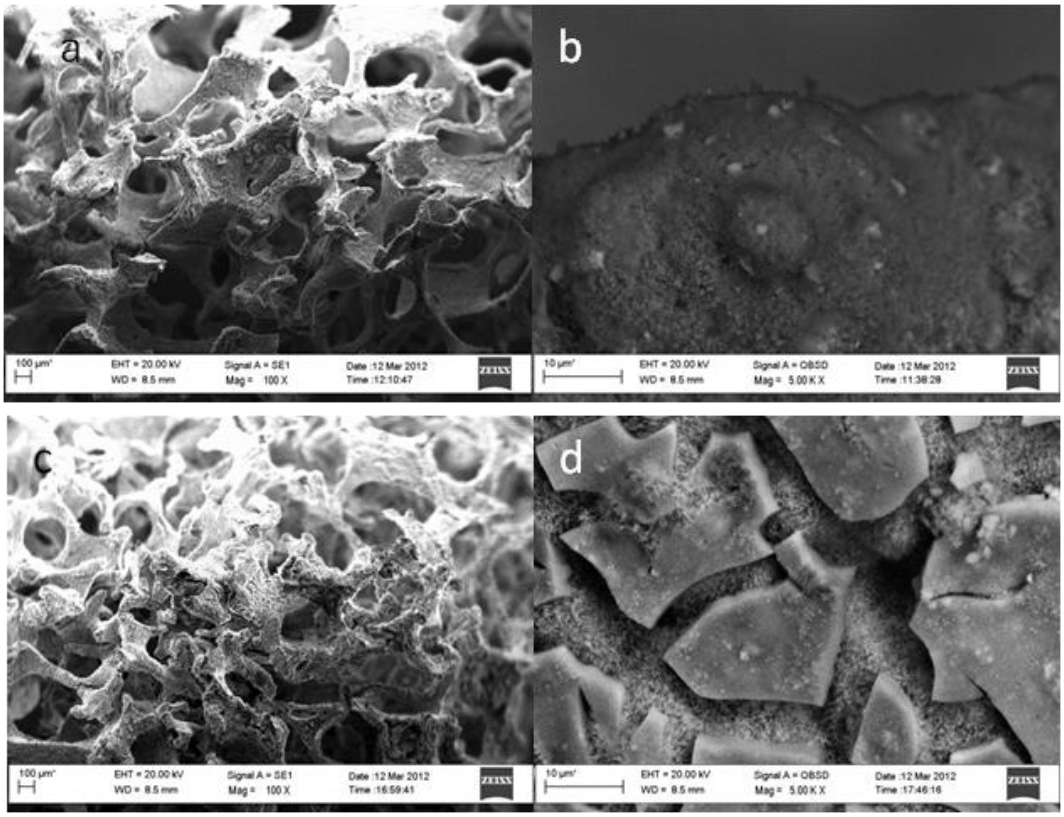

Figure 99: Used samples synthesized at -1.2 V for 2000 s with a three points plug in absence of KNO_3 from an electrolytic solution with 5:70:25 (a and b) and 2:70:25 (c and d) Rh:Mg:Al molar ratios

From the comparison of the collected data, the similar catalytic activity observed for the catalysts prepared from a solution containing a 5:70:25 Rh:Mg:Al molar ratio respect to that with a higher amount of Rh is a consequence of the better dispersion and the size of the metal particles in the sample. The higher aggregation rate found out for in the Rh-enriched sample does not optimize the performances of the active phase, that was instead the feature obtained in the synthesis carried out with a minor Rh content plating solution. However, a further decrease of the amount of rhodium during the synthesis leads to a too small particles formation, that is responsible for the lowering of catalytic activity.

As far as Ni was found to be an active catalyst in CPO of CH_4 (chapter 3), it was added to the composition of the catalyst in order to test its catalytic activity in combination with that of Rh. The best set up indentified was used and syntheses at -1.2 V for 2000 s for a RhNiMgAl plating solution with a molar ratio of 2:15:55:28 were performed. A three layer system seems to be detected in this case. The lower one, in close contact with the foam surface, results to be Mg enriched, with a Mg:Ni molar ratio close to the expected one and a low Rh amount. In the middle layer the Mg content decreases noticeably, while a variable Ni:Rh molar ratio (always higher than 1) is observed. Finally in the upper part ahigher amount of Rh is found, with a Ni:Rh lower than 1. The presence of Al is always higher than expected, but this behavior has been already discussed before.

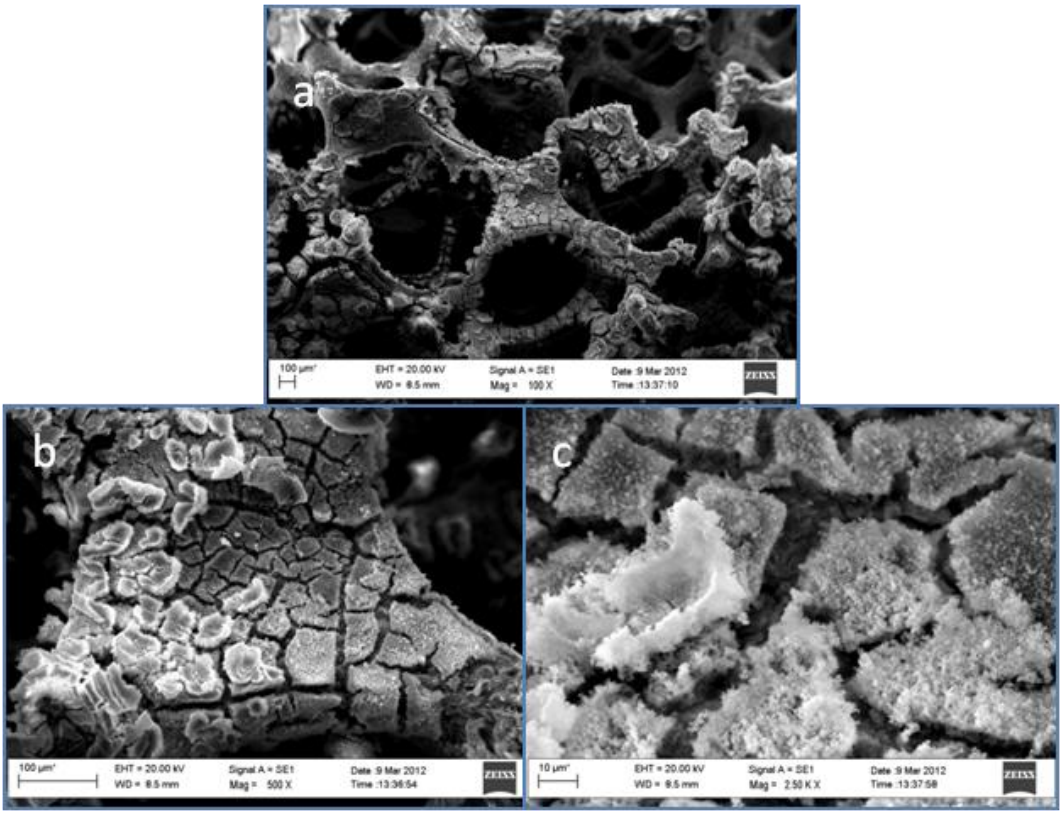

Figure 100: Sample synthesized at -1.2 V for 2000 s with a three points plug in absence of KNO_3 from an electrolytic solution with 5::15:55:70:25 Rh::Ni:Mg:Al molar ratio

The described behavior could be quite in agreement with the observations that were done for the samples without the presence of $Ni(OH)_2$. It in fact precipitates in a pH range between that of $Mg(OH)_2$ and that of $Rh(OH)_3$ and $Al(OH)_3$. In the previous samples a Mg enriched layer was deposited at first, probably because of the more basic pH value reached at the beginning of the synthesis, and the growth of Rh and Al particles and aggregates was noticed. (These observations are also in according with what observed on Pt plates during MgAl-LDHs and NiAl-LDHs synhesized in the chapter on the study of pH evolution at the WE.)

The explanation of this behavior is probably the lowering of the pH during the synthesis, it maybe due to an increased difficulty of NO_3^- ions to reach the electrodic surface or the lowering of the effective applied potential due to the growth of a insulating layer on the foam surface. So the formation of a Ni enriched layer between a Mg and a Rh enriched layers is probably due to the difference in the pH required for the precipitation.

After calcination the presence of the three layers has been noticed more difficultly by SEM analysis, but in some zones the crack development allows to observe clearly the stratification of the catalyst flakes, although two main layer seem to be detected (Figures 101a and 101b). These observations point to solid state reaction during the calcination process, resulting in sort of compaction between the Mg and the Ni enriched layers, and the Ni and the Rh enriched layers. Moreover, the EDS analysis shows some zones where the Mg:Ni molar ratio is about 1-2 with a low Rh content, and some zones with a lower Mg amount and a higher Ni-Rh molar ratio (up to 1) is detected.

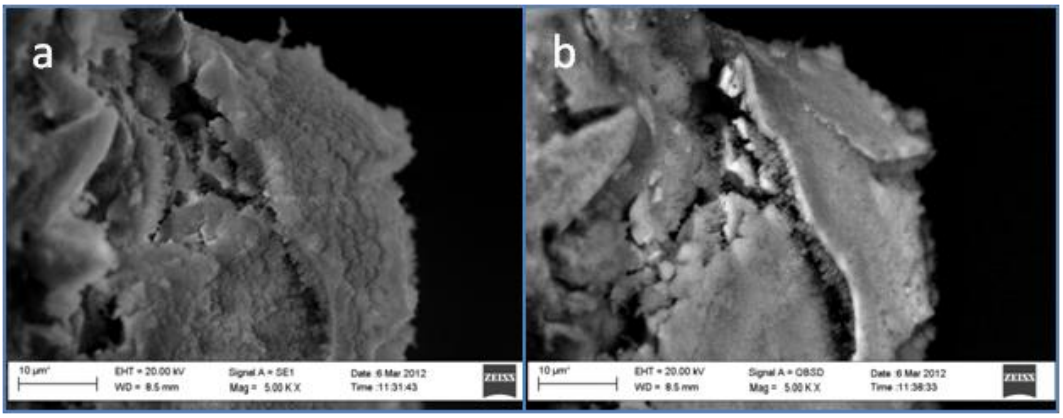

Figure 101: Calcined sample synthesized at -1.2 V for 2000 s with a three points plug in absence of KNO_3 from an electrolytic solution with 5::15:55:70:25 Rh::Ni:Mg:Al molar ratio

The same catalytic tests have been performed employing the bimetallic. The same trend has been observed for both CH_4 conversion and selectivity to CO and H_2. A lowering is in fact observed when a feed mixture CH_4/O_2/He 2/1/4 v/v is employed in conversion and yelds. However, higher value are always observed as far as the Ni containing catalyst is concerned.

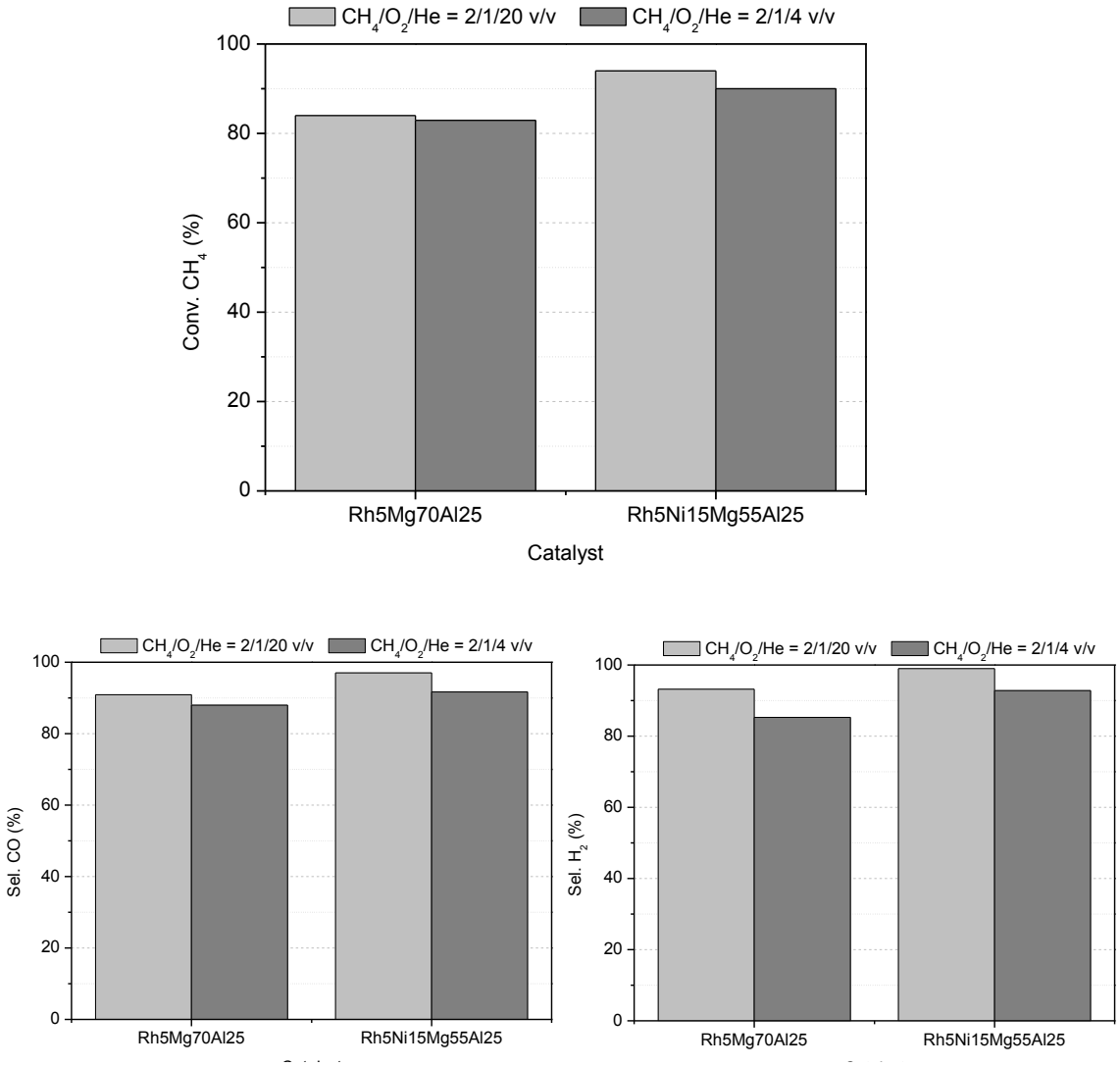

Figura 102: Comparison of the catalytic performances in CPO when Ni is added to the composition of the catalyst

SEM and EDS analyses of the used sample containing Ni do not show any unexpected behavior too. The presence of some exposed crusts has further confirmed the multilayer nature of the coating described before (Figure 103a and 103b). A good coating degree is still observed and the presence of metal particles and aggregates has been shown by back scattering images also in this case.

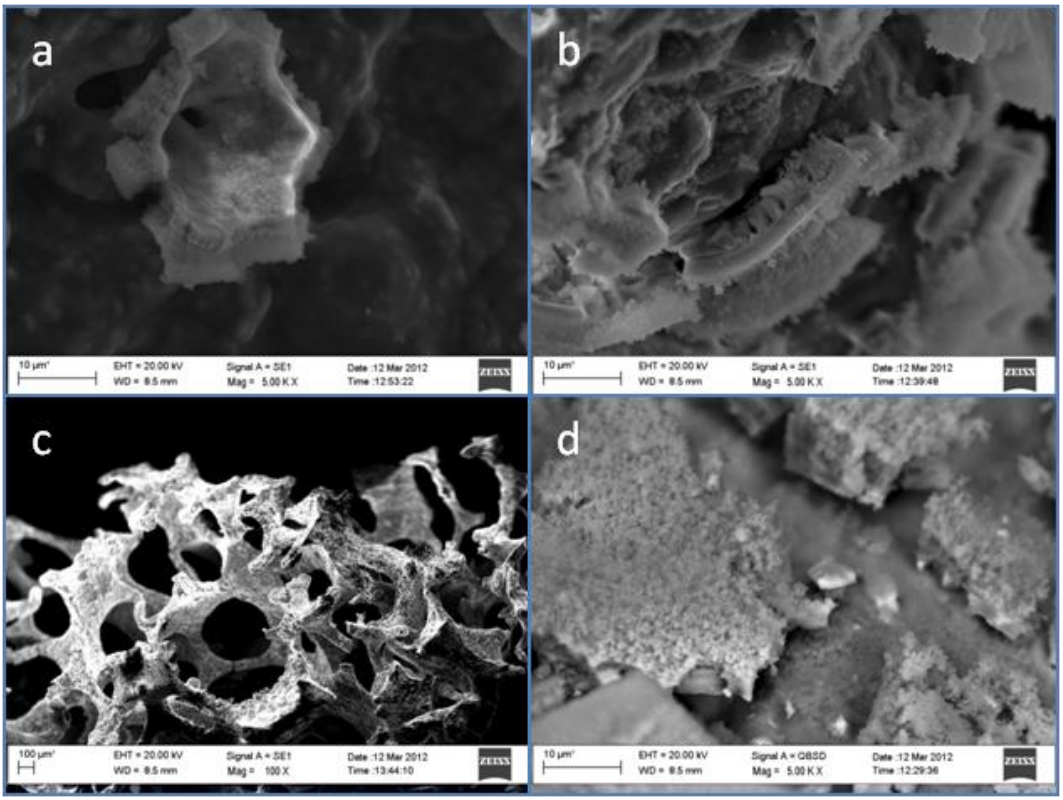

Figure 103: Used sample synthesized at -1.2 V for 2000 s with a three points plug in absence of KNO_3 from an electrolytic solution with 5::15:55:70:25 Rh::Ni:Mg:Al molar ratio

The increasing of catalytic performances obtained with the addition of Ni to the plating solution respect to the sample with the same amount of Rh is due to the presence of the bi-metallic phase deposited, that is active in the CPO reaction. The enhanced multilayer coating system seems not to be a limiting factor in the development of catalysts with this composition.

6. CONCLUSIONS

In this research work the optimization of the electrochemical system of LDHs as catalytic precursors on FeCrAlY foams was carried out.

Preliminary sintheses were performed on flat surfaces in order to easily characterize the deposited material.

From the study of pH evolution vs time at different cathodic potentials applied to a Pt electrode, the theoretical best working conditions for the synthesis of single hydroxides ($Al(OH)_3$, $Ni(OH)_2$, $Mg(OH)_2$) and LDH (2:1 and 3:1 MgAl, 2:1 and 3:1 NiAl) compounds was achieved. A preliminary estimation of the pH reached at the surface of the WE after the application of the chosen potential was carried out employing acid-base indicators. Subsequently, a more reliable measurement performed employing a glass electrode.

In order to define the optimal potential for the synthesis of a particular LDH compound, the collected data were compared with the interval of precipitation determined by titration with NaOH. However, the characterization of the deposited material on Pt surfaces did not confirm the presence of a pure and homogeneous LDH phase even if the employed working conditions were the best, on the basis of the results obtained from titration. Different compositions were found depending on the analyzed points, and different morphologies were observed for both MgAl-LDHs and NiAl-LDHs. These results point out a sequential deposition linked to the pH of precipitation of the involved elements. An LDH phase always precipitate at first as confirmed by XRD and SEM/EDS experiments by carryng out syntheses for different times. Especially for the longest deposition time (1000 s), which assure the obtainment of thick film, a 'stratified' structure was evidenced by SEM/EDS. In particular, the elemental composition revealed on LDH phase which was enriched in Mg^{2+} (or Ni^{2+}) in the layer nearer to the Pt surface, whereas the outer layer resulted enriched in Al^{3+}.

The same behavior was observed during the synthesis of the RhMgAl LDH on FeCrAlY foam as catalytic precursor. Several parameters were considered in order to optimize the synthesis. A strong influence on the initial pH of the electrolyte solution was observed, particularly as far as the reduction of the easier reducible metal, i.e. Rh, was concerned. The correction of the pH to a value of 3.8 resulted adeguate to avoid the presence of Rh^0 particles in the synthesized precursor samples.

According to the data collected for MgAl and NiAl LDHs on Pt plates, the applied potential strongly affected the composition and the amount of deposited materials, and therefore the catalytic performances of the sample.

The employment of an electrochemical cell with a cylindrical round counter electrode and the increase of the plugging points between the metallic foams and the potentiostat assures a better charge exchange and amore uniform potential, leading to a more homogeneous coating of the foam surface at a macroscopic scale. However, at a microscopic scale, a difference in composition and thickness of the coating was actually present between tips and flat zones, as detected by EDS analyses for all the synthesized samples.

The syntheses carried out in stirred solutions in order to allow a better diffusion of the ionic species inside the foam and, therefore, to obtain a good precipitation also in the inner partwas not successful. Moreover, the reduction of Rh in the plating solution was observed, particularly for a high applied potential, such as -1.3 V. In such conditions the solution turned darker because of the presence of metallic particles.

The employment of lower pore density foams seemed to solve partially the problem of solution permeation, but a low coverage degree was still observed in the inner part of the foam.

The absence of KNO_3 during the electrochemical synthesis of the catalytic precursor lead to an increase in the amount of deposited active phase and, therefore, to increase in the catalytic performances of the sample.

Good conversion of CH_4 and selectivity to CO and H_2 were obtained in steam reforming reaction for the sample synthesized from a plating solution with a Rh:Mg:Al molar ratio 11:70:19 at -1.2 V for 2000 s. In the case of CPO of methane, the best catalyst was that with the same molar ratio, as just said above, but synthesized at -1.1 V for 3000 s. The influence of the molar ratio of the elements in the electrolytic solution was investigated too. In order to obtain high catalytic performances and to use a low amount of rhodium, the optimal composition resulted 5:70:25 for the Rh:Mg:Al molar ratio.

The addition of nickel to the plating solution (Rh:Ni:Mg:Al molar ratio = 5:15:55:25) led to an increased activity for the CPO reaction, as expected, since Ni also is an active center in this reaction

.

7. FUTURE DEVELOPMENT

Several features have to be improved in order to optimize the synthesis of catalysts precursors on metallic foams.

The discussed sequential deposition that takes place on both Pt plates and metallic foams is one of the main undesired behaviors which were observed. Although good results were obtained in catalytic tests, further studies have to be carried out in order to better understand the precipitation mechanism.

Another problem is the development of cracks on both fresh and calcined samples. In the first case the optimization of the drying phase will be attempted by the employment of a lyophilizer. The resulting freeze-drying process is expected to induce a lower formation of cracks in comparison with the drying in oven at 40 °C.

As far as the calcined samples are concerned, the processes that lead to the crack development have been outlined previously during the data discussion. In order to reduce the stress caused by the difference in the thermal expansions of the metal alloy and the deposited material, the calcination could be effected more slowly.

Some experiments, such as the employment of stirring solutions or the use of foams with lower pores density, were already carried out. However, a good coating degree of the inner part of the foam, that is expected to cause an improvement of catalytic performances, was not been reached yet. A new electrochemical in-flow cell was designed and developed in order to solve this problem.

7.1 THE FLOW CELL

It consists in a glass pipe through which the working solution is fed by a HPLC pump connected to the bottom of the cell. The solution then flow from the upper part of the cell to the reservoir tank. This could be a very interesting device since the expensive metal salts employed for the synthesis be recycled from the solution, so limiting the production of high cost wastes.

The electrochemical compartment is placed in the central part of the cell the metallic foam could be located inside a porous ceramic cylinder (1.4 cm diameter) thanks to a glass rod that is inserted through the bottom part of the pipe. Three Pt wires inserted in the rod are employed to plug the foam and the potentiostat. A Pt wire, which works as CE, is rolled up on the outer part of the ceramic cylinder. It is immersed in a supporting electrolyte solution contained in a glass pipe which is wound round the main pipe. Once the pourous membrane is hydrated, the current flow between the foam and the CE, while minimizing the diffusion of the working solution from the central pipe to the supporting electrolyte compartment. The reference electrode is located in the upper part of the main pipe. Since the cell geometry does

not allow to the RE to be placed, a Luggin capillary is inserted cross the upper part of the cell until it reaches the foam surface.

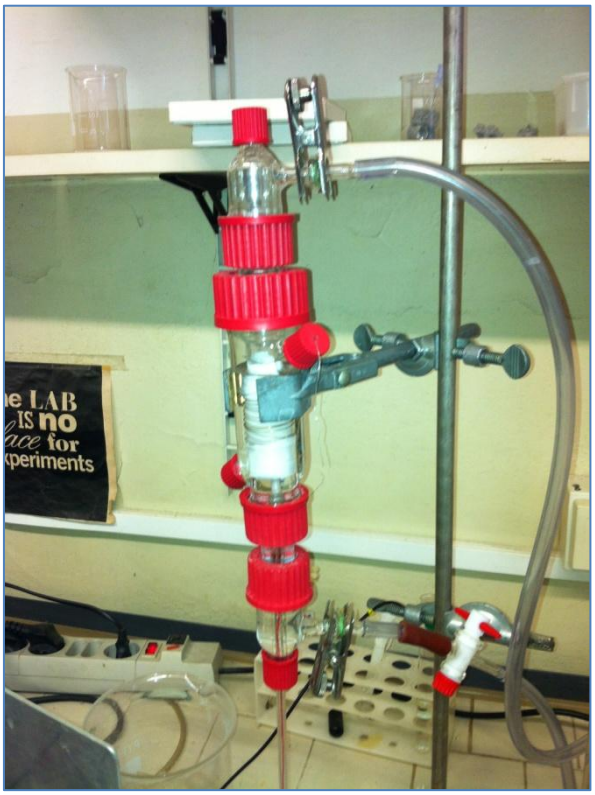

Figure 104: the flow cell

The cell has been already realized but just a few tests have been performed and no results can reported at present.

8. BIBLIOGRAFIA

1. R. M. Navarro, M. A. Pena, J. L. G. Fierro, Chemical Review 107 (2007) 3952;
2. H. Argun, F. Kargi, International Journal of Hydrogen Energy 36 (2011) 7443-7459;
3. R. Guil-Lopez, R.M. Navarro, M.A. Pena, J.L.G. Fierro, International Journal of Hydrogen Energy 36 (2011) 1512-1523;
4. X. Deng, H. Wang, H. Huang, M. Ouyang, International Journal of Hydrogen Energy 35 (2010) 6475-6481;
5. www.iea.org/Textbase/techno/essentials.htm
6. A. Dermibas, Progress in Energy and Combustion Science 33 (2007) 1;
7. J.D. Holladay, J. Hu, D.L. King, Y. Wang, Catalysis Today 139 (2009) 244–260;
8. S. C. Tsang, J. B. Claridge, M. L. H. Green, Catalysis Today 23 (1995) 3;
9. Z. Chen, Y. Yan, S. S. E. H. Elnashaie, Chemical Engineering Science 58 (2003) 4335;
10. M. E. E. Abashar, 29 (2004) 799;
11. M. A. Pena, J. P. Gomez, J. L.G. Fierro, Applied Catalysis A: General 144 (1995) 7;
12. www.iea.org/papers/2006/hydrogen.pdf
13. M. E. E. Abashar, Internation Journal of Hydrogen Technology 29 (2004) 799;
14. D. Levin, L. Pitt, M. Love, Internation Journal of Hydrogen Energy, 29 (2004) 173;
15. S. K. Ryi, J. S. Park, D. K. Kim, T. H. Kim, S. H. Kim, Journal of Membrane Science, 339 (2009)189;
16. B. S. Kwak, J. Kim, M. Kang, International Journal of Hydrogen Energy, 35 (2010) 1829;
17. A. Vita, L. Pino, F. Cipiti, M. Lagana, V. Recupero, International Journal of Hydrogen Energy 35 (2010) 9810;
18. A. Fonseca Lucredito, E. M. Assaf, Journal of Power Sources 159 (2006) 667;
19. A. Fonseca, E.M. Assaf, Journal of Power Sources 142 (2005)154;
20. F. Basile, P. Benito, G. Fornasari, M. Monti, E. Scavetta, D. Tonelli, A. Vaccari, Catalysis Today 157 (2010) 183–190;
21. F. Basile, P. Benito, G. Fornasari, M. Monti, E. Scavetta, D. Tonelli, A. Vaccari, 10th International Symposium "Scientific Bases for the Preparation of Heterogeneous Catalysts"E.M. Gaigneaux, M. Devillers, S. Hermans, P. Jacobs, J. Martens and P. Ruiz (Editors) (2010);
22. L. D. Vella, S. Specchia, B. Lorenzut, T. Montini, P. Fornasiero, Combustion Colloquia 2009, 32nd Meeting on Combustion;
23. A. Donazzi, A. Beretta, G. Groppi, P. Forzatti, Journal of Catalysis 255 (2008) 241;
24. R. Horn, K. A. Williams, N.J.Degenstein, L. D. Schmidt, Journal of Catalysis 242 (2006) 92;
25. G. A. Deluga, J. R. Salge, L. D. Schmidt, X. E. Verykios, Science 13 (2004) 993;
26. D. K. Linguras, D. Kondariedes, X. E.Verykios, Applied Catalysis B: Environmental 43 (2003) 345;

27. A. Lucretio Fonseca, G. Jerkiewickz, E. M. Assaf, Applied Catalysis B: Environmental 84 (2008) 106;
28. J. Zhang, N. Zhao, W. Wei, Y. Sun, International Journal of Hydrogen Technology 35 (2010) 11776;
29. A. Fonseca Lucretio, G. Jerkiewickz, E. M. Assaf, Applied Catalysis A: General 333 (2007) 90;
30. takehira
31. Z. P. Xu, J. Zhang, M. O. Adebajo, H. Zhang, C. Zhou, Applied Clay Science 53 (2011) 139–150;
32. A. N. Ay, B. Zümreoglu-Karan, A. Temel, L. Mafra, Applied Clay Science 51 (2011) 308–316;
33. K. H. Goha, T.T. Lima, Z. Dong, Water Research 42 (2008) 1343–1368;
34. P. Brateman, Z. P. Xu, F. Yarberry, Layered Double Hydroxides (LDH), in Handbook of Layered Materials (Ed. S. M. Auerbach, K. A. Carrado, P. K. Dutta), 2004, p. 373;
35. G. H. A. Therese, P. V. Kamath, Chemistry of Matererials 12 (2000) 1195-1204
36. A. Zamaniyan, Y. Mortazavi, A. A.Khodadadi, H. Manafi, Applied Catalysis A: General 385 (2010) 214;
37. S. Roy, T. Bauer, M. Al-Dahhan, P. Lehner, T. Turek, AIChE Journal, 50 (2004) 2918;
38. R. M. Heck, S. Gulati, R. J. Farrauto, Chemical Engineering Journal 82 (2001) 149;
39. P. Avila, M. Montes, E. E. Miro, Chemical Engineering Journal 109 (2005) 11–36
40. T. Sanders, P. Papas, G. Veser, Chemical Engineering Journal 142 (2008) 122–132
41. A.N. Pestryakov, V.V. Lunin, A.N. Devochkin, L.A. Petrov, N.E. Bogdanchikova, V.P. Petranovskii, Applied Catalysis A: General 227 (2002) 125–130
42. P. Sepulveda, J. G. P. Binner, Journal of the European Ceramic Society 19 (1999) 2059-2066;
43. J. W. Geus, J. C. van Giezen, Catalysis Today 47 (1999) 169-180;
44. X. K. Phana, H. Bakhtiary-Davijanya, R. Myrstadb, P. Pfeifer, H. J. Venvika, Anders Holmen, Applied Catalysis A: General 405 (2011) 1–7;
45. D. Lehmhus, C. Mrchner, J. Banhart, Metallschaume, (ed. Willey) (2000) 474-477;
46. L. Giani, G. Groppi, E. Tronconi, Industrial and Engineering Chemistry Resesearch 44 (2005) 4993-5002;
47. T.Knorr, P. Heinl, J. Schwerdtfeger, C. Korner, R. F. Singer, B. J. M. Etzold, Chemical Engineering Journal 181-182 (2012) 725;
48. V. Meille, Applied Catalysis A: General 315 (2006) 1;
49. L. C. Almeida, F. J. Echave, O. Sanz, M. A. Centeno, J. A. Odriozola, M. Montes, 10th International Symposium “Scientific Bases for the Preparation of Heterogeneous Catalysts” (Ed. E.M. Gaigneaux, M. Devillers, S. Hermans, P. Jacobs, J. Martens and P. Ruiz) (2010)
50. M.J. Schoning, D. Tsarouchas, L. Beckers, J. Schubert, W. Zander, P. Kordo, H. Luth, Sensors and Actuators B 35 (1996) 228;
51. C. Agrafiotis, A. Tsetsekou, Journal of the European Ceramic Society 22 (2002) 423;

52. G. H. A. Therese, P. V. Kamath, Journal of Applied Electrochemistry 28 (1998) 539;
53. P. V. Kamath, G. H. A. Therese, Journal of Solid State Chemistry 128 (1997) 38;
54. L. Indra, M. Dixit, P. V. Kamath, Journal of Power Sources 52 (1994) 93;
55. E. Scavetta, A. Mignani, D. Prandstraller, D. Tonelli, Chemistry of Materials, 19 (2007) 4523;
56. G. Wang, Y. Wei, W. Zhang, X. Zhang, B. Fang, L. Wang, Microchimica Acta 168 (2010) 87–92;
57. E. Scavetta, L. Guadagnini, A. Mignani, D. Tonelli, Electroanalysis 20 (2008) 2199;
58. A. Khenifi, Z. Derriche, C. Forano, V. Prevot, C. Mousty, E. Scavetta, B. Ballarin, L. Guadagnini, D. Tonelli, Analytica Chimica Acta, 654 (2009) 97-102;
59. W. De Nolf, K. Janssens, Surface and Interface Analysis, 42 (2010) 411-418;
60. J. T. Matsushima, F. Trivinho-Strixino, E. C. Pereira, Electrochim. Acta 51 (2006) 1960;
61. T. Honda, K. Murase, T. Hirato, Y. Awakura, J. Appl. Electrochem. 28 (1998) 617;
62. J. W. Boclair, P. S. Braterman, Chemistry of Matererials, 11 (1999) 298-302;
63. Z. P. Xu, H. C. Zeng, Journal of Physycal Chemistry B 105 (2001) 1743;
64. K.W. Li, N. Kumada, Y. Yonesaki, T. Takei, N. Kinomura, H. Wang, C. Wang, Materterials Chemistry and Physics 121 (2010) 223;
65. R. Chegroune, E. Salhi, A. Crisci, Y. Wouters, A. Galerie, Oxididation of Metals 70 (2008) 331;
66. F. Basile, P. Benito, G. Fornasari, V. Rosetti, E. Scavetta, D. Tonelli, A. Vaccari, Applyed Catalysis B: Environ. 91 (2009) 563;
67. Y. Hamlaoui, F. Pedraza, L. Tifouti, Corrossion Science 50 (2008) 2182;
68. C. Agrafiotis, A. Tsetsekou, J. Eur. Ceram. Soc. 20 (2000) 815;
69. F. Basile, G. Fornasari, M. Gazzano, A. Kiennemann, A. Vaccari, Journal of Catalysis 217 (2003) 245;
70. C.P. Hwanga, C.T. Yeha, Q. Zhub, Catalysis Today 51 (1999) 93;
71. F. Basile, P. Benito, G. Fornasari, A. Vaccari, Applied Clay Science 48 (2010) 250.